Amirkhanov Institute of Physics
of Dagestan Federal Research Centre of the
Russian Academy of Sciences
Kotelnikov Institute of Radioengineering and Electronics
of Russian Academy of Sciences
Chelyabinsk State University

DAGESTAN CALORIC DAYS: Functional Materials and Their Applications

BOOK OF ABSTRACTS

May 27–31, 2026
Manas, Dagestan, Russia

Chelyabinsk
Publishing House of Chelyabinsk State University
2026

УДК 620
ББК Ж3
D11

ORGANIZING COMMITTEE
Co-Chairs:
A. M. Aliev, Makhachkala, Russia
V. V. Koledov, Moscow, Russia
S. V. Taskaev, Chelyabinsk, Russia

PROGRAM COMMITTEE
A. A. Amirov, Makhachkala, Russia; A. B. Batdalov, Makhachkala, Russia;
V. D. Buchelnikov, Chelyabinsk, Russia; I. V. Bychkov, Chelyabinsk, Russia;
Fengxia Hu, Beijing, PR China; A. G. Gamzatov, Makhachkala, Russia;
Jing Wang, Beijing, PR China; A. P. Kamantsev, Moscow, Russia;
V. V. Khovaylo, Moscow, Russia; V. V. Marchenkov, Ekaterinburg, Russia;
A. V. Mashirov, Moscow, Russia; A. K. Murtazaev, Makhachkala, Russia;
V. V. Sokolovskiy, Chelyabinsk, Russia; M. A. Zagrebin, Chelyabinsk, Russia

LOCAL COMMITTEE
M. D. Alieva, Makhachkala, Russia; A. T. Kadyrbardeev, Makhachkala, Russia;
A. A. Mukuchev, Makhachkala, Russia; L. N. Khanov, Makhachkala, Russia;
D. M. Yusupov, Makhachkala, Russia; Zhao Zhiyuan, Moscow, Russia;
M. V. Matyunina, Chelyabinsk, Russia

D11 **Dagestan Caloric Days**: Functional Materials and Their Applications : Book of Abstracts (May 27-31, 2026, Manas, Dagestan, Russia) / Persons responsible for publication: M. V. Matyunina, M. A. Zagrebin. Chelyabinsk : Publishing House of Chelyabinsk State University, 2026. 180 p.

ISBN 978-5-7271-2140-5

This book of abstracts presents results of modern fundamental and applied research in the fields of condensed matter physics, functional magnetic materials, and advanced energy conversion technologies. Primary focus is placed on magneto-, electro-, and elastocaloric effects in Heusler alloys, rare-earth compounds, multiferroics, and shape-memory materials.

The book reflects the interdisciplinary nature of modern research: along with experimental techniques (direct measurement of adiabatic temperature changes, thermal imaging diagnostics, pulsed magnetometry, and microwave spectroscopy), theoretical and computational approaches are widely represented, including ab initio calculations, Monte Carlo methods, machine learning, and numerical modeling of caloric and levitation systems.

The materials in this book will be useful to researchers, graduate students, and engineers specializing in solid-state physics, modern materials science, cryogenic engineering, and the development of energy-efficient cooling technologies.

The materials are published in the author's version.

УДК 620(082)
ББК Ж3я431

ISBN 978-5-7271-2140-5 © Chelyabinsk State University, 2026

Localized Phase of Skyrmions in a Ferromagnetic Film with a Defect

D. I. Abdrakhmanov[1, a], I. F. Sharafullin[1, b]

[1]Ufa University of Science and Technology, Ufa, Russia
[a]e-mail: *dron.boiko@mail.ru@mail.ru*
[b]e-mail: *sharafullinif@yandex.ru*

Skyrmions — opologically stable magnetic structures — are considered promising memory [1] and logic [2] elements in spintronic devices due to their small size (up to 100 nm), stability at room temperatures [3], and the ability to be controlled by current [4] or electric field [5]. One of the challenges for practical implementation is the controlled localization of skyrmions in specified positions [6]. The use of crystal lattice defects that create local potential wells can pin skyrmion phases [7].

This paper considers the Heisenberg model on a triangular lattice consisting of two ferromagnetic layers (Fig. 1, *a*). The first layer is char-

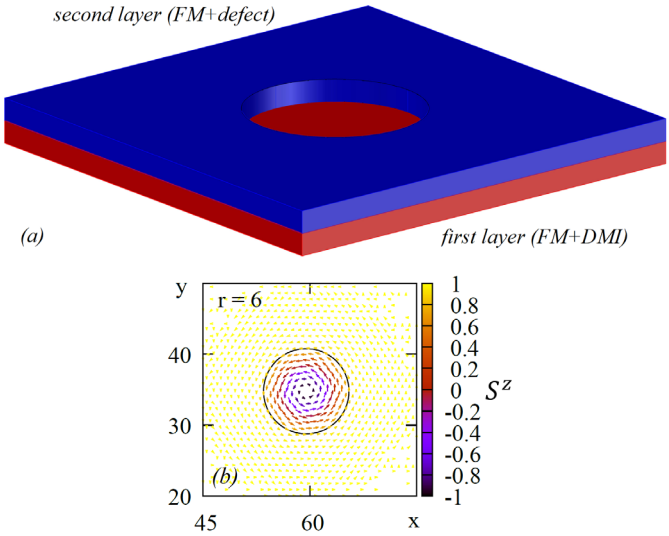


Fig. 1. (a) Schematic of the ferromagnetic film model. (b) Spin configuration of the ground state of the first layer at $D=-0.5$, $h=0.2$ with a defect in the second layer. The boundary of the defect in the second layer is indicated in black

acterized by ferromagnetic exchange and in-plane Dzyaloshinskii-Moriya interaction (DMI). Spins on the second layer with the defect only interact through exchange. The external magnetic field is directed perpendicular to the plane of the bilayer film. The Hamiltonian of the system has the form:

$$H = -\frac{1}{2}\sum_{i,j} J^m_{i,j} \cdot \vec{S}_i \cdot \vec{S}_j -$$

$$-\frac{1}{2} D \sum_{i,j} \left\{ e^x_{i,j} \left(S^y_i S^z_j - S^z_i S^y_j \right) - e^y_{i,j} \left(S^x_i S^z_j - S^z_i S^x_j \right) \right\} - \vec{h} \sum_i \vec{S}_i . \qquad (1)$$

The defect in the second layer is specified by modifying the exchange interaction parameter according to the formula:

$$J^m_{i,j} = J^0 \left(1 + \tanh \left(\frac{\left| \vec{K}_{ij} \right| - R}{\vartheta} \right) \right). \qquad (2)$$

The ground state of the system was determined using the steepest descent method with periodic boundary conditions. The topological charge was calculated using the Berg — Luscher method [8; 9].

The addition of a second ferromagnetic layer does not change the overall trend of the topological charge dependence on external field $q_T(h)$, but shifts the region of existence of skyrmion phases toward lower external fields. When the defect in the second layer is taken into account, a nonzero topological charge is retained beneath the defect in regions of phase diagram where a ferromagnetic phase would be observed otherwise (Fig. 1b). This means that the hole-type defect in the second layer locally weakens the stabilizing effect of the external field, allowing DMI to form a skyrmion phase in the first layer only in the region below the defect. As the defect diameter increases, the area with suppressed interlayer exchange interaction increases, leading to the formation and localization of several skyrmions by the defect.

This work was carried out within the framework of the state assignment, agreement № 075-03-2024-123/1 dated 02/15/2024.

[1] A. Fert, V. Cros, J. Sampaio, *Nat. Nanotechnol*. 8, 152–156, (2013).

[2] X. Zhang, M. Ezawa, Y. Zhou, *Sci. Rep*. 5, 1–8, (2015).

[3] O. Boulle et al. *Nat. Nanotechnol*. 11, 449–454, (2016).

[4] Y. Tchoe, J. H. Han, *Phys. Rev. B*. 85, 174416, (2012).

[5] Y. Okamura et al. *Nat. Commun*. 7,12669, (2016).

[6] A. Derras-Chouk, E. M. Chudnovsky, *J. Phys. Condens. Matter*. 33, 195802, (2021).

[7] K. Fallon et al. *Small*. 16, 1907450, (2020).

[8] B. Berg, M. Lüscher, Nucl. *Phys. B*. 190, 412–424, (1981).

[9] J. V. Kim, J. Mulkers, *IOP SciNotes*. 1, 025211, (2020).

Direct Measurements of Adiabatic Temperature Change in $DyCo_2$ Alloy in Ultra-low Magnetic Fields

N. Z. Abdulkadirova[1, a], A. G. Gamzatov[1], A. M. Aliev[1], Jing Wang[2], Fengxia Hu[2]

[1]Amirkhanov Institute of Physics of DFRC of RAS, Makhachkala 367003, Russia

[2]Beijing National Laboratory for Condensed Matter Physics, Institute of Physics, Chinese Academy of Sciences, Beijing 100190, PR China

[a]e-mail: *nnurizhat@mail.ru*

Traditionally, direct measurements of the adiabatic temperature change ΔT are conducted in fields of the order of 1–2 T, where the signal is maximal and experimental difficulties are minimized. However, the region of ultra-low magnetic fields (less than 50 Oe) remains the least studied due to the smallness of the effect and the need for specialized

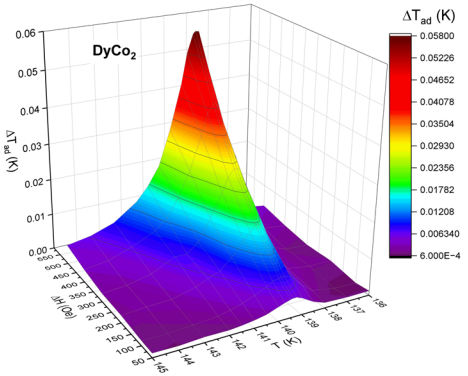


Fig. 1. Temperature dependence of ΔT_{ad} for $DyCo_2$ alloy in magnetic fields from 50 to 500 Oe

experimental techniques. It is in the limit of weak fields (on the order of the coercive force) that the physical mechanisms determining the nature of the phase transition begin to dominate.

This study presents the results of direct measurements of the adiabatic temperature change ΔT_{ad} of the binary $DyCo_2$ alloy in weak magnetic fields from 50 to 500 Oe (Fig. 1), conducted using a highly sensitive modulation method. It is shown (Fig. 1) that even at such low fields, the effect is recorded with a good signal-to-noise ratio, and its temperature dependence allows for a scaling analysis of the critical behavior. Measurements of the phase shift between the applied magnetic field and the temperature response of the sample were also carried out. A scaling analysis of the obtained results was also performed.

The study was supported by the Russian Science Foundation, grant № 24-12-00362, https://rscf.ru/en/project/24-12-00362/.

Magnetocaloric Effect of the $Tb_{0.25}Dy_{0.25}Ho_{0.25}Er_{0.25}Co_2$ Alloy in Weak Magnetic Fields

M. D. Alieva[1, a], N. Z. Abdulkadirova[1], A. G. Gamzatov[1], A. M. Aliev[1]

[1]Institute of Physics named after H. I. Amirkhanov DFRC RAS, Makhachkala, Russia

[a]e-mail: *totalfailure@mail.ru*

The magnetocaloric effect (MCE) has prospects not only for practical use in solid-state cooling technology, but is also an important parameter in terms of studying the nature of magnetic phase transitions. The study of the MCE in weak magnetic fields is particularly effective in terms of studying phase transitions. Currently, direct measurements of the MCE are mainly conducted in moderate or strong fields to assess the prospects of materials for solid-state cooling technology. Direct measurements of the MCE in weak magnetic fields have been conducted rarely due to the limitations of the classical direct measurement method. However, mea-

surements in weak magnetic fields can provide extensive information about magnetic phase transitions. In this study, we used a highly sensitive modulation method for measuring the MCE, which was developed in our laboratory, to conduct measurements in magnetic fields of tens of ergs. The results of direct measurements of the adiabatic temperature change in the high-entropy alloy $Tb_{0.25}Dy_{0.25}Ho_{0.25}Er_{0.25}Co_2$ in weak magnetic fields from 50 E to 3000 E are presented. We measured the temperature and magnetic field dependencies of ΔT_{ad} and performed a detailed analysis of the magnetic field dependencies near the ferromagnet-paramagnet phase transition.

This work was supported by the Russian Science Foundation grant № 24-12-00362, https://rscf.ru/en/project/24-12-00362/.

Application of Reactive Additive and Electron Beam Processing to Create Porous-Monolithic Material Based on TiNi

S. G. Anikeev[1, a], N. V. Artyukhova[1], S. A. Pakholkina[1], E. A. Bolshevich [1]

[1] Laboratory of Medical Materials Science, Tomsk State University, Tomsk, Russia

[a]e-mail: *anikeev_sergey@mail.ru*

Modern reconstructive surgery and traumatology place high demands on bone implant materials. They must simultaneously possess the necessary and sufficient mechanical strength, durability under cyclic loads, and the ability to effectively integrate with surrounding body tissues. Among metallic biocompatible materials, titanium nickelide (TiNi)-based alloys occupy a special place, demonstrating a unique combination of high corrosion resistance, fatigue strength, and functional properties (shape memory and superelasticity). These properties are due to reversible thermoelastic martensitic transformations between the high-temperature austenitic B2 phase and the low-temperature martensitic B19’ phase.

Porous-monolithic (PM) TiNi-based materials represent a promising class of biocompatible materials that combine the advantages of monolithic and porous structures. The key technological challenge in creating PM materials is the formation of a strong and stable bond between the porous and monolithic components. Traditional methods, such as diffusion and reaction sintering of TiNi powder onto a monolithic substrate, despite their effectiveness, have significant drawbacks. High temperatures and long processing times lead to thermal degradation of the monolithic substrate (softening), as well as the formation of a heterogeneous phase structure in the porous layer. The presence of brittle secondary intermetallic phases (such as Ti_2Ni, $TiNi_3$) and oxycarbonitride inclusions Ti_4Ni_2(O, N, C) reduces the corrosion resistance and mechanical integrity of the coating under cyclic loading in an aggressive biological environment.

To address these interrelated issues, this paper proposes and explores an integrated two-stage technological approach. The first stage is aimed at minimizing the thermal impact on the monolithic substrate. This is achieved using reaction-diffusion sintering, which incorporates titanium and nickel powders into a TiNi-based charge as an activating exothermic additive. The heat generated by the synthesis reaction reduces the overall sintering temperature by approximately 150 K compared to traditional methods, preventing undesirable changes in the monolith structure and promoting the formation of a durable, graded transition layer between the substrate and the porous coating.

The second stage of the technology involves modifying the surface of the resulting porous-monolithic composite with a pulsed low-energy high-current electron beam (LEHCEB). The short-term, concentrated energy exposure causes localized melting and recrystallization of the surface layer, leading to its homogenization, smoothing of the microrelief, and dissolution and dispersion of secondary phase particles. Simultaneously, the treatment activates the surface, intensifying the formation of a dense passive oxide film based on TiO_2, which is a determining factor in increasing corrosion resistance.

This work addresses the pressing scientific and technical challenge of developing and comprehensively studying a method for producing porous-monolithic materials based on titanium nickelide. The technology is based on the synergy of two key processes: reaction-diffusion sintering with an activating additive for low-temperature formation of a composite with a high-quality transition layer, followed by electron-beam processing

to create a homogeneous, corrosion-resistant layer with optimized topography on its surface, free of harmful impurity phases. Implementation of this approach is aimed at creating a new generation of biocompatible implants with a predetermined property gradient, combining high structural characteristics with excellent bioactivity and long-term stability in the body. It has been established that the use of a monolithic titanium nickelide alloy grade TN-10 in combination with TiNi powder, produced by calcium hydride reduction, with a fraction of 100–160 μm and the reactive addition of Ti and Ni powders at a sintering temperature of 1100°C, enables the creation of a porous monolithic material with a predominant content of the austenitic phase B2(TiNi) and a proportion of secondary phase particles Ti_2Ni and Ti_4Ni_2(O, N, C) oxycarbides based on them of no more than 17%. The NSEP modification improves corrosion resistance and reduces the corrosion rate in NaCl environments by homogenizing the material's phase and chemical composition.

This work was supported by the D. I. Mendeleyev Scientific Foundation as part of the Tomsk State University Development Program (Priority 2030).

The Influence of Chromium Alloying on the Structural Features and Phase Composition of a Monolithic Material Based on Ti_2Ni

N. V. Artyukhova[1, a], S. G. Anikeev[1], S. A. Pakholkina[1], E. A. Bolshevich[1], V. V. Loban'[1]

[1] Laboratory of Medical Materials Science, Tomsk State University, Tomsk, Russia

[a]e-mail: *artyukhova_nad@mail.ru*

The physical and chemical advantages of hydrogen will make it an important synthetic fuel in the future [1]. Currently, hydrogen can be stored as a gas in composite cylinders and as a liquefied gas at cryogenic temperatures in tanks with screen-vacuum insulation [2]. The first method, in pressurized cylinders, has the disadvantage of low gas bulk density,

while the second method, increasing pressure to 600 bar, is associated with safety risks. Metal hydride storage has been proposed as a safe and technologically advanced storage alternative [1]. The technology is based on the ability of metals and intermetallic compounds to reversibly absorb large volumes of hydrogen, forming hydrides. In this state, hydrogen is in a bound state, which reduces the risk of leaks and explosions, ensures high storage density at low pressures, and also allows storage in a compact solid-phase form [1; 2].

A Ti_2Ni alloy has been selected as the basis for the hydrogen carrier. It has an $E9_3$ cubic structure and is characterized by satisfactory kinetics and a capacity of up to ~2.1 wt.% H_2 [3]. Alloying it with chromium allows us to optimize its sorption properties, influencing the metal-hydrogen bond energy, the size of interstitials, and the stability of the material during cycling. The choice of chromium is justified by its ability to form hydrides, the proximity of its atomic radius (128 pm) to nickel (124 pm), and its proven effectiveness in TiNi-based systems [3]. The aim of this study is to identify the effects of chromium alloying on the microstructure of monolithic Ti_2Ni-based materials.

In this work, we investigated monolithic Ti_2Ni-based alloy samples with different Cr contents: 0, 0.5, 1, 1.5 at.%, obtained by induction melting using an ISV-0.004 melting furnace. The feedstock was sponge titanium, electrolytic nickel in the form of plates, and NiCr wire. All components were melted in a crucible. Heating, holding, and pouring the melt into the chill mold were carried out in an argon atmosphere at a pressure of 1 atm. Microstructure analysis was performed using optical and scanning electron microscopy on AXIO Zoom V16 and Quanta 200 3D microscopes. Pre-ground samples were treated with an aqueous solution of HNO_3: HF : H_2O acids. X-ray diffraction analysis of the samples was performed at room temperature using a Shimadzu XRD-6000 diffractometer.

The structure of the monolithic Ti_2Ni-based material, both pristine and chromium-doped, is characterized by the presence of dendrites. The formation of the dendritic structure is associated with the phenomenon of concentration supercooling, which occurs ahead of the moving crystallization front, destabilizing its flat shape and promoting the formation of cellular and dendritic growth forms. With an increase in the Cr concentration to 1 at.%, an increase in the number and size of dendrites is observed. At the maximum chromium content (1.5 at.%), the dendritic

morphology changes from branched to lamellar. The contrast between the structural components for the chromium-doped samples indicates different chromium concentrations within the structural elements. During crystallization, chromium is displaced from the growing dendrite to the phase boundary, leading to its accumulation and enrichment of the residual melt in the interdendritic layers. A study of the structural and phase composition revealed that the introduction of chromium in the studied concentration range does not lead to the formation of new phases. The phase composition is characterized by the presence of only the Ti_2Ni phase. However, an increase in the lattice parameter is observed, from 11.3298 Å for the original sample to 11.3400 Å for the sample doped with 1.5 at.% Cr.

The X-ray diffraction pattern reveals a shift of all diffraction reflections toward smaller reflection angles. This indicates an increase in interatomic distances in the crystal lattice. This expansion is caused by the dissolution of chromium atoms in the Ti_2Ni matrix, which creates an elastic microstress field. An increase in the lattice parameter promotes an increase in octahedral voids, which contributes to an increase in the material's capacitance. In this case, the most promising addition is 1.5 at.% Cr, which provides the maximum increase in the lattice parameter.

The study was supported by the Russian Science Foundation grant No. 25-79-10232, https://rscf.ru/project/25-79-10232/.

[1]. Schlapbach, L., Züttel, A. *Nature*. 414, 6861 (2001).

[2]. Tarasov B. P., Lototsky M. V., Yartys V. A. *Russian Chemical Journal*. 6. 34–48 (2006).

[3]. Kulabukhova N. A., Poletaev G. M., Starostenkov M. D., Kulagina V. V., Potekaev A. I. *Russian Physics Journal.* 54(12). 1394–1400 (2012).

Effect of Alloying on the Thermoelectric Properties of the Half-Heusler FeVSb Alloy at Low Temperatures

A. B. Batdalov[1, a], A. A. Mukhuchev[1], A. V. Khovailo[2]

[1]Institute of Physics named after H. I. Amirkhanov DFRC RAS, Makhachkala, Russia
[2]National University of Science and Technology "Moscow Institute of Steel and Alloys," Moscow, Russia
[a]e-mail: *ab.batdalov@gmail.com*

Ternary intermetallic compounds, called Heusler alloys, are usually divided into full Heusler alloys with a stoichiometry of X_2YZ, and half-Heusler alloys, the stoichiometric composition of which is defined as XYZ, where, as a rule, X and Y are transition metals, and Z is a chemical element of the main group.

Full Heusler alloys are interesting because they exhibit a series of phase transitions of various natures, and their practical interest is associated with gigantic values of the MCE, which can find application in magnetic refrigeration technology [1].

Interest in half-Heusler alloys based on Fe-V-Sb is primarily associated with the possibility of their practical application in the technology of direct conversion of thermal energy into electrical energy (Seebeck effect) and vice versa (Peltier effect).

It can also be noted that the elements included in these thermoelectrics are thermally stable, inexpensive and environmentally safe [2; 3].

The most important parameter determining the efficiency of a thermoelectric material is its thermoelectric figure of merit

$$ZT = \frac{\sigma s^2}{\kappa} T,$$

where σ is the electrical conductivity, s is the thermoelectric power, κ is the thermal conductivity, T is the temperature, and σS^2 is sometimes called the power parameter. As can be seen from the expression for ZT, the efficiency of a thermoelectric can be increased by either increasing the power parameter σS^2 or decreasing the overall thermal conductivity.

However, the problem is that the coefficients determining ZT values are interrelated, making it difficult to select materials with optimal characteristics. The most common way to increase ZT currently is to reduce the thermal conductivity of phonons by enhancing scattering by nanoscale inhomogeneities. Inhomogeneities comparable to the wavelength of thermal phonons effectively scatter phonons, leading to an increase in ZT. FeVSb iron-based half-Heusler alloys exhibit noteworthy thermoelectric properties among other half-Heusler alloys [3; 4].

A significant drawback of such alloys is their high thermal conductivity, which limits their potential for use as thermoelectric converters, prompting researchers to seek ways to reduce thermal conductivity. One way to reduce thermal conductivity is iso- and heteroelectronic substitution of V atoms with transition metal atoms, such as Hf and Ti. The results of such studies at room temperature and above are presented in [5]. It should be noted that half-Heusler alloys of the FeVSb type are classified as medium-temperature thermoelectrics, and our studies at low temperatures (from nitrogen and above) are more of a fundamental nature, related to the mechanisms of electron and phonon scattering.

This paper presents the results of a study examining the effect of alloying on the thermal conductivity, thermoelectric power, and electrical resistance of a half-Heusler FeVSb alloy at low temperatures. The transition metals Hf and Ti were used as alloying elements. Traditional methods were used for the measurements: the steady-state heat flux method for thermal conductivity, the differential method for thermoelectric power, and the four-probe method for electrical resistance.

The samples for the study were obtained by inductive melting followed by mechanical alloying, spark plasma sintering followed by annealing. The results obtained from the study can be summarized as follows.

Alloying samples with transition metals Hf and Ti leads to a sharp decrease in thermal conductivity and a reversal of the Seebeck coefficient, as well as a significant increase in electrical resistance. The power factor increases with temperature, which is associated with an increase in the Seebeck coefficient.

Within the experimental accuracy, a magnetic field of 80 kOe has no effect on the measured coefficients. Phonon thermal conductivity completely dominates the electronic component over the entire temperature range studied.

The obtained results indicate an increase in the rate of phonon scattering on inhomogeneities arising from alloying the initial alloy with heavy metals and are discussed within the framework of modern theoretical concepts.

The work was carried out with the financial support of a grant from the RSF № 25-29-00410 (https://rscf.ru/project/25-29-00410/).

[1] A. B. Batdalov, L. N. Khanov, Jr. and A. M. Aliev. J. *Appl. Phys*. 129, 12 (2021).

[2] M. Zou, J-F. Li, T. Kita. J. *Sob. St. Chem*. 198, 125 (2013).

[3] D. P. Yong, R. J. Cava, A. P. Ramirez. *J. Appl. Phys*. 87, 317 (2000).

[4] R. Hasan, S-C Ur. *Trans. Electr. Electron Materials*. 19, 106 (2018).

[5] A.El-Khouly, A. M. Adam, Jr. and E. M. Elsehly. *J. All. And Comp*. 886, 16136 (2021)

Temperature Relaxation Time of the Elements of the Gas Thermal Switch of a Cryogenic Magnetic Refrigerator

O. V. Belova[1, a], S. S. Morkovin[1], K. A. Kolesov[2], A. V. Mashirov[2, b]

[1] Bauman Moscow State Technical University, Moscow, Russia
[2] Kotelnikov Institute of Radioengineering and Electronics of Russian Academy of Sciences, Moscow, Russia
[a] e-mail: *ovbelova@bmstu.ru,*
[b] e-mail: *a. v.mashirov@mail.ru*

The development of magnetic cooling technology is associated not only with the household use of materials with a magnetocaloric effect [1], but also with the development of cryogenic magnetic refrigerators for liquefying natural gas or hydrogen [2]. The aim of this work is to experimentally determine the relaxation time of the elements of a gas thermal switch in the cryogenic temperature range and compare it with a mechanical thermal switch with the same mass and dimen-

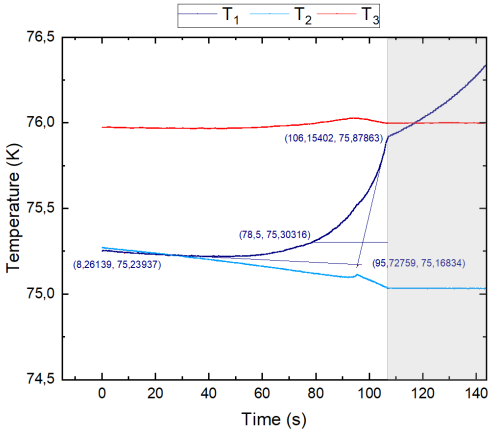


Fig. 1. T_1 is the value of the temperature relaxation time of the $GdNi_2$ sample, T_2 is the value of the copper heat receiving cylinder and T_3 is the change in the temperature of the heat shield surrounding them

sional parameters. The relaxation time at a temperature level of 75 K was determined experimentally with a ratio of the mass of the copper heat sink and the magnetocaloric working body $m_{Cu}/m_{GdNi_2} = 49$, which is about 10.4 seconds (Fig. 1). It has been established that the relaxation times of the contact pair of a cryogenic mechanical thermal switch with an indium thermal interface and a cryogenic gas thermal switch with similar weight and size parameters are practically the same. An assessment is made of the heat removal capacity of a single stage of a cryogenic magnetic refrigerator cascade with a gas thermal switch.

[1] J. Liang et al., *Appl. Therm. Eng*. **284**, 129144 (2025).

[2] L. Cirillo et al., *Int. J. of Refrigeration*. **179**, 184–203 (2025).

Thermoelectric Properties of Selected Double Half-Heusler Alloys

V. D. Buchelnikov[1, a], V. V. Sokolovskiy[1], S. V. Taskaev[1]

[1]Chelyabinsk State University, Chelyabinsk, Russia
[a]e-mail: *buche@csu.ru*

In this study, we investigate the thermoelectric properties of seven double half-Heusler alloys using a combined theoretical and experimental approach. The alloys under consideration are Zr_2Ni_2InSb, $V_2FeNiGe_2$, Ti_2Pt_2InSb, Ti_2Ni_2InSb, $Ti_2FeNiSb_2$, $Nb_2FeNiSn_2$, and $Hf_2FeNiSb_2$. Using density functional theory, the Boltzmann transport equation, and the quasi-Debye approximation, we calculated the Seebeck coefficient (S), electrical conductivity (σ), total thermal conductivity ($\kappa = \kappa_{el} + \kappa_{latt}$), and thermoelectric figure of merit (ZT). Our calculations show that all the studied alloys exhibit low lattice thermal conductivity, ranging from 5.7 to 10 W/(m·K) at room temperature. The ZT values ($ZT = S^2\sigma T/\kappa$) at 300 K fall within the range of 0.16–0.32. At elevated temperatures, ZT is predicted to reach values of approximately 1–2. For instance, the ZT of $Ti_2FeNiSb_2$ reaches unity at 500 K. Experimental measurements of the properties were also performed for selected alloys, confirming their potential for application in thermoelectric devices

This work was supported by the Russian Science Foundation Project № 24-12-20016 (https://rscf.ru/en/project/24-12-20016/).

Electrocaloric Effect During Ferroelectric Phase Transition in Ceramic Samples $BaTiO_3$

M. S. Bybik[1, a], A. P. Kamantsev[1], D. S. Kalenov[1], A. P. Orlov[1], K. V. Lopukhin[1], V. V. Koledov[1], A. A. Amirov[2, b], G. A. Shandryuk[3, c], D. A. Kuzmin[4], I. V. Bychkov[1, 4, d]

[1] Kotelnikov Institute of Radioengineering and Electronics of RAS, Moscow, Russia
[2] Institute of Physics named after H. I. Amirkhanov of RAS, Makhachkala, Russia
[3] A. V. Topchiev Institute of Petrochemical Synthesis of RAS, Moscow, Russia
[4] Chelyabinsk State University, Chelyabinsk, Russia
[a]e-mail: *ne.znachit.nichego@yandex.ru*
[b]e-mail: *amiroff_a@mail.ru*
[c]e-mail: *gosha@ips.ac.ru*
[d]e-mail: *bychkov@csu.ru*

The development of methods for measuring the electrocaloric effect (ECE) is a prerequisite for unlocking the full potential of ferroelectric materials in solid-state cooling. An example of a non-contact method for direct measurements of the ECE with time resolution of the adiabatic change in temperature ΔT and electrical polarization P in ferroelectric materials is provided in [1].

The purpose of this work is to study the ECE in $BaTiO_3$ with simultaneous registration of electrical polarization. A theoretical model of ferroelectric materials with martensitic phase transitions (PTs) based on modified Landau-Khalatnikov kinetic equations was also developed, taking into account the nonlinear interaction between the ferroelectric and elastic subsystems of the solid. A numerical algorithm for solving a system of coupled differential equations was implemented, and computer simulations of hysteresis phenomena in $BaTiO_3$ as a model object were performed.

The dielectric spectroscopy of $BaTiO_3$ samples was previously performed, and the temperature dependencies of the relative permittivity, impedance, and tangent of the loss angle at frequencies of 1, 10, and 100 kHz were obtained during heating and cooling near the ferroelectric PT. The obtained dependencies exhibit the characteristic temperature

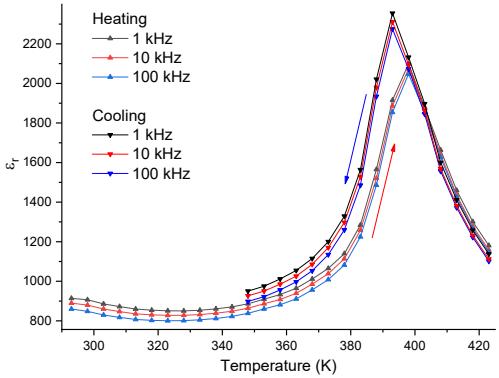


Fig. 1. Temperature dependence of the relative permittivity ε_r of a $BaTiO_3$ ceramic sample at frequencies of 1, 10, and 100 kHz during heating and cooling

hysteresis between the ferroelectric and paraelectric phases, which is typical for the first-order PTs.

The temperature dependencies of the relative permittivity ε_r of the $BaTiO_3$ ceramic sample at frequencies of 1, 10, and 100 kHz during heating and cooling are shown in Fig. 1 and exhibit a characteristic temperature hysteresis at the 1st-order PT between the ferroelectric and paraelectric phases, which is consistent with the known data [2].

The ECE was measured using a direct method. The setup includes a thermostat with a ferroelectric sample in the form of a "tablet" with dimensions of Ø10×4 mm and silver plates enclosed in a vacuum chamber. The electrical circuit allows for the application of pulsed and harmonic electrical signals to the sample under study, *in situ* measuring the in situ dynamics of electrical polarization and temperature changes in the sample.

The ability to correlate the dynamics of the ECE with the dynamics of electrical polarization will allow us to better understand the kinetics of the ferroelastic martensitic PT and establish the power limits of thermodynamic machines based on it.

The study was supported by a grant from the Russian Science Foundation. № 25-19-00942, https://rscf.ru/project/25-19-00942/.

[1] Fischer, J., Döntgen, J., Molin, et al. *Rev.Sci. Instrum.*, 94(4), 043906 (2023).

[2] M. Acosta, N. Novak, V. Rojas, et. al. *Appl. Phys. Rev.*, 4(4), 041305 (2017).

Spin Wave Emission Upon the Decay of a Discrete Breather in a Chain of Magnetic Nanoparticles

D. A. Kuzmin[1], E. G. Ekomasov[2], I. V. Bychkov[1, a]

[1]Chelyabinsk State University, Chelyabinsk, Russia
[2]Ufa University of Science and Technology, Ufa, Russia
[a]e-mail: *bychkov@csu.ru*

Nonlinear magnetic wave phenomena in periodic arrays of magnetic nanoparticles have attracted considerable attention for quite a long time [1–7]. Discrete breathers (DBs) [8–10] represent temporally periodic and spatially localized excitations. Previously, the existence of DBs was theoretically predicted for chains of magnetic nanodots coupled by dipole-dipole interaction [11] and for chains of magnetic nanoparticles without dissipation [12]. However, under realistic experimental conditions, the influence of dissipative processes cannot be excluded. The present work is devoted to investigating the possibility and conditions for the existence of DBs in a chain of magnetic nanoparticles, taking these features into account.

A chain of cylinder single-domain permalloy nanoparticles interacting via dipole-dipole interaction is considered (see Fig. 1). A fifth-order Runge — Kutta numerical method was used for the analysis.

The study reveals that taking dissipation into account fundamentally changes the dynamics of DBs. In contrast to conservative models, DBs have a finite lifetime. During the decay process, their oscillation frequency decreases, and the energy of the localized excitation is converted into spin wave emission into the chain. It is shown that decreasing the distance between particles (strengthening the dipole-dipole coupling) significantly reduces the lifetime of DBs and increases the frequency of the emitted spin wave packets. The decay of DBs transforms them into a source of directional spin wave packets. It is shown that the velocity of this packet (group velocity) depends on the distance between particles and exhibits a distinct minimum at a specific value (~120 nm), which was not observed in models without dissipation. DBs demonstrate stability both with an increase in the number of excited particles in the core (up to 5 particles) and with changes in the total chain length (from 10 to 50 particles).

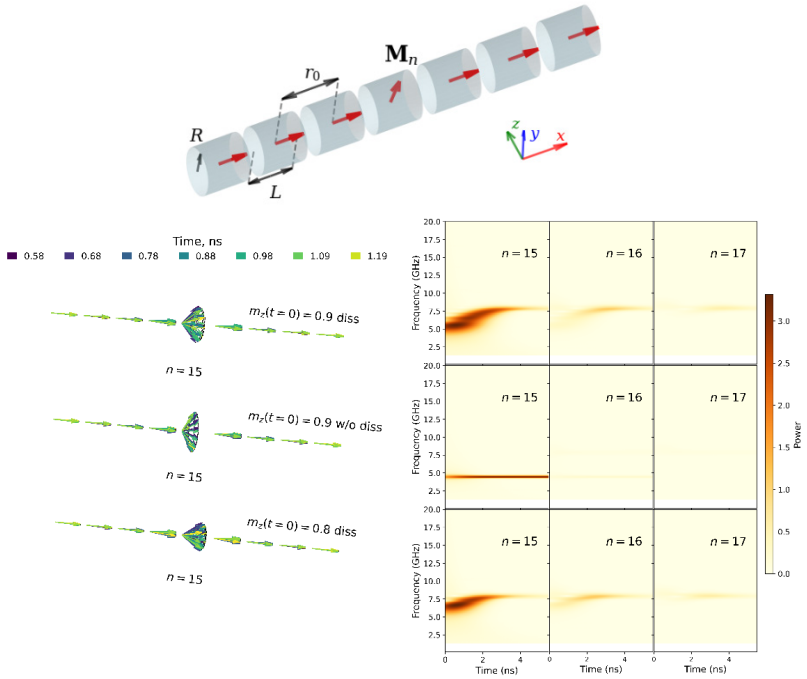


Fig. 1. A chain of cylinder single-domain permalloy nanoparticles interacting via dipole-dipole interaction shows localized non-linear magnetization precession leading to spin wave emission upon the decay

Dissipation not only suppresses DBs but also enables the controlled generation of spin wave packets with a controllable velocity using them. Possible methods for exciting DBs in experiments are discussed: using ultrafast optical remagnetization, spin torque, or resonant microwave excitation. The obtained results open new prospects for the application of nonlinear dynamics of magnetic nanoparticles in magnonics and spintronics, for example, for creating magnonic switches or sources of spin waves based on the controlled decay of localized excitations.

The work was carried out within the framework of State Assignments № 075-00188-26-00.

[1] P. C. Waterman, N. E. Pedersen, *J. Appl. Phys*. 59, 2609 (1986).

[2] P. Vavassori et al., *J. Appl. Phys*. 88, 999 (2000).

[3] A. Yu. Galkin, B. A. Ivanov, *JETP* 109, 77 (2009).

[4] S. A. Dzyan, B. A. Ivanov, *JETP* 116, 984 (2013).

[5] T. Shinjo et al., *Science* 289, 930 (2000).

[6] M. Pardavi-Horvath, G. S. Makeeva, O. A. Golovanov, *IEEE Trans. Magn*. 44, 3067 (2008).

[7] S. Ishizaka, K. Nakamura, *J. Magn. Magn. Mater*. 210, 15 (2000).

[8] A. A. Ovchinnikov, *Sov. Phys. JETP* 30, 147 (1970).

[9] S. Flach, A. V. Gorbach, *Phys. Rep*. 467, 1 (2008).

[10] S. V. Dmitriev et al., *Phys. Usp*. 59, 446 (2016).

[11] R. L. Pylypchuk, Y. Zolotaryuk, *Low Temp. Phys*. 41, 733 (2015).

[12] D. A. Kuzmin, I. V. Bychkov, E. G. Ekomasov, *J. Magn. Magn. Mater*. 629, 173250 (2025).

Hysteresis and Kinetics of 1st Order Phase Transitions in Heusler Alloys Under High Magnetic Fields

E. T. Dilmieva[1]

[1]Kotelnikov Institute of Radioengineering and Electronics of RAS, Moscow, Russia
e-mail: *kelvit@mail.ru*

The growing demand for energy-efficient technologies stimulates intensive research into functional materials with strongly coupled magnetic, structural, and electronic subsystems. Among these, Heusler alloys exhibiting first-order magnetostructural phase transitions are of particular interest due to their pronounced magnetocaloric effect and its potential for solid-state cooling and energy conversion applications. However, such transitions are inherently accompanied by hysteresis and complex kinetics, which significantly limit their practical efficiency. Hysteresis leads to irreversible losses and incomplete phase transformation under cyclic operation, thereby reducing the fraction of usable thermal energy. In addition, the characteristic transition times, often reaching tens or even hundreds of seconds, impose constraints on the

operating frequency of magnetocaloric devices [1; 2]. High magnetic fields also play a crucial role, as phenomenological theories suggest that the suppression of hysteresis and the achievement of reversible phase transitions may require fields on the order of ~30 T, which are experimentally challenging to realize [3]. This necessitates the development of specialized experimental methodologies capable of probing phase transitions under extreme conditions.

This talk is organized along two main research directions. First, advanced experimental methodologies for magnetic fields up to 30 T and a wide temperature range (4.2–320 K) have been developed and implemented for the investigation of magnetostructural phase transitions, based on the simultaneous measurement of multiple macroscopic properties. This approach ensures strictly identical thermodynamic conditions and enables direct investigation of the kinetics of interacting subsystems during the phase transition [4]. Second, experimental results obtained under extreme conditions are presented for Heusler alloys of the Ni—Mn—In and Ni—Mn—Ga families, focusing on the kinetics and relaxation of the phase transition, as well as on the mechanisms governing the formation and control of hysteresis. Particular attention is paid to the role of the structural subsystem alongside the magnetic one in the magnetostructural transition under conditions of high magnetic fields and low temperatures [4].

[1] R. Costa, E. Lovell, R. et.al., J. *Phys. D: Appl. Phys*., 56, 155001 (2023).

[2] E. Lovell, A. M. Pereira, et.al., *Adv. Energy Mater*., 5, 1401639 (2015).

[3] Yu. Koshkid'ko, E. Dilmieva, et.al., *J. All.Compd*., 904, 164051 (2022).

[4] A. Soares, E.Dilmieva, et.al., Preprint available at Research Square [https://doi.org/10.21203/rs.3.rs-8917871/v1]

Dynamics and Structural Changes of Magnetic Vortices of Different Polarity in Spin-transfer Nanooscillators

E. G. Ekomasov[1, a], R. A. Faskhutdinov[1], D. K. Kabanov[1], V. S. Kudashev[1]

[1]Ufa University of Science and Technology
[a]e-mail: *ekomasovEG@gmail.com*

One of the promising multilayer technical devices in spintronics is the microwave spin-transfer nanooscillator (STNO) [1]. The most studied case is that of three-layer nanopillars, which have two permalloy magnetic layers of different thicknesses separated by a nonmagnetic spacer layer. In the magnetic layers (for certain dimensions), a magnetic vortex can exist as the ground state. Cases of vortex-based STNOs are investigated, where a vortex exists in one or both magnetic layers (see, e. g., [1]). It has been shown experimentally and theoretically that the vortex dynamics in a two-vortex STNO can change dramatically compared to the case of a single-vortex STNO [1; 2].

For the case of a two-vortex STNO of small and medium diameter, the SPIN PM package was used to describe the dynamic change in the vortex structure, several possible scenarios of vortex motion, and possible structural phase transitions between them, depending on the magnitude of the spin-polarized current. Diagrams of the frequency and radius of stationary coupled oscillations of magnetic vortices as functions of the spin-polarized current magnitude were constructed. Using effective equations of coupled dynamics for the vortex cores, possible trajectories and frequencies for the stationary regime of coupled vortex oscillations were found for both the same and different polarities.

The work was carried out within the framework of a state assignment, agreement No. 075-03-2024-123/1 dated February 15, 2024, topic No. 324-21.

[1] K. A. Zvezdin, E. G. Ekomasov, The Physics of Metals and Metallography 123, 201–219 (2022)

[2] A. Hanif, A. A. Rahim, H. Maab, Physica B: Condensed Matter. 668, 415203 (2023)

Phase Stability and Martensitic Transformations in Ni—Co—Ti Heusler Alloys

K. R. Erager[1, a], V. V. Sokolovskiy[1], V. D. Buchelnikov[1]

[1]Chelyabinsk State University, Chelyabinsk, Russia
[a]e-mail: *eragerk@rambler.ru*

Heusler alloys are a class of intermetallic compounds characterized by an ordered crystal structure and a wide range of functional properties, including magnetic shape memory, the magnetocaloric effect, magnetoresistance, etc. Classical examples of Heusler alloys include binary and ternary systems based on Ni—Mn—Ga, Ni—Fe—Ga, and Co—Ni—Al. The Ni—Co—Ti system is of significant interest for the development of various technological materials, such as permanent magnets, shape memory alloys, and high-entropy alloys.

Theoretical investigations of the structural and magnetic properties of the Ni—Co—Ti Heusler alloy family were carried out using the VASP software package [1; 2] within the framework of the PBE exchange-correlation functional approximation [3]. The crystal structure of the regular $L2_1$ and inverse XA lattices was defined using 16-atom cubic and tetragonal cells of space group symmetry No. 225 (Cu_2MnAl prototype) and No. 216 (Hg_2TiCu prototype), respectively. Geometric optimization of the structures was performed via ionic relaxation, allowing changes in atomic positions, cell shape, and volume.

In this theoretical study, a comprehensive analysis of the structural and magnetic properties of the ternary Ni-Co-Ti system was performed for the cubic ($L2_1$, XA) and tetragonal ($L1_0$, XA_t) phases. First-principles calculations revealed key regularities governing the stability and functional characteristics of alloys in this system. The main result of this work is the establishment of a thermodynamic preference for martensitic phases for most compositions within the system.

The work was supported by the Young Scientists Support Fund of Chelyabinsk State University.

[1] G. Kresse, J. Furthmüller, *Phys. Rev. B.* 54, 11169 (1996).

[2] G. Kresse, D. Joubert, *Phys. Rev. B.* 59, 1758 (1999).

[3] J. P. Perdew, K. Burke, M. Ernzerhof, *Phys. Rev. Lett*. 77, 3865 (1996).

Stability of Magnetic Skyrmions in Nanomodified Films to the Influence of External Magnetic Fields

M. A. Filippov[1, a], R. M. Vakhitov[1], A. A. Khakimullina[1], A. A. Akhmetova[1]

[1]Ufa University of Science and Technology, Ufa, Russia
[a]e-mail: *mikhail.filippov.99@mail.ru*

Magnetic skyrmions are topologically stable vortex-like inhomogeneities. Due to their unique physical properties, they have attracted the attention of researchers in recent years and hold potential for use in next-generation spintronic devices. The Dzyaloshinskii — Moriya interaction (DMI) is the primary contributor to the stabilization of magnetic skyrmions in various materials, but maintaining a delicate balance of material parameters characterizing other interactions in magnetic materials is also essential. This process can be simplified by using nanomodified films with locally modified parameters. For example, films with a "potential well" type defect [1] can be used, in the region of which the magnetic anisotropy abruptly decreases.

To use magnetic skyrmions in spintronic devices, some methods of their control are required, therefore, in this study, the effect of an external magnetic field on their structure was considered. The study was carried out by the method of micromagnetic modeling in the OOMMF software package [2]. Initially, stable states of magnetic skyrmions were obtained in a thin film in the form of a disk with a radius $R = 150$, in the center of which there was a defect of radius $R_0 = 30$ nm. In the defect region, the magnetic anisotropy constant takes the value K_{u2}, and in the rest of the disk K_u, where $K_{u2} < K_{u1}$. The material parameters of the film correspond to multilayer films of the Co/Pt type. Then, the effect on the obtained stable states of a perpendicular magnetic field co-directed with the orientation of the skyrmion core magnetization was considered. For a given field direction, the skyrmion magnetization reversal occurs according to the following scenario: its core begins to expand with increasing field strength until it occupies the entire disk [3]. This mechanism is realized in the absence of a defect when $K_{u2} = K_{u1} = 0.3 \cdot 10^6$ J/m^3 (for small DMI $D = 1 \cdot 10^{-3}$ J/m^2). The skyrmion size in the absence of a field (Fig. 1 a) was $R_{sk0} = 19$ nm; at the

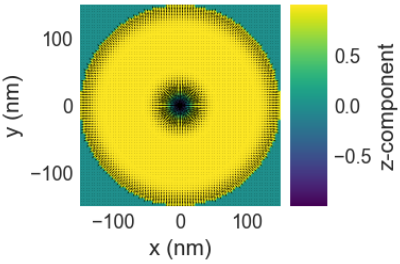


Fig. 1a

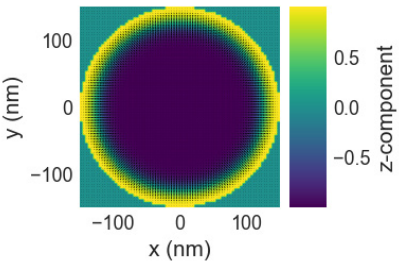


Fig. 1b

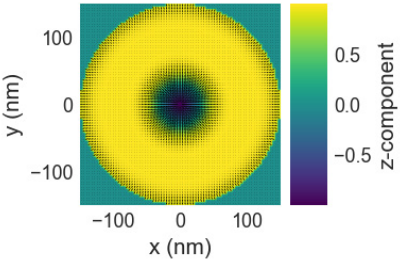


Fig. 1c

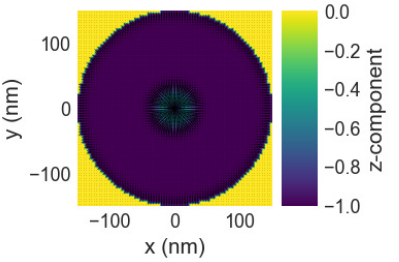


Fig. 1d

critical field value before the skyrmion annihilation $H_{cr} = 34$ mT, its size increased to $R_{sk} = 135$ nm, that is, it occupies almost the entire disk (Fig. 1b). In the presence of a defect ($K_{u1} = 0.3 \cdot 10^6$ J/m^3, $K_{u2} = 0$), the initial skyrmion size is $R_{sk0} = 37$ nm. At $H_{cr} = 115$, the skyrmion has a size of $R_{sk} = 44$ nm (Fig. 1c). With a further increase in the external field, the skyrmion transforms into a non-topological soliton (Fig. 1d), and then the disk undergoes a complete magnetization reversal in the direction of the field.

Based on the above, we can conclude that stabilizing skyrmions at a defect allows for the production of skyrmions of a specific size ($R_{sk0} \approx R_0$), while increasing their resistance to external magnetic fields. Furthermore, the film magnetization reversal process undergoes changes, preventing the skyrmion from expanding across the entire disk due to the limitations of the defect, and also switching to a different type of magnetic vortex-like inhomogeneity.

The authors are grateful for the financial support of the State assignment of Russian Federation for the implementation of scientific research by laboratories (№ 075-03-2024-123/1 15.02.2024).

[1] R. M. Vakhitov, et al, *Lett. on Mater*., **15(4)**, 344–349 (2025).

[2] M. J. Donahue, D. G. Porter, *OOMMF User's Guide, Version 1.0 Interagency Report.*, National Institute of Standards and Technology, Gaithersburg, MD. 1999.

[3] T. B. Winkler, et al, *Phys. Rev. Appl*., **16(4)**, 044014 (2021).

Influence of Thermo-mechanical Treatment on the Microstructure, Magnetic and Magnetocaloric Properties of $Ni_{50}Mn_{18.5}Ga_{25}Cu_{6.5}$ Alloy

R. Yu. Gaifullin[1, a], M. I. Nagimov[1], V. I. Mitsiuk[2], A. M. Aliev[3], A. A. Mukhuchev[3], A. T. Kadyrbardiev[3], I. I. Musabirov[1]

[1] Institute for Metals Superplasticity Problems of RAS, Ufa, Russia

[2] Scientific-Practical Materials Research Centre, NAS of Belarus, Minsk, Belarus

[3] Amirkhanov Institute of Physics, DFRC of RAS, Makhachkala, Russia

[a]e-mail: *gaifullin_1998@bk.ru*

The relevance of studying Ni-Mn-based Heusler alloys is due to the presence of unique functional effects, such as the magnetocaloric effect (MCE) and magnetically induced deformations observed at room temperatures, where martensitic transformation occurs. The magnetocaloric effect is of growing interest due to its potential application in the development of highly efficient and environmentally friendly room-temperature magnetic refrigeration technology. The main obstacle to the practical implementation of such systems is the low fatigue strength of Heusler alloys. One method for improving the mechanical properties of the material is thermo-mechanical treatment (TMT). However, in the case of Heusler alloys, it is important to consider that the treatment can significantly reduce the magnitude of the functional effects. Therefore, the alloy structure after TMT must not only have increased strength but also ensure a sufficient functional effect.

This paper presents the results of a study of the influence of TMT on the microstructure, magnetic properties, and magnetocaloric effect

in the $Ni_{50}Mn_{18.5}Ga_{25}Cu_{6.5}$ alloy. The alloy was subjected to multi-axial isothermal forging (MIF) using two different methods:

1) 7 upsetting stages at 700 °C. The total true strain was $e \approx 2.59$.

2) 4 upsetting stages at 700 °C, followed by 3 more upsetting stages at 600 °C. The total true strain was $e \approx 2.41$.

As a result of the TMT by the MIF method, the initial alloy microstructure, characterized by large equiaxed grains ≈300 μm in size, is transformed into a bimodal "necklace" microstructure, in which large grains 200–300 μm in size are surrounded by a fine-grained interlayer with grain sizes of approximately 10–20 μm. A comparative microstructural analysis of the alloy after MIF using these two different methods revealed a similar structure. The only difference is in the proportion of fine-grained structure. In an alloy specimen deformed at 700 °C with a subsequent decrease in the deformation temperature to 600 °C in the final stages of upsetting, the proportion of fine-grained structure is higher.

A combined analysis of the temperature dependence of magnetization and differential scanning calorimetry data allows us to conclude that a magnetostructural phase transformation occurs in the alloy in all structural states.

Analysis of the magnetocaloric effect data shows that for the alloy in its initial state during the direct martensitic transformation, in a magnetic field of 1.8 T, the peak adiabatic temperature change is $\Delta T_{ad} = 1.2$ K, while for the alloy sample after MIF at 700 °C, $\Delta T_{ad} = 1.37$ K. For the alloy sample deformed according to the second scheme, $\Delta T_{ad} = 0.95$ K.

The present work was accomplished according to the state assignment of IMSP RAS.

Dynamics of the Magnetocaloric Effect in $DyCo_2$ and $Dy_{0.25}Tb_{0.25}Ho_{0.25}Er_{0.25}Co_2$ Alloys: Frequency and Cyclic Stability

A. G. Gamzatov[1, a], N. Z. Abdulkadirova[1], A. M. Aliev[1], Jing Wang[2], Fengxia Hu[2]

Amirkhanov Institute of Physics of DFRC of RAS, Makhachkala 367003, Russia
Beijing National Laboratory for Condensed Matter Physics, Institute of Physics, Chinese Academy of Sciences, Beijing 100190, PR China
[a]e-mail: *gamzatov_adler@mail.ru*

In recent years, research into the effect of cyclic magnetic field frequency on the magnitude and stability of magnetocaloric effects under long-term exposure to cyclic magnetic fields has become increasingly important. As a rule, these studies are carried out under conditions as close as possible to the operating characteristics of magnetocortic cooling devices (operating frequencies of 0.1–20 Hz). Consequently, these data allow us to make recommendations on the long-term applicability of magnetocaloric materials in magnetic refrigeration technology.

This paper presents the results of direct measurements of the adibatic temperature change (ΔT_{ad}) in $DyCo_2$ and $Dy_{0.25}Tb_{0.25}Ho_{0.25}Er_{0.25}Co_2$ alloys

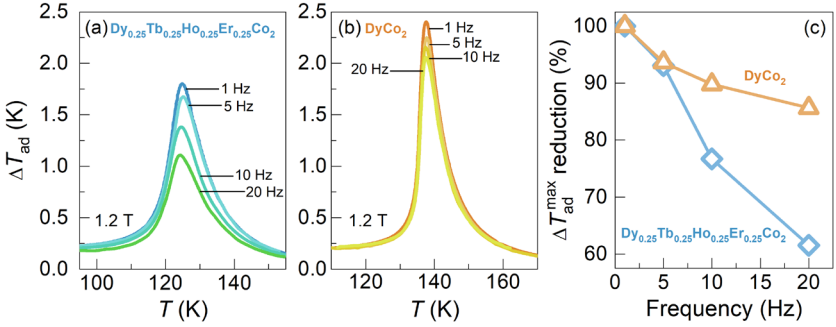


Fig. 1. a) Dependence $\Delta T_{ad}(T)$ for $Dy_{0.25}Tb_{0.25}Ho_{0.25}Er_{0.25}Co_2$ in a field of 1.2 T for different frequencies, b) Dependence $\Delta T_{ad}(T)$ for $DyCo_2$, c) Dependence $\Delta T_{max}(f)$ for both samples (figure is taken from the [1])

in cyclic magnetic fields (1.2, 1.8 and 8 T). As we can see from Fig. 1, the $Dy_{0.25}Tb_{0.25}Ho_{0.25}Er_{0.25}Co_2$ sample demonstrates a stronger frequency dependence of ΔT_{ad} than the $DyCo_2$ alloy. The paper discusses possible mechanisms for such a difference in the frequency dependences of ΔT_{ad}.

The study was supported by the Russian Science Foundation, grant № 24-43-00156 (https://rscf.ru/en/project/24-43-00156/).

[1] Zhengying Tian, et.al., *Acta Materialia*. 299 12147 (2025)

The Effect of Hydrostatic Pressure on the Magnetic and Structural Properties of the $Ni_{1.5}Co_{0.5}Mn_{1.375}Ti_{0.625}$ Alloy

R. R. Garipov[1, a], V. V. Sokolovskiy[1], M. V. Matunina[1]

[1]Chelyabinsk State University, Chelyabinsk, Russia
[a]e-mail: *ravil.garipov2209@gmail.com*

Shape memory Heusler alloys are promising caloric materials. However, traditional Heusler alloys such as Ni—Mn—X (where X is an *sp*-element) are quite brittle due to *p-d* covalent hybridization, which causes material degradation during cyclic phase transitions. Alloys consisting solely of *d* metals address this issue. Among the most popular are NiCoMnTi-based alloys. These Heusler alloys exhibit excellent ductility and significant mechanical strength due to *all-d* bonding. Furthermore, these alloys exhibit high magnetocaloric effect values. The magnetocaloric effect (MCE) is a phenomenon associated with the heating or cooling of a magnetic material when the external magnetic field strength changes [1]. This makes NiCoMnTi-based alloys excellent materials for use in magnetic refrigeration technology.

The aim of this work is to theoretically investigate the structural, magnetic and magnetocaloric properties of the $Ni_{1.5}Co_{0.5}Mn_{1.375}Ti_{0.625}$ alloy under hydrostatic pressure of up to 12 kbar. The calculations were performed within the density functional theory (DFT) using the Vienna

Ab-initio Simulation Package (VASP) [2; 3] and spin-polarized relativistic Korringa-Kohn-Rostoker (SPR — KKR) [4] software packages. Electron — ion interactions were modeled by the projector — augmented wave (PAW) [3] method, while the exchange-correlation effects were treated within the generalized gradient approximation (GGA) in the formulation of Perdew, Burke and Ernzerhof (PBE) [5]. In the VASP software package, the procedure of geometric optimization of cubic austenite and tetragonal martensite phases with ferromagnetic (FM) and ferrimagnetic (FiM) ordering was carried out at different pressures of 3, 6, 9 and 12 kbar. The $Ni_{1.5}Co_{0.5}Mn_{1.375}Ti_{0.625}$ alloy was analyzed in a 32-atom supercell obtained by translating four atoms of the primitive cell in the 2×2×2 direction. The $L2_1$ and $L1_0$ structures were studied. For each structure, the equilibrium lattice parameters, tetragonal distortion ratio, formation energy, magnetic moment, total electron density of states (DOS), and the contribution of each element to the DOS were calculated. The DOS was obtained using two methods: the PAW method implemented in VASP and by solving the Green's function equation using the KKR method. In the next step, the results of the two methods were compared and the dependence on hydrostatic compression up to 12 kbar was investigated.

The figure below shows, as an example, the graphs of the DOS, reflecting the total DOS and the contribution of each atom to it in the absence of hydrostatic pressure, obtained by the SPR — KKR method. These data were calculated for the volume-only relaxation mode for the $L2_1$ and $L1_0$ structures. As a result, it was revealed that the main

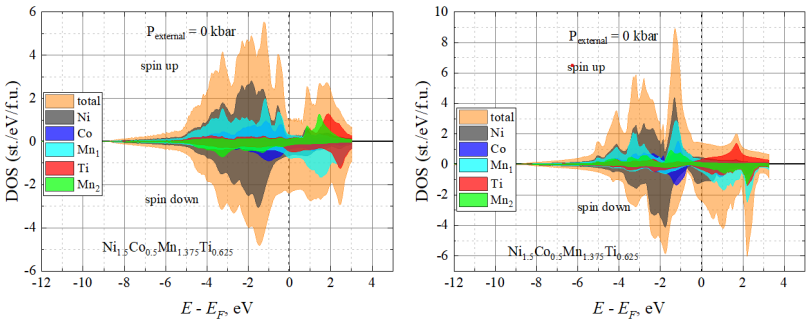


Fig. 1. DOS of $Ni_{1.5}Co_{0.5}Mn_{1.375}Ti_{0.625}$ alloy in the absence of hydrostatic pressure for $L2_1$ and $L1_0$ structures. Mn atoms located at the regular Mn sublattice are labeled as Mn_1, Mn atoms occupying Ti sites denoted as Mn_2

contribution to the DOS in the cubic phase is made by Mn_1, Ti and Ni atoms. In the tetragonal phase, the highest DOS values are demonstrated by Mn_1, Ni and Co atoms. This work examines the effect of hydrostatic pressure on the structural, magnetic, and magnetocaloric properties of the $Ni_{1.5}Co_{0.5}Mn_{1.375}Ti_{0.625}$ alloy. As a result, the electronic structure and DOS near the Fermi level change only slightly. It is shown that both phases meet the criteria for mechanical stability: austenite exhibits increased ductility under compression, while martensite retains high rigidity.

The work was supported by Russian Science Foundation, Project № 25-12-20024, https://rscf.ru/project/25-12-20024/.

[1] V. Franco, J. S. Blázquez, J. J. Ipus, J.Y Law, L. M. Moreno Ramírez, A. Conde, *Progress in Materials Science.* 93, 112–232 (2018)

[2] G. Kresse, J. Furthmüller, *Physical Review B*. 54, 11169–11186 (1996)

[3] G. Kresse, D. Joubert, *Physical Review B*. 59, 1758–1775 (1999)

[4] H. Ebert, D. Koedderitzsch, J. Minar, *Reports on Progress in Physics*. 74, 096501 (2011)

[5] J. P. Perdew, K. Burke, M. Ernzerhof, *Phys. Rev. Lett*. 77, 3865–3868 (1996).

The Effect of Substitution of Mn by Pd on the Structure and Thermomagnetic Properties of the $Mn_{1-x}Pd_xCoGe$ Alloys (where x = 0.03, 0.05, 0.07 and 0.1)

K. Kutynia[1], A. Przybył[1], P. Gębara[1, a]

[1]Department of Physics, Częstochowa University of Technology, Armii Krajowej 19 Av., 42–200 Częstochowa, Poland
[a]e-mail: *piotr.gebara@gmail.com*

The aim of the present work is to study the influence of a partial substitution of Mn by Pd on structure, thermomagnetic properties and phase transitions in half-Heusler MnCoGe alloys. The XRD studies revealed a coexistence of the orthorhombic TiNiSi-type and hexagonal

Ni_2In-type phases. Deep analysis of the XRD pattern supported by the Rietveld analysis showed that the changes in lattice constants and content of recognized phases depended on the Pd addition. An increase of palladium in alloy composition at the expense of manganese induced a rise of the Curie temperature. The values of ΔS_M measured for the change of external magnetic field ~5T equaled 8.88, 23.99, 15.63 and 11.09 for $Mn_{0.97}Pd_{0.03}CoGe$, $Mn_{0.95}Pd_{0.05}CoGe$, $Mn_{0.93}Pd_{0.07}CoGe$ and $Mn_{0.9}Pd_{0.1}CoGe$ alloy, respectively. The highest magnetic entropy change ΔS_M was observed for sample with Pd content $x = 0.05$ induced by magnetostructural phase transition. The analysis of the n vs. T curves allowed to confirm XRD and DSC results of an occurrence of magnetostructural transition in $Mn_{0.95}Pd_{0.05}CoGe$ and $Mn_{0.93}Pd_{0.07}CoGe$ alloys samples.

Symmetry of Phase Transitions in Ni_2MnIn

A. V. Golovchan[1]

[1] Galkin Donetsk Institute for Physics and Engineering, Donetsk, Russia
e-mail: *golovchan12@yandex.ru*

Currently, significant interest is being shown in materials with a strong coupling between the crystal lattice and the magnetic subsystem, which leads to first-order magnetostructural phase transition. Among such materials, Heusler alloys of the Ni—Mn—In family [1] are of particular interest. In these alloys, the strong coupling between the magnetic and lattice subsystems leads to an enhancement of various effects in the phase transition region, such as giant magnetoresistance, the magnetocaloric effect, magnetically controlled shape memory effect, magnetostriction, and others.

A well-known theoretical model of phase transitions in Heusler alloys [2] is based on the consideration of a single channel of martensitic transformation: from a cubic to a tetragonal phase, which works well for the Ni—Mn—Ga system, but is not applicable to the Ni—Mn—In system. In this model, according to experimental data [3], during the martensitic

transformation, the cubic crystal structure ($L2_1$, space group $Fm\bar{3}m$) transforms into a monoclinic one (space group I2/m).

The work presents the results of a group-theoretical analysis of structural phase transitions in Ni_2MnIn corresponding to a star with a wave vector $\overrightarrow{k_{11}} = (0,0,0)$. The experimentally observed martensitic transformation corresponds to the irreducible representation (IR) Γ_5^+ (k11t7 in Kovalev's notation). The structural transformation is described by three order parameters: two-component $\vec{\eta} = (\eta_1, \eta_1, \eta_2)$ (IR Γ_5^+), one-component ψ (IR Γ_1^+) and $\vec{\phi} = (\phi, -1.732\phi)$ (IR Γ_3^+). $\vec{\eta}$ determines the displacements of Ni atoms $\left(\frac{1}{2} - \eta_1\sqrt{2}, 0, \frac{3}{4} - \eta_2\right)$ in the monoclinic phase and monoclinic deformations of the unit cell $\eta_1 = (\epsilon_{xy} + \epsilon_{xz})/\sqrt{2}$, $\eta_2 = \epsilon_{yz}$. One-component parameters $\psi = (\epsilon_{xx} + \epsilon_{yy} + \epsilon_{zz})/\sqrt{3}$ and $\phi = (2\epsilon_{yy} - \epsilon_{xx} - \epsilon_{zz})$ are responsible for the change in volume (ψ) and tetragonal distortion (ϕ) of the unit cell.

This work was supported by the RSF, project № 25-19-00587, https://rscf.ru/project/25-19-00587/.

[1] H.-L. Yan, X.-M. Huang, C. Esling, *Front. Mater*. 9, 812984 (2022).

[2] V. D. Buchelnikov, V. S. Romanov, A. T. Zayak. *J. Magn. Magn. Mater*. 191, 203–206 (1999)

[3] H. Yan, Y. Zhang, A. Senyshyn, H.-G. Brokmeier, C. Esling, X. Zhao, L. Zuo *Acta Mater*. 88, 375–388 (2015).

The Modeling of a Dynamic Magnetocaloric Effect in $(LaFe_{11.6}Si_{1.4})_{100-x}Cu_x$ (x = 0, 5, 10, 15) Alloy Doped by Cu

P. A. Igoshev[1,2,3, a], A. G. Vedernikova[3], A. G. Gamzatov[1, b]

[1] Institute of Physics named after H. I. Amirkhanov DFRC RAS, Makhachkala, Russia
[2] M. N. Mikheev Institute of Metal Physics UB RAS, Ekaterinburg, Russia
[3] Ural Federal University, Ekaterinburg, Russia
[a] e-mail: *igoshev_pa@imp.uran.ru*
[b] e-mail: *gamzatov_adler@mail.ru*

The study of first-order phase transitions in magnetic materials is of significant interest for the development of new functional devices, particularly magnetic refrigeration systems based on the magnetocaloric effect. A question of great practical importance is the stability of the magnetocaloric effect magnitude in an alternating magnetic field of low frequency.

Compounds of the La—Fe—Si family are itinerant-electron metamagnets [1; 2] that exhibit a significant magnetocaloric effect and strong magnetostriction, which offers promising prospects for their application as active magnetic regenerators, working bodies in magnetic refrigerators [3]. In this work, we investigated the effect of copper doping concentration on the field dependencies of magnetization as a function of the external magnetic field for $(LaFe_{11.6}Si_{1.4})_{100-x}Cu_x$ (x = 0, 5, 10, 15) system. It was experimentally established that the pure sample (x = 0) exhibits a classical first-order metamagnetic transition with a sharp magnetization jump (see Fig. 1, *a*). As the copper content increases to x = 5, the critical transition field shifts toward lower values, and the magnitude of the magnetization jump decreases (see Fig. 1, *b*). At copper concentrations of x = 10 and x = 15, the jump in the field dependence disappears entirely, indicating a crossover in the transition order from first to second. The description of these two types of transitions within a single model is of significant theoretical interest and is crucial for practical applications.

The experimental data for the M(H) field dependencies were analyzed using Landau theory. The free energy of the system was represented as an expansion in powers of magnetization:

$$F(M,H)=\frac{1}{2}AM^2+\frac{1}{4}BM^4+\frac{1}{6}CM^6-HM. \quad (1)$$

Based on the comparison between theory and experiment, the expansion coefficients A, B, and C [4] were determined. The calculation results are shown in Fig. 1. A good agreement with the experimental data is observed, which justifies the use of expression (1) for modeling the magnetocaloric effect in low-frequency alternating magnetic fields within the framework of the relaxation model.

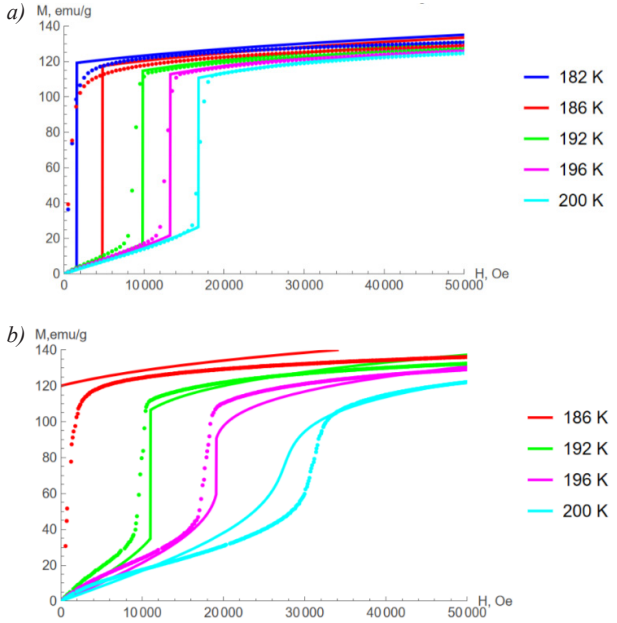


Fig. 1. Magnetization curves M(H) for x = 0 (a) and x = 5 (b) copper content at various temperatures near the metamagnetic transition temperature $T = T_c$. H varies in the range from 0 to $5 \cdot 10^4$ Oe. Points represent experimental data, solid lines represent the results of calculations based on the Landau functional (1) of the $(LaFe_{11.6}Si_{1.4})_{100-x}Cu_x$ alloy

The investigation of dynamic magnetocaloric effect in alternate magnetic field is measured and compared with the results of relaxation model $dM/dt = -\Gamma\partial F/\partial M$ with $F(M, H)$ given by Eq. (1).

The study was supported by the Russian Science Foundation, Grant № 24-43-00156 (https://rscf.ru/en/project/24–43–00156/).

[1] S. Fujieda, A. Fujita and K. Fukamichi. *Appl. Phys. Lett.* 81, 1276 (2002).

[2] A. Fujita, S. Fujieda, Y. Hasegawa and K. Fukamichi. *Phys. Rev. B.* 67, 104416 (2003).

[3] F. Long, Y. Song, J. Chen. *La (Fe, Si/Al) 13-based materials with exceptional magnetic functionalities: a review.* OAE Publishing Inc., 2024.

[4] P. A. Igoshev, A. G. Vedernikova and A. G. Gamzatov. *Phys. Met. Metallogr*. 126, 1087 (2025).

The Study of Ferrimagnetic Ordering and Magnetocaloric Effect in the Hubbard Model for a Simple Cubic and a Base-centered Cubic Lattices

P. A. Igoshev[1,2, a], A. N. Boyko[2]

[1] Institute of Physics named after H. I. Amirkhanov DFRC RAS, Makhachkala, Russia

[2] M.N. Mikheev Institute of Metal Physics UB RAS, Ekaterinburg, Russia

[a]e-mail: *igoshev_pa@imp.uran.ru*

The role of magnetic phase separation for the first-order transition in metals is a challenge up to now. It acquires a new sound in the context of magnetocaloric effect (MCE) description. It was found that phase separation effects result in giant kinks or changing of the sign of MCE value [1–4].

We consider the MCE for the Hubbard model on the simple cubic (SC) and base-centered (BCC) lattices within nearest neighbor hopping approximation taking into account the first-order phase transition-forced phase separation (PS) consistently[5; 6]. The Hubbard model Hamiltonian reads

$$H = -t\sum_{\langle ij\rangle\sigma} c^{\dagger}_{i\sigma}c_{j\sigma} - h\sum_{i\sigma}\gamma_{\sigma}c^{\dagger}_{i\sigma}c_{i\sigma} + U\sum_{i} c^{\dagger}_{i\uparrow}c_{i\uparrow}c^{\dagger}_{i\downarrow}c_{i\downarrow}, \qquad (1)$$

t is nearest-neighbor hopping integral, $\gamma_{\sigma} = \pm 1$, $h = 2\,\mu_B H$ is a magnetic field $c_{j\sigma} / c^{(\dagger)}_{i\sigma}$ — annihilation/creation Fermi operators at site $i(j)$ with spin projection σ, U is an on-site Coulomb interaction parameter.

To capture qualitatively these effects we treat the ferromagnetic (FM), antiferromagnetic (AFM) and ferrimagnetic (Fi) ordering within the Hartree — Fock approximation. Actual magnetic phase provides a minimum of thermodynamic grand potential at fixed chemical potential μ. Within this approach a magnetic phase transition manifests itself by a jump in phase parameters (electron filling n, ferromagnetic component of magnetization m_f and staggered component of magnetization m_a). Key role for an entropy change $\Delta S = S(h) - S(0)$, ($S(h)$ is an entropy in magnetic field h) plays the fact that there are two different temperature scales corresponding to the disappearance of PS at $h = 0$ and at finite h.

A phase diagram for $U = 5t$ is shown in Fig. 1. There is a narrow stripe of Fi phase and two wide PS regions away from it: PM—Fi and Fi—AF M. One can see that PS regions are very sensitive to the magnetic field applied: at $0.18t < T < 0.19t$ for PS Fi—AFM; at $0.17t < T < 0.20t$ for PS PM—Fi.

The calculation of $\Delta S(T)$ results for $n = 0.80$, $n = 0.81$ and $n = 0.82$ are shown in Fig. 2. The entropy jump is observed precisely at the phase separation boundaries and increases with increasing filling. This is due to the boundary between the phase separations of PM—Fi, PM—AFM and pure Fi. We found that the results for SC lattice are similar to that for the square lattice [1].

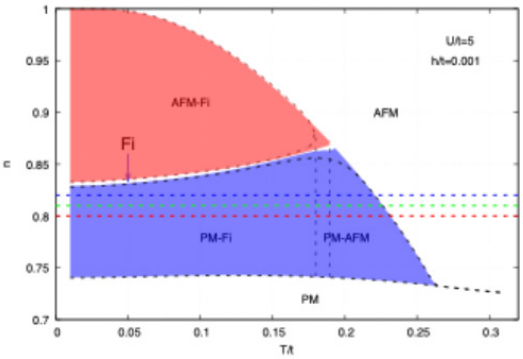


Fig. 1. Phase diagram for the Hubbard model (1) for the SC lattice at U/t = 5. The filled area corresponds to the PS at h = 0, the dashed lines restrict PS region at h = 0.001t. The vertical dashed lines represent the second-order phase transition separating. The horizontal lines, corresponding to n = 0.8, 0.81 and 0.82 marks filling values for which the $\Delta S(T)$ the calculation result is shown

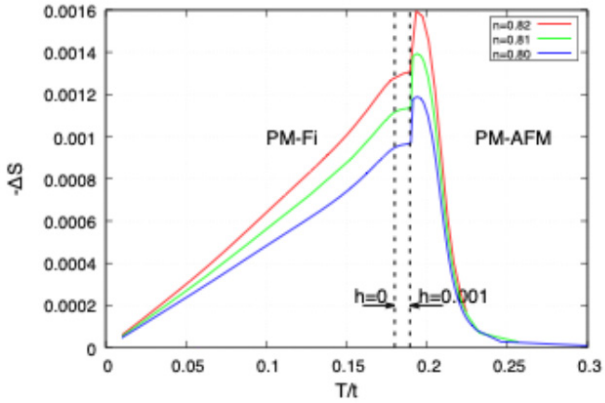


Fig. 2. $\Delta S(T)$ *for n = 0.80,0.81,0.82 (horizontal lines in Fig. 1). Here the vertical lines correspond to the boundaries between the PM—Fi and PM—AFM regions for h = 0 and h = 0.001*

The study was supported by the Russian Science Foundation, Grant № 24-43-00156 (https://rscf.ru/en/project/24-43-00156/).

[1] P. A. Igoshev, L. N. Gramateeva and A. V. Lukoyanov, *Phys. Chem. Chem. Phys*., 25, 6995 (2023)

[2] V. V. Ivchenko and P. A. Igoshev, *Phys. Rev. B*. 104, 024425 (2021).

[3] P. A Igoshev, I. A. Nekrasov, *Phys. Rev. B*. 110, 134406 (2024).

[4] P. A. Igoshev, *Phys. Met. Metallogr*. 124,1112 (2023).

[5] P. A. Igoshev, M. A. Timirgazin, A. A. Katanin, A. K. Arzhnikov, V. Yu. Irkhin, *Phys. Rev. B*. 81, 94407 (2010).

[6] P. A. Igoshev, M. A. Timirgazin, V. F. Gilmutdinov, A. K. Arzhnikov and V. Y. Irkhin, *J. Phys.: Condens. Matter.* 27, 446002 (2015).

Transformation of $k\varpi$-skyrmions on Columnar Defects of the "Potential Well" Type

R. M. Vakhitov[1], G. F. Ilyasova[1, a], M. A. Filippov[1], R. V. Solonetsky[1]

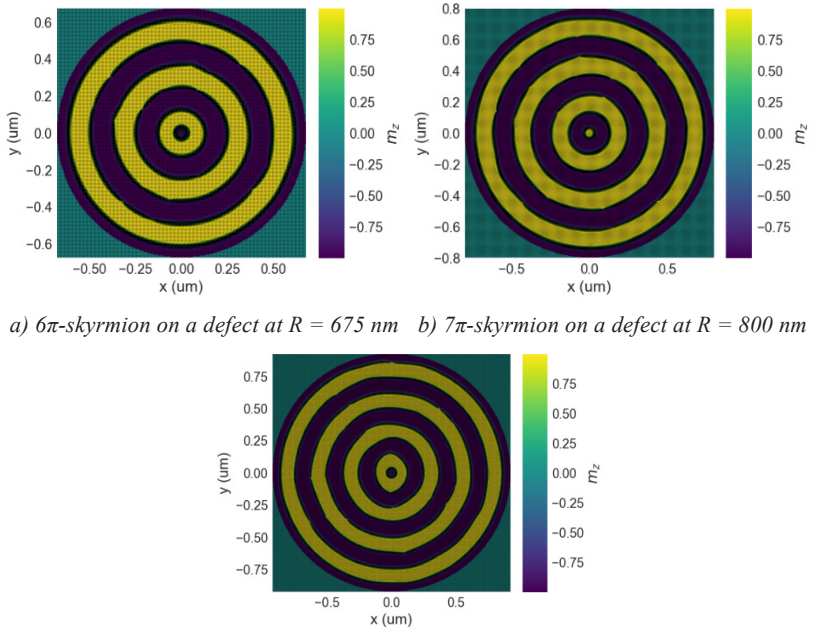
[1]Ufa University of Science and Technology, Ufa, Russia
[a]e-mail: *galiya.siraeva2014@yandex.ru*

Recently, the scope of research into magnetic skyrmions, their properties, the influence of various factors on them, the magnetic materials in which they are stabilized, etc., has increased significantly. This interest was prompted by their potential for use in the development of various spintronic devices.

In most studies, skyrmions are stabilized in chiral magnets due to the presence of the Dzyaloshinsky — Moriya interaction (DMI), but certain limitations to their stabilization in such magnets have been identified [1]. Therefore, interest has arisen in searching for non-chiral magnetic materials in which stable skyrmion states can arise in the absence of DMI. One of the most acceptable methods for obtaining stable skyrmions in them is the creation of modified magnetic films [2], in which, by irradiating their surface with a localized beam of He^+ ions, regions with altered values of the material parameters of the films are created, in particular, with a reduced value of the uniaxial anisotropy constant. As a result, such a sample forms a lattice of "potential well" defects, on which magnetic skyrmions are stabilized under certain conditions. In most studies, the term "magnetic skyrmion" is understood as a vortex-like inhomogeneity in which the unit magnetization vector $\mathbf{m} = \mathbf{m}(r)$ changes its direction by 180° when moving radially from the center ($r = 0$) to the periphery ($r = \infty$) of the film (π-skyrmion). In [3], it was theoretically predicted that in uniaxial ferromagnetic films with DMI, the existence of skyrmions with a more complex structure is possible, the so-called $k\pi$-skyrmions ($k \in 1, 2, 3\ldots$), in which the "twist" of the vector $\mathbf{m}$ occurs at an angle multiple of 180°. Such structures can be obtained both in chiral [4] and non-chiral [5] magnets.

In [5], stable states of 2π, 3π, and 4π-skyrmions were experimentally detected at room temperature (T = 300 K).

In the present work, the conditions for stabilizing kπ-skyrmions in a magnetouniaxial confined film in the form of a disk containing a columnar defect of the "potential well" type were examined. Based on the obtained results, it follows that the presence of such a defect — whose material parameter values can be reduced — has a positive effect on the stability of magnetic textures and leads to $k\pi$-skyrmions (k = 1, 2, 3, 4) becoming stable at smaller disk sizes. Furthermore, it was found that for large disk radius values (R>1 150 nm), the existence of kπ-skyrmions with k = 5, 6, 7, 8 is possible (Fig. 1), which, in the absence of defects in the disk, can emerge as stable structures — but only at larger disk dimensions. At the same time, it should be noted that such structures have not yet been obtained experimentally nor studied in detail theoretically.



a) 6π-skyrmion on a defect at R = 675 nm *b) 7π-skyrmion on a defect at R = 800 nm*

c) 8π-skyrmion on a defect at R = 925 nm

Fig. 1. Images of k π-skyrmions with different k stabilized in the presence of defect R_0 = 50 nm, Ku_2 = 0 J/m³ using Ubermag

The work was carried out within the framework of the state assignment of the Russian Federation for scientific research by laboratories (Theory, modeling and production of thin-film, nanostructured and hybrid structures (FRRR-2024-0001))

[1] R. Tomasello, K. Y. Guslienko et al., *Phys. Rev. B*. 97, 060402 (2018)

[2] M. V. Sapozhnikov, S. N. Vdovichev, O. L. Ermolaeva et al., *Appl. Phys. Lett*. 109, 042406 606 (2016)

[3] A. Bogdanov, A. Hubert. *J. Magn. Magn. Mater*. 195, 182 (1999)

[4] M. Beg, R. Carey, W. Wang et al., *Sci Rep*. 5, 17137 (2015)

[5] J. Jiang, Y. Wu, L. Kong, Y. Wang, J. Li, Y. Xiong, J. Tang, *Acta Mater*. 215, 117084 (2021)

Confined Crystallization of Patterned $MAPbBr_{3-x}Cl_x$ Microcrystals

J. Wang[1], P. Zhang[1], Y. Zhang[1], Y. Fang[1], O. Ivasenko[1, a]

[1]State Key Laboratory of Bioinspired Interfacial Materials Science, Institute of Functional Nano & Soft Materials (FUNSOM), Soochow University, Suzhou 215123, P. R. China

[a]e-mail: *ivasenko@suda.edu.cn*

Mixed-halide perovskite single crystals combine low defect densities with continuously tunable band gaps, making them promising materials for optoelectronic applications. However, controlled patterning of such compositionally tunable microcrystals remains largely unexplored. Here, we demonstrate template-assisted confined crystallization of periodic $MAPbBr_{3-x}Cl_x$ single-crystal microstructures on diverse substrates.

We show that spatial confinement and applied pressure govern mass transport and crystal growth, leading to distinct morphological regimes (Fig. 1): thick, continuous microcrystals at the periphery and isolated arrays in the central confined regions. Structural and elemental analyses (SEM, AFM, XRD, EDX) confirm high crystallinity and mixed-halide composition governed by precursor stoichiometry. Varying the Br/Cl ratio enables fine-tuning of the band gap (2.2–2.9 eV), thereby controlling

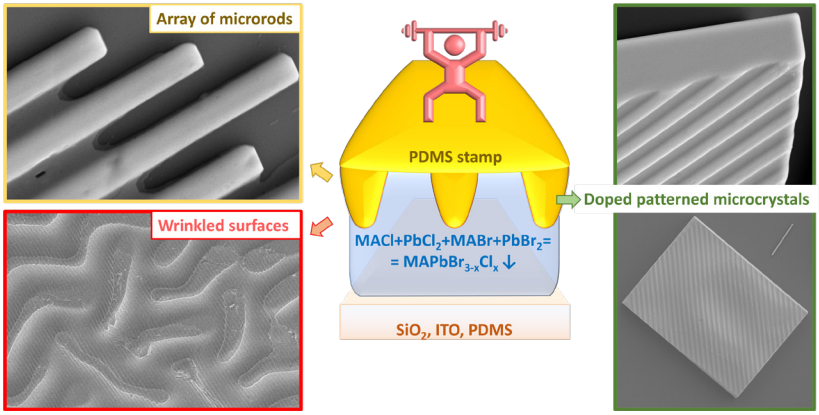


Fig. 1. Representative patterned microstructures of $MAPbBr_{3-x}Cl_x$

the optical absorption and photoluminescence. Furthermore, we identify several confinement-specific effects, including strain-induced wrinkling and spatial growth heterogeneity [1].

Our approach showcases a convenient protocol for initial screening and optimization of crystallization conditions in multicomponent systems and can be readily extended to other perovskite and non-perovskite systems. It provides insight into nucleation, growth, and doping processes under confinement, facilitating the rational design of bandgap-engineered patterned microstructures for advanced optoelectronic applications.

This research was funded by the National Natural Science Foundation of China (Grant № 22372110) and the Suzhou Key Laboratory of Surface and Interface Intelligent Matter (Grant No. SZS2022011).

[1] J. Wang, P. Zhang, Y. Zhang, Y. Fang and O. Ivasenko. Crystals, *in press* (2026).

To Possibility of Magnetic Field Quanta Using for Coherent Caloritronics

S. V. Gratowski[1], G. N. Izmaïlov[1, a], V. V. Koledov[1]

[1] Kotelnikov Institute of Radioengineering and Electronics of RAS, Moscow, Russia

[a]e-mail: *gizmailov@mail.ru*

Quantum mechanics in a magnetic field has the peculiarity that the integral of the momentum circulation along a closed loop is proportional to the integer number of magnetic field flux quanta $\Phi_0 = h/2e$. This has many practical implications. For example, a SQUID — a ring-shaped connection of superconductors separated by bridges called Josephson junctions (*JJs*) — can be adapted as a valve for Φ_0, quanta penetrating the superconducting ring. Since the flow of Cooper pairs through the depends on the phase difference of the wave functions $\Psi = |\Psi| e^{i\phi}$, they thereby form a macroscopic condensate state (the superconducting phase). Here $\phi = 2\pi\Phi/\Phi_0$. At T<0,5 Tc and $T < \Delta/k_B$, heat in a superconductor is transferred not by phonons or Cooper pairs, but by quasiparticles (single-electron excitations above the energy gap Δ). Their tunneling heat flux through the DP is proportional to J_Q, which depends on the phase ϕ ($J_Q \propto \cos(2\pi\Phi/\Phi_0)$), which ensures the interference of "thermal waves" (quasiparticle tunneling amplitudes). This opens the possibility of a counterintuitive entropy flow from the cold terminal to the hot one. As is well known, the second law of thermodynamics is not violated if it is formulated for the total entropy of a closed system, including all degrees of freedom (mechanical, quantum, phase). Local reverse heat transfer can be compensated by increasing the entropy in other subsystems or by external work. As shown in [1], in a thermal interferometer using a SQUID, the quantum coherence of the tunneling current is ensured by quasiparticles possessing phase coherence. Thus, by varying the external magnetic flux (Φ) penetrating the SQUID ring, we change the phase difference on the DP. The effective density of state and the tunneling probability of quasiparticles become phase-dependent. As a result, the wave functions of quasiparticles tunneling through the left and right arms of the SQUID

interfere. This is directly analogous to an optical interferometer, in which the phase difference of light waves modulates the light intensity at the detector. Here is the thermal conductivity $G_{th} = dJ_{th}/dT$ oscillates with a period Φ_0: $G_{th}(\Phi) = G_0\left[1 + V\cos\left(2\pi\Phi/\Phi_0\right)\right]$, by abruptly changing the interference of photons through quantum phase differences (0, π, 2π…). V — interference contrast. This leads to jumps in the entropy of the controlled phase, which leads to the conservation of $\Delta S_{full} \geq 0$. Ultimately, the SQUID operates as a thermal modulator. In other words, by changing the magnetic field in the superconductor, we can vary the amount of heat flowing from a hotter reservoir to a colder one. This is analogous to the operation of a field-effect transistor, where the magnetic field plays the role of the electric field strength (gate voltage). The conclusion [1] was experimentally confirmed in [2] and other works from 2012 to 2024. This feature is embodied in ultra-low-temperature caloritronics — a field of thermal processes where flows are controlled through coherent quantum effects, and not only through classical thermal conductivity. Design requirements for the creation of basic logic elements on lumped Josephson junctions, the architecture of a thermal diode, and a thermal transistor have been formulated. New devices, which effectively utilize changes in material conductivity, exhibit increased response speed (ns–μs) compared to the response speed of conventional thermal switches (μs–ms). It is proposed to use modern devices in nanocalorimeters, bolometers, and noise thermometry.

Another effect occurring in SQUIDs is the generation of terahertz radiation. This radiation is generated by coherent tunneling of Cooper pairs through a stack of intrinsic Josephson junctions in superconductors such as BSCCO and YBCO. The frequency is determined by the Josephson ratio $f = (2e/h)V \approx 483.6$ Ghz/mVB and its value lies in the range of GHz÷THz. The source is compact: (active element dimensions (mesa) ~ 400·80·1.5 μm^3, system size: tabletop cryostat (~0.01 m^3), operating temperature < 80 K. The generator has the advantage of narrow radiation directivity, output power < 0.61÷0.63 mW at 0.51 THz (synchronization 3 mesa), high coherence. Obviously, high-resolution spectroscopy, quantum metrology, communications are the field of activity of such a generator, cryogenic compatibility, facilitating integration into quantum systems [5; 6].

This work was carried out within the framework of by state assignment of Kotelnikov IRE RAS.

[1] F. Giazotto, M. J. *Martínez-Pérez, Nature* 492, 401–405 (2012).

[2] F. Giazotto, *Nature Phys.* 11, 527 (2015)

[3] A. Fornieri, C. Blanc, R. Bosisio, S. D'Ambrosio, F. Giazotto, *Nature Nanotechnol*. 11, 258 (2016).

[4] E. Strambini, S. D'Ambrosio, F. Vischi, F. S. Bergeret, Yu. V. Nazarov, F. Giazotto, *Nature Nanotechnology* 11, 1055–1059 (2016)

[5] E. A. Borodianskyi, V. M. Krasnov, *Nature Commun*. 8, 1742 (2017).

[6] S. V. Shitov, *Technical Physics*, 68, 11 (2023).

Oscillations of Magnetic Solitons in Multilayer Structures as a Basis for Creating a Spin-wave Generator

D. K. Kabanov[1, a], E. G. Ekomasov [1], I. F. Sharafullin [1]

[1] Ufa University of Science and Technology
[a]e-mail: *danya.kabanov.95@mail.ru*

Modern experimental capabilities in nanotechnology and magnetic measurements are stimulating in-depth studies of the dynamics of magnetic inhomogeneities, especially in multilayer magnetic structures, whose demand in various applications are steadily growing. Theoretical analysis of the one-dimensional dynamics of these inhomogeneities in ferromagnetic multilayers, which represent a periodic sequence of layers of different thicknesses and with different magnetic properties (in particular, anisotropy), reveals a connection with the problem of soliton interaction with impurities in the sine-Gordon equation (SGE) [1]. It was shown in [2] that the dynamics of domain walls in multilayer structures can lead to the generation of stable localized solitons that act as sources of spin waves.

In this work, we investigate the possibility of creating a spin-wave generator based both on domain wall pinning and on magnetic breath-

ers and solitons excited in a three-layer ferromagnetic structure. It is established that the layer parameters of the structure directly affect the characteristics of the generated spin waves, allowing control of their amplitude and frequency. Particular attention is paid to the application of the autoresonance method using a weak alternating magnetic field to achieve controlled generation of high-amplitude spin waves. The frequency of these waves is fixed and is determined both by the intrinsic properties of the magnetic breather and by the frequency of the applied field.

The work was carried out within the framework of a state assignment, agreement № 075-03-2024-123/1 dated February 15, 2024, topic № 324-21.

[1] M. A. Shamsutdinov, I. Yu. Lomakina, V. N. Nazarov, A. T. Kharisov, D. M. Shamsutdinov. *Ferro- and Antiferromagnetodynamics. Nonlinear Oscillations, Waves, and Solitons*. Nauka, Mosco, 456 (2009).

[2] E. G. Ekomasov, V. N. Nazarov, K. Yu. Samsonov, R. R. Murtazin. "Possibility of Controlling the Dynamics and Structure of a Magnetic Soliton in a Three-Layer Ferromagnetic Structure". *Technical Physics Letters*, 47(10), 15–18 (2021).

Reversibility of the Inverse Magnetocaloric Effect During Forward and Reverse Martensitic Transitions in Heusler Alloy $Ni_{36.5}Co_{13.5}Mn_{35}Ti_{15}$

A. T. Kadirbardeev[1,2, a], A. G. Gamzatov[1,2], A. M. Aliev[1], K. Qiao[3], H. Zhang[3]

[1]Amirkhanov Institute of Physics DFRC RAS, Makhachkala, Russia
[2]Chelyabinsk State University, 454001 Chelyabinsk, Russia
[3]University of Science and Technology Beijing, Beijing, China
[a]e-mail: *anvar.kadirbardeev@gmail.com*

"All-d-metal" Heusler alloys have recently shown giant magnetocaloric effect (MCE) values along with increased mechanical characteristics, especially alloys with the chemical formula NiCoMnTi, replacing p-d hybridization with d–d hybridization among transition metals increases their ductility, which in turn affects the martensitic transition (MT) and its behavior in a magnetic field.

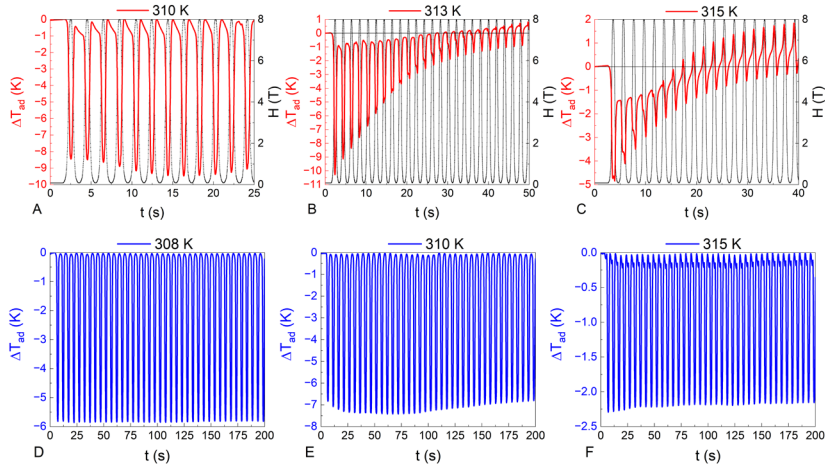


Fig. 1. A, B, C) Direct measurements of the time dependences of ΔT_{ad} (red line) in heating mode; D,E,F) ΔT_{ad} (blue line) in cooling mode in magnetic field of 8 T

In this work, direct measurements of the adiabatic temperature change ΔT_{ad} in a magnetic field of 8 T were carried out in two modes (Fig.1): 1) heating mode (reverse MT) from the martensitic phase; 2) cooling mode (forward MT) from the austenitic phase. From the data obtained, it can be concluded that in mode 1, the value of ΔT_{ad} is higher than in mode 2, but decreases with each new cycle of magnetic field application. This effect may be due to the fact that with reverse MT, the martensitic phase is unstable and quickly transforms into an austenitic one, which is not observed with forward MT.

This work was financially supported by Russian Science Foundation (№ 25-12-20024, https://rscf.ru/en/project/25-12-20024/)

Relation Between Magnetic and Magnetocaloric Properties Near the Phase Transition Point in the La—Fe(Mn, Co—Si) Alloy

Adler Gamzatov[1, a], Petr Igoshev[1,2], Nurizhat Abdulkadirova[1], Anvar Kadirbardeev[1]

[1]Amirkhanov Institute of Physics, Dagestan Federal Research Center of the Russian Academy of Sciences, 367003, Makhachkala, Russia
[2]M.N. Mikheev Institute of Metal Physics of Ural Branch of Russian Academy of Sciences, 620180, Ekaterinburg, Russia
[a]e-mail: *gamzatov_adler@mail.ru*

The results of measurements of magnetization, longitudinal magnetostriction and entropy change in the $LaFe_{11.1}Mn_{0.1}Co_{0.7}Si_{1.1}$ alloy in magnetic fields up to 180 kOe are presented. A detailed correlation analysis of the studied parameters near the Curie temperature is carried out [1].

In contrast to standard Bean — Rodbell and Stoner — Edwards — Wohlfarth theories the temperature and magnetic field dependence of longitudinal magnetostriction cannot be reduced to the squared magnetization. Instead, we found biquadratic dependence of the magnetostriction on the magnetization value whose coefficients are temperature dependent. At the critical point the coefficient at squared magnetization vanishes which is a similar situation to MnSi. Such behavior can be qualitatively explained within a set of ideas of spin-fluctuation theories developed by Moriya and Takahashi stating forth power of magnetization dependence of magnetostriction at critical temperature, especially in weak magnetic fields.

Magnetocaloric effect and a magnetostriction exhibit strong temperature dependence near the critical temperature. The form the temperature dependence of these quantities is bell-shaped and similar. At the same time, in a close vicinity of critical temperature exhibit rigid correlation between ΔS_M and $\lambda_{||}$, $\Delta S_M = -\varkappa(T_C)\lambda_{||}$, $\varkappa = 9.52\,10^3$ J/kg K. The value of the corresponding coefficient can be taken from a simple theory of magnetostriction based on the Heisenberg model with an exchange integral depending on a lattice parameter. This relationship not only deepens our

understanding of magnetoelastic phenomena in the critical region, but also provides a valuable tool for the design and optimization of materials for magnetic refrigeration. The formal deviation of the coefficient $\varkappa(T)$ from the critical value $\varkappa(T_C)$ at a strong difference between the temperature and the critical one can have two sources: firstly, this is the method of estimating the change in entropy through the specific heat data, which makes some artifactual contribution to it far from T_C, and secondly, this is the different role of spin fluctuations at T_C and far from T_C.

The obtained results manifest the remarkable role of magnetoelastic interaction and spin fluctuations in the alloy $LaFe_{11.1}Mn_{0.1}Co_{0.7}Si_{1.1}$.

The study was supported by the Russian Science Foundation, grant № 24-43-00156 (https://rscf.ru/en/project/24-43-00156/).

[1] A. G. Gamzatov, et. al. *J. Magn. Magn. Mater*. 642, 173865 (2026).

Elastocaloric Effect in 3d-metals Ribbons Measured by Thermal Imager and Ultrafast Fiber-optical Temperature Sensor

A. P. Kamantsev [1, a], D. A. Karpukhin[1], E. V. Morozov[1], L. N. Butvina[2, b]

[1]Kotelnikov Institute of Radioengineering and Electronics of RAS, Moscow, Russia

[2]Prokhorov General Physics Institute of Russian Academy of Sciences, Dianov Fiber Optics Research Center, Moscow, Russia

[a]e-mail: *kaman4@gmail.com*

[b]e-mail: *lnbutvina@gmail.com*

The thermoelastic properties and the elastocaloric effect (ECE) were studied in melt spun ribbons (with sequent heat treatment) of the *3d*-metals based alloys in polycrystalline states under periodic mechanical stress with frequency up to 50 Hz. The polycrystalline ribbons demonstrated the thermoelastic martensitic transition and the shape memory effect (SME). The studies were made on improved setup which the firstly

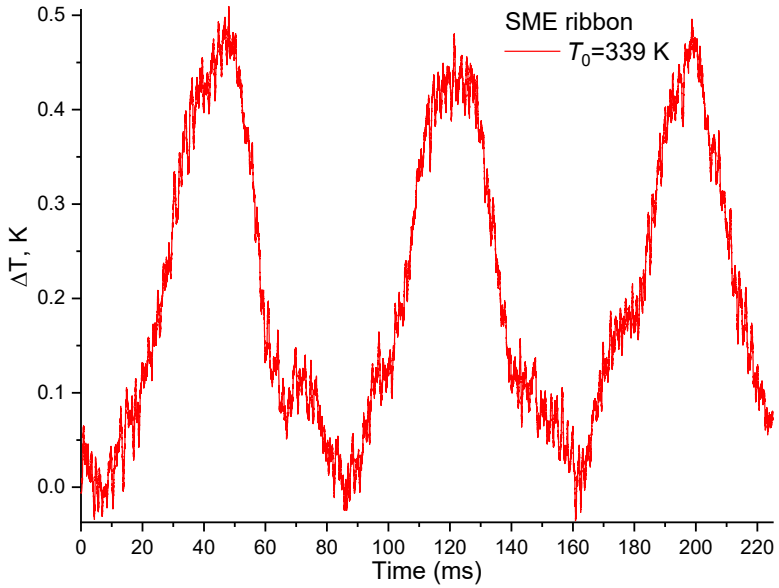


Fig. 1. The ECE in Ti_2NiCu ribbon under periodic mechanical stress with relative deformation ε = 1.28% at T_0 = 339 K

described in [1]. We used two temperature measurement principles. The first principle is using the thermal imager *Pergam Spectr 640 UC* with frame rate of 100 Hz. The second principle is using the ultrafast fiber-optical temperature sensor (FOTS) described in details in [2]. The ECE measured by FOTS in the polycrystalline Ti_2NiCu ribbons at initial temperature T_0 = 339 K was ΔT = 0.5 K under relative deformation ε = 1.28% (Fig. 1). It is shown that the ECE value does not depend on the frequency of external action in the range from 0 to 50 Hz.

The study was supported by a grant from the Russian Science Foundation № 25-19-00942, https://rscf.ru/project/25-19-00942/

[1] Morozov E., Kuznetsov D., Kalashnikov V., et al. *Crystals*, 11(8), 949 (2021).

[2] Kamantsev A. P., Amirov A. A., Yusupov D. M., et al. *Phys. Metal. Metallogr.* 124(11), 1075–1091 (2023).

Machine Learning and Neural Networks Methods for Magnetocaloric Materials

O. I. Urzhumtsev[1, a], D. A. Kanurin[1, b], A. A. Amirov[2, c]

[1]Physics faculty, Lomonosov Moscow State University, Moscow, 119991, Russia
[2]Amirkhanov Institute of Physics of Dagestan Federal Research Center, Russian Academy of Sciences Makhachkala, 367015, Russia
[a]e-mail: *urjumtsev@amtc.org*
[b]e-mail: *kanurin.da18@physics.msu.ru*
[c]e-mail: *amiroff_a@mail.ru*

Machine learning (ML) has recently emerged as one of the key tools for the accelerated discovery of magnetocaloric materials. Its primary value lies not only in predicting the magnitude of the magnetocaloric response based on composition and descriptors, but also in enabling rapid ranking of candidate materials for subsequent experimental validation. It has already been demonstrated that ML approaches can lead to the actual discovery of promising compounds: in the work by de Castro *et al.*, machine learning was employed to screen materials, resulting in the experimental identification of a strong magnetocaloric effect in HoB_2 [1].

In another study focused on predicting magnetic entropy change from chemical descriptors, a large dataset covering several classes of magnetocaloric materials was compiled, and the Random Forest model outperformed a number of alternative methods, including neural networks. These findings indicate that, for magnetocaloric applications, the critical factor is not the choice of a "trendy" model architecture per se, but rather the proper alignment between the model, feature set, and data structure [2].

For magnetocaloric systems, it is crucial that model training is performed on properly curated and physically consistent data. Therefore, when constructing a dataset, it is essential to rely on data from validated research groups, preserve experimental metadata, and clearly distinguish the intrinsic physical effects from measurement artifacts. In this context, the quality of the underlying dataset is not a secondary factor, but rather a central component of the ML approach in magnetocaloric research.

The report considers a broad range of approaches — from classical regression algorithms to neural networks — in the context of two practical tasks: prediction of magnetocaloric properties and screening of new candidates for experimental validation. Particular attention is paid not only to model accuracy, but also to uncertainty quantification, as it determines how reliably ML can be used to guide subsequent synthesis and measurement efforts. Recent studies demonstrate that high average accuracy does not necessarily guarantee model reliability when applied to new classes of materials. Therefore, in materials science applications, robustness, proper uncertainty calibration, and rigorous validation on independent datasets are of particular importance [3].

The research was supported by the Russian Science Foundation (project № 25-43-20052).

[1] P. B. d. Castro, K. Terashima, T. D. Yamamoto *et al. NPG Asia Mater* 12,35(2020).

[2] H. Ucar, D. Paudyal, K. Choudhary. *Computational Materials Science*, 209, 111414, 0927–0256(2022).

[3] D. Varivoda et al. *Appl. Phys. Revs*. 10, 2. (2023).

Multistimulus Magnetic Refrigeration: from Materials to Cooling Cycles

D. Yu. Karpenkov[1,2], R. A. Makarin[2], A. Yu. Karpenkov[1, a], M. V. Zheleznyi[1,2]

[1]National University of Science and Technology MISIS, Moscow, Russia
[2]Lomonosov Moscow State University, Moscow, Russia
[a]e-mail: *karpenkov_d_y@mail.ru*

Multi-stimulus cooling cycles — simultaneous application of magnetic field, temperature, and mechanical stress — offer significant advantages over conventional magnetic refrigeration: pressure tunes the Curie temperature (~10 MPa/K), reducing the required permanent magnet volume; a 40 K operating range becomes feasible with 400 MPa; and hysteresis

losses can be actively managed. This work establishes scientific foundations for next-generation refrigerators using these cycles.

Optimal heat exchanger geometry. Numerical simulations (1–10 Hz) compared plate and rod regenerator fillers. Optimal plate thickness: 180 μm at 10 Hz to 600 μm at 1 Hz (porosity 10% → 2–3%). Optimal rod diameter: 100 μm at 10 Hz to 400 μm at 1 Hz (porosity 25% → 14%). Plate geometry yields 10–20% higher specific cooling power.

Adaptation of La(Fe, Si)$_{13}$ compounds. Cast $La_{1.12}Fe_xSi_{1.4}$ (x = 11.6–14.6) with 12% excess La were hydrogenated in two modes. Increasing Fe from x = 11.6 to 14.6 raises reinforcing BCC Fe—Si phase from 6 to 23 vol%, boosting yield strength from 830 to 1353 MPa. Hydrogenation degrades strength, but mode 2 (vacuum heating, slow H_2 infusion) gives twice the strength of mode 1. Optimal composition: $LaFe_{11.55}Si_{1.45}$ + 18.7 vol% Fe-Si hydrogenated via mode 2 achieves yield strength >400 MPa (sufficient for 40 K T_C shift) while retaining ΔT_{ad} = 2.75 K at 1.85 T. The Fe—Si phase arrests crack propagation when >15 vol%.

Phenomenological model. An analytical equation of state describes first-order ferromagnetic transitions under magnetic field (h), temperature (t), and pressure (p). Pressure increases shift the critical region to lower temperatures and increase thermal hysteresis; magnetic field shifts it to higher temperatures and reduces hysteresis. This enables control of phase transition parameters.

Mastering of hysteresis. It has been experimentally established that the width of the field hysteresis in first-order phase transition magnetocaloric materials exhibits a non-monotonic dependence on the magnetic field sweep rate. As the magnetization rate increases, the hysteresis width initially grows, reaches a maximum, and then decreases. This behavior is attributed to the temperature change of the sample during magnetization and demagnetization. At high field sweep rates, adiabatic conditions are approached, and the sample heats up or cools down by the magnitude of the direct or inverse magnetocaloric effect. This shifts the local temperature of the sample relative to the nominal isothermal measurement temperature, thereby distorting the shape of the hysteresis loop and altering its width.

Simulations that include adiabatic heating/cooling make it possible to predict the actual shape of the field-dependent magnetization curves and, most importantly, to determine the magnitude of external mechanical stress that must be applied to the sample to minimize both field and

temperature hysteresis. It is shown that an appropriately chosen pressure shifts the critical region of the phase transition, reducing hysteresis energy losses and improving the efficiency of the multi-stimulus cooling cycle.

Selective multi-stage cascade cycle with reservoirs. A novel cycle using a single working body with pressure-tunable T_C and buffer reservoirs achieved 15.6 K cooling (three reservoirs, T_C = 289.5, 284.3, 279.1 K) after 1543 cycles — far exceeding the single-stage MCE limit of 5.2 K. The selective cycle with one material and pressure tuning reached 15 K cooling after 7134 cycles.

These integrated results — optimal plate geometry, non-destructive hydrogenation, predictive modeling, hysteresis characterization, and the cascade cycle — provide a complete pathway to efficient multi-stimulus magnetic refrigerators.

This work was carried out within the framework of a state assignment and partially supported by the RSF, project № 25-22-00371.

Experimental Technique for Studying the Kinetics of the Heusler Alloy $Ni_{50.5}Mn_{33.4}In_{15.6}V_{0.5}$ During the Phase Transition Near the Curie point

D. A. Karpukhin[1, a], V. V. Koledov[1], I. I. Musabirov[2, b], A. M. Aliev[3, c], A. G. Gamzatov[3], N. Z. Abdulkadirova[3], S. V. Taskaev[4, d]

[1]Kotelnikov Institute of Radioengineering and Electronics of RAS, Moscow, Russia

[2] Institute of Problems of Superplasticity of Metals of the Russian Academy of Sciences, Ufa, Russia

[3]Amirkhanov Institute of Physics of the Russian Academy of Sciences, Makhachkala, Russia

[4] Chelyabinsk State University, Chelyabinsk, Russia

[a]e-mail: *interceptor1986@mail.ru*

[b]e-mail: *irekmusabirov@imsp.ru*

[c]e-mail: *lowtemp@mail.ru*

[d]e-mail: *s.v.taskaev@gmail.com*

The purpose of this work is to experimentally study the dependencies of thermodynamic parameters of temperature and magnetization in magnetic fields of the order of 1 T in the Geissler $Ni_{50.5}Mn_{33.4}In_{15.6}V_{0.5}$ alloy near related phase transitions “in situ”, that is, in dynamics, directly during the phase transition.

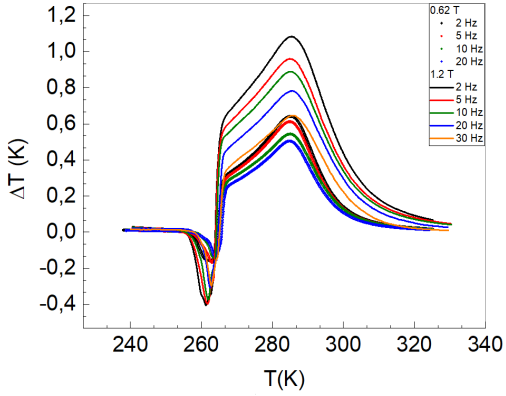


Fig. 1. Temperature dependencies of the magnetocaloric effect in $Ni_{50.5}Mn_{33.4}In_{15.6}V_{0.5}$ in field H= 0,62 and 1,2 T at frequencies f = 2…30 Hz

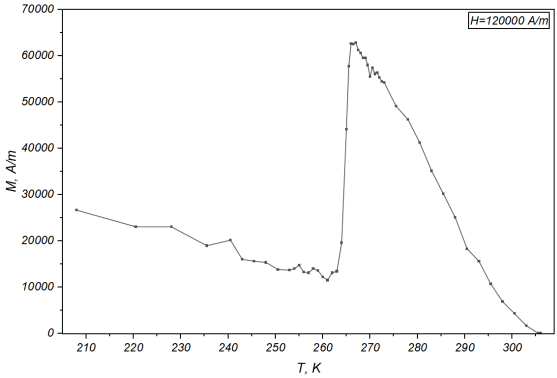


Fig. 2. Graph of the sample magnetization dependence on temperature at an applied external field of H=0.15 T in the alloy $Ni_{50.5}Mn_{33.4}In_{15.6}V_{0.5}$

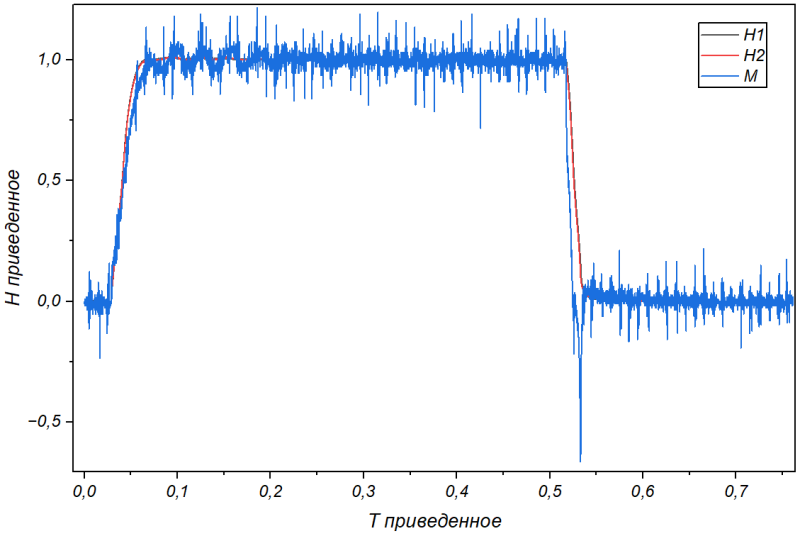


Fig. 3. The values of the applied fields without H1 and with the H2 sample, and its magnetization M in a 0.56 T field during a single 500 ms pulse

To study the kinetics of the MCE (Fig. 1), the technique described in [1] was used. The original experimental setup allows us to determine the Curie point from the magnetization graph of the $Ni_{50.5}Mn_{33.4}In_{15.6}V_{0.5}$ sample at a temperature of 291 K in a small field of H = 0.15 T on Fig. 2.

In fields of 0.56 T and higher, it is possible to see the applied field values without $H1$ and with the $H2$ sample and its magnetization M, as

shown in Fig. 3. Based on the graphs, it can be observed that the magnetization M lags behind the rate of increase of the *H*1 and *H*2 fields in a single 500 ms pulse.

The applied technique allows us to determine the Curie point in the $Ni_{50.5}Mn_{33.4}In_{15.6}V_{0.5}$ alloy and show the minimum limit for the maximum rate of phase transition.

The study was supported by a grant from the Russian Science Foundation № 25-19-00942, https://rscf.ru/project/25-19-00942/

[1] A. M. Aliev, et al., *J. Al. Com*.676, 601–605 (2016).

Microwave Response of VO_2 and $V_{0.98}W_{0.02}O_2$ Powder Materials in the 8–12 GHz Microwave Range in the Phase Transition Region

D. Y. Kazakov[1, a], I. V. Bychkov[1], D. A. Kuzmin[1], A. G. Fazlitdinova[1]

[1]Chelyabinsk State University, Chelyabinsk, Russia
[a]e-mail: *danielatk304@yandex.ru*

The current development of microwave electronics, radio photonics, and next-generation (6G) communication systems requires the creation of dynamically reconfigurable devices capable of adaptively controlling signal parameters in real time. One of the most promising materials for such applications is vanadium dioxide (VO_2), which exhibits a reversible semiconductor-to-metal phase transition at around 340 K. This transition is accompanied by a sharp jump in conductivity and a significant change in the complex permittivity over a wide frequency range, including microwaves. Despite the large number of studies devoted to VO_2 thin-film structures, experimental investigations of the electrodynamic characteristics of powdered vanadium dioxide in the microwave range remain fragmentary.

In this work, powders of pure vanadium dioxide (VO_2) and tungsten-doped vanadium dioxide ($V_{0.98}W_{0.02}O_2$) were studied. The particle size

in the first case was less than 100 nm, and in the second case less than 10 μm. The phase purity in both cases exceeded 99%. Moisture content and oxygen non-stoichiometry were not determined. Temperature dependences of the transmission, reflection, and absorption coefficients of microwave radiation in the 8–12 GHz range were investigated. Tungsten doping was chosen because it can lower the phase transition temperature to around room temperature [1]. For each sample, X-ray diffraction analysis was performed to monitor the phase composition; measurements were carried out in both heating and cooling modes, and hysteresis dependences were constructed. The presented results can be used for designing devices for microwave response control based on powder materials through doping and thermal exposure.

The structural properties of the samples were investigated using the traditional X-ray diffraction method with a D8 Advance diffractometer (Bruker) using Cu-Kα radiation at room temperature. The results of X-ray diffractometry of the samples are shown in Fig. 1.

The study of the samples' properties in the microwave frequency range was carried out using the waveguide method in a 10×23 mm waveguide with a setup based on the R2M-40 scalar network analyzer, shown in Figure 2. The thickness of all samples was 7.9 mm. The measurement results are presented in Fig. 3.

It was found that the phase transition temperature for the VO_2 powder was 60±0.5 °C, with a hysteresis width of ΔT = 8.5±0.5 °C; for $V_{0.98}W_{0.02}O_2$, the corresponding values were 19±0.5 °C and ΔT = 3.2±0.5 °C. The amplitude values of the coefficients at the phase transition are presented in Table 1.

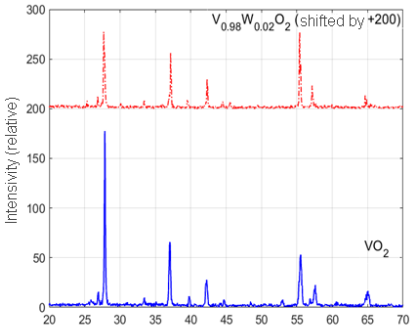


Fig. 1. Diffractometry of VO_2 u $V_{0.98}W_{0.02}O_2$ (shifted by +200)



Fig. 2. General view of the R2M-40 instrument

Table 1

Parameter	VO_2		Change	$V_{0.98}W_{0.02}O_2$		Change
	30 °C	80 °C		14 °C	30 °C	
T, %	57.1422	96.0670	+68.12%	54.90281	55.43879	+0.98%
R, %	1.9238	0.0006	–99.97%	1.855261	0.752041	–59.46%
A, %	40.9340	3.9324	–90.39%	43.74144	43.55694	–0.42%

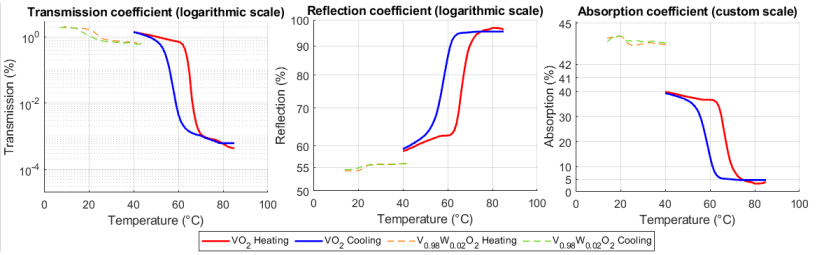


Fig. 3. Transmission, reflection, and absorption coefficients of VO_2 and $V_{0,98}W_{0,02}O_2$

[1] G. Pan, J.Yin, K. Ji et al. *Scientific Reports*. 7, 6132 (2017).

The Influence of Defects in Nanomodified Films on the Properties of Magnetic Skyrmions

A. A. Khakimullina[1, a], R. M. Vakhitov[1], M. A. Filippov[1]

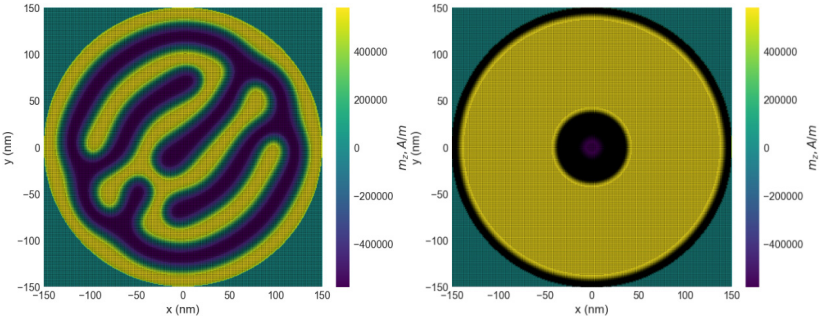
[1]Ufa University of Science and Technology, Ufa, Russia
[a]e-mail: *a_khakimullina@bk.ru*

In modern world, the rapid growth of data volumes, driven by the development of artificial intelligence, is stimulating the search for alternative methods of information processing and storage. One of the most promising areas in this field is the use of systems based on magnetic skyrmions — nanoscale vortex-like structures possessing a topological charge. They combine the following unique properties: topological protection, small size, controllability by low-density spin-polarized currents,

etc. Magnetic skyrmions are considered as the basis for non-volatile memory devices, logic, and neuromorphic computing [1].

The main obstacle to the practical implementation of spintronic devices based on skyrmions remains their stabilization in magnetic materials. The primary interaction responsible for the generation of skyrmions in magnetic materials is the Dzyaloshinskii — Moriya interaction (DMI), but at present there also exist alternative stabilization methods that mitigate the influence of DMI. These include the use of nanomodified films with "potential well" type defects, in the region of which the magnetic anisotropy decreases, ensuring the existence of skyrmions with weak DMI or even its absence [2–4].

The aim of this work is to investigate the two-factor influence of DMI and a "potential well" type defect on the stabilization of magnetic skyrmions. The study was carried out using micromagnetic modeling in the OOMMF software package [5]. A disk-shaped film with a radius $R = 150$ nm and a thickness $h = 1$ nm was considered as the calculation model. A columnar defect with a radius $R_0 = 30$ nm is located in the center of the disk, within which the perpendicular magnetic anisotropy K_{u2} is less than the magnetic anisotropy K_{u1} in the rest of the film, i. e., the condition $K_{u2} < K_{u1}$ is satisfied. The K_{u2} value varied between 0 and K_{u1}, allowing for the consideration of different defect depths. The modeling took into account the exchange interaction, DMI ($D = 4.0 \cdot 10^{-3}\ J / m^2$), magnetic anisotropy ($K_{u1} = 0.6 \cdot 10^6\ J / m^3, K_{u2} = \left(0 \div K_{u1}\right)$) and magnetostatic interaction. The material parameters of the model correspond to multilayer Co/Pt films. Initially, the film is uniformly magnetized.



a) $K_{u2} = 0.6 \cdot 10^6\ J / m^3$ b) $K_{u2} = 0.3 \cdot 10^6\ J / m^3$

Fig. 1. Magnetic structures on a disk at $K_{u1} = 0.6 \cdot 10^6\ J / m^3$ *: a) 2π-skyrmion with a labyrinth domain structure; b) π-skyrmion*

Modeling showed that in the absence of a defect, a deformed 2π-skyrmion with a labyrinth domain structure forms on the disk. However, when introducing a columnar defect, where the anisotropy value is halved ($K_{u2} = 0.3 \cdot 10^6 \ J/m^3$), the magnetic texture becomes axially symmetric and is simplified to a single π-skyrmion stabilized in the defect region (Fig. 1).

Thus, the introduction of a defect and variation of its parameters make it possible to control the formation of magnetic skyrmions of a specific type, allowing the stabilization of axially symmetric structures in specified regions of the film (in the defect region). This fact opens up new possibilities for the design of spintronic devices.

The work was carried out with financial support from the state assignment for scientific research conducted by laboratories (Design of New Materials (FRRR-2024-0001)).

[1] K. K. Mishra, et al., *Appl. Phys. Rev*. 12(1), 011315 (2025).

[2] M. V. Sapozhnikov et al., *J. Appl. Phys*. 109(4), 042406 (2016).

[3] R. M. Vakhitov, R. V. Solonetsky, A. A. Akhmetova, M. A. Filippov, *Symmetry.* 14(3), 612 (2022).

[4] R. M. Vakhitov, A. A. Akhmetova, M. A. Filippov, A. A. Khakimullina. *Letters on Materials*. 15(4), 344–349 (2025).

[5] M. J. Donahue, D. G. Porter National Institute of Standards and Technology, Gaithersburg, MD (1999).

Magnetocaloric Effect and Magnetostriction in Cyclic Magnetic Fields

L. N. Khanov[1, a], A. M. Aliev[1]

[1] Amirkhanov Institute of Physics of DFRC of RAS, Makhachkala, Russia
[a]e-mail: *hanov82@mail.ru*

The primary objective of research in solid-state cooling is the discovery and development of materials exhibiting a giant and stable magnetocaloric effect (MCE). These materials are intended to serve as working

substances in practical magnetic refrigeration devices. Such materials should not only exhibit a large adiabatic temperature change (ΔT_{ad}) or isothermal entropy change (ΔS) under moderate magnetic fields (1–2 T), but also retain their performance over extended periods during repeated exposure to cyclic magnetic fields. This long-term stability is critically important for the commercial viability of magnetic refrigeration systems.

In this context, compounds exhibiting first-order magnetostructural phase transitions are of particular interest, as the giant MCE in these materials arises from the coupled contributions of the magnetic and lattice subsystems. It is precisely in such systems that record-high ΔT_{ad} values are achieved; however, their practical application is limited by hysteresis-related irreversibility, functional degradation, and a strong dependence on magnetic and thermal history. Consequently, contemporary research focuses not only on identifying new systems with a large MCE, but also on the targeted optimization of their functional stability. To gain a comprehensive understanding of the MCE characteristics in these materials, simultaneous measurements of ΔT_{ad} and magnetostriction λ are essential. Such measurements enable the quantitative separation of the magnetic and lattice contributions to the overall MCE, which in turn allows for targeted optimization of magnetocaloric properties:

– if the dominant contribution stems from lattice entropy, performance can be enhanced by tuning the crystal structure and magnetoelastic interactions,

– if the magnetic contribution dominates, optimization can be achieved through chemical doping or modification of exchange interactions.

It is important to note that such measurements are most informative when conducted under cyclic (alternating) magnetic fields. This approach exhibits the reversible MCE by excluding irreversible processes associated with hysteresis and defect structures, which are inevitably present during a single field sweep near a magnetostructural phase transition.

Direct measurements of the ΔT_{ad} under cyclic magnetic fields were performed using a modulation method on an experimental setup developed in our laboratory [1]. Magnetostriction λ was measured using a strain-gauge technique [2].

A chromel-constantan differential thermocouple was used to measure the temperature response of the sample. One junction was attached to one side of a plane-parallel sample, while a strain gauge was mounted on the opposite side. Signals from both sensors were simultaneously recorded

using a DXA-205C two-channel Lock-in. Cyclic magnetic fields were generated using various systems capable of creating fields up to 8 T at frequencies up to 0.3 Hz.

The materials selected for investigation were polycrystalline Heusler alloys of the Ni—Mn—In family, which exhibit a magnetostructural phase transition (MSPT) and a giant MCE near room temperature. ΔT_{ad} and λ were measured for an alloy with the nominal composition $Ni_{43.18}Mn_{45.15}In_{11.67}$ across the MSPT temperature range under a cyclic magnetic field with an amplitude of 1.8 T. The $\lambda(T)$ and $\Delta T_{ad}(T)$ curves show a strong correlation, with their peaks coinciding, thereby indicating a strong coupling between the lattice and magnetic subsystems.

Simultaneous measurements of $\Delta T_{ad}(t)$ and $\lambda(t)$ were also performed at constant temperatures under continuous cyclic magnetic field application: at the temperature corresponding to the maximum MCE (286 K), as well as below (279 K) and above (289 K). Prior to each measurement, the sample was cooled from the high-temperature austenitic phase ($T > T_C$) to a temperature well below the martensitic transformation temperature, then heated to the desired temperature, after which the cyclic magnetic field was applied. Each measurement at a given temperature lasted one hour.

The results demonstrate that prolonged exposure to a cyclic magnetic field leads to a gradual decrease in both ΔT_{ad} and λ. This indicates the occurrence of processes causing cyclic degradation of the magnetocaloric and magnetostrictive properties, likely attributable to both hysteresis-related irreversibility within the thermal hysteresis loops and incomplete phase transformations during cyclic field application.

This study was funded by the Russian Science Foundation, grant № 24-12-00362, https://rscf.ru/en/project/24-12-00362/.

[1] A. M. Aliev, A. B. Batdalov, V. S. Kalitka. *JETP Letters* 90, 663 (2009).

[2] S. I. Novikova, *Thermal Expansion of Solids* (Nauka, Moscow, 1974) [in Russian].

Magnetization Dynamics in Various Magnetic Films

D-H. Kim[1, 2]

[1]Department of Physics, Chungbuk National University, Cheongju, South Korea
[2]Advanced-Basic-Convergence Research Institute, Chungbuk National University, Cheongju, South Korea

Magnetization dynamics over wide timescales will be introduced, including from an ultraslow thermally activated magnetization reversal via Barkhausen jumps to an ultrafast photoinduced magnetization dynamics involved with energy transfer among spin, electron, and lattice. Thermally activated magnetization reversal behavior in CoFeB multilayer films, together with microscopic magnetic domain observation, is investigated by means of magneto-optical Kerr effect microscopy. Temperature-dependent and strain-dependent magnetic behavior for Co/2D heterostructure will be also discussed based on magneto-Raman measurement result. Magnon observation in ferrimagnetic materials based on the magneto-Raman study will be also discussed. Lastly, ultrafast spin dynamics involved with THz emission behavior due to the matching timescale of sub-ps magnetoelectric interaction will be discussed for various magnetic multilayer films. Equilibrium and non-equilibrium energy transfer among sub-physical systems will be discussed.

Thermal Expansion and Microstructural Evolution of a Ni—Mn—Ga—Si Alloy Following Stepwise Annealing of the Deformed State

K. K. Kirilyuk[1, a], I. I. Musabirov[1]

[1]Institute for Metals Superplasticity Problems of the Russian Academy of Sciences, Ufa, Russia
[a]e-mail: *kirkonst2002@mail.ru*

Currently, Heusler alloys are considered promising materials. Their diverse properties, such as magnetocaloric and elastocaloric effects [1], make this group of alloys suitable for use in the development of various microactuators or magnetic cooling systems. However, their use is complicated by the material's high thermal cycling brittleness and, consequently, sample failure due to defect accumulation during multi-cycle phase transformations. In this work, we investigate the effect of reducing internal stresses in the alloy on thermal expansion in the martensitic transformation region.

An alloy ingot was obtained by arc melting in an argon atmosphere. To obtain an equiaxed structure, additional vacuum induction remelting was performed. The alloy was then subjected to strain-tempering treatment by multi-axial isothermal forging at 700 °C with a strain ratio of $e = 3.19$. A 9×1×1 mm³ specimen was prepared to study the microstructure and thermal expansion properties. Stepwise annealing of the specimen was performed at temperatures ranging from 400 to 800 °C in 100 °C increments. After each annealing, the microstructure and thermal expansion of the specimen in the martensitic transformation region were examined.

An examination of the microstructure of the sample in the as-forged condition revealed the presence of large martensitic grains measuring 100–300 μm, surrounded by a layer of fine grains approximately 5 μm in size. Stepwise annealing of the specimen does not result in a significant change in the microstructure. Complete recrystallization of the microstructure takes place after annealing at 800 °C. Results of the dilatation study in the martensitic transformation region show that the length of the specimen decreases abruptly by 0.43% during the direct transformation. As the annealing temperature of the sample increases, the magnitude

of the jump decreases and reaches 0.28% after annealing at 800 °C. Complete recrystallization of the microstructure should have led to the removal of internal stresses of deformation origin and should contribute only to the anharmonic shortening of the polycrystalline specimen's length during direct martensitic transformation. However, complete recrystallization of the microstructure should have led to the elimination of internal stresses of deformation origin and contributed only to an inharmonic shortening of the polycrystalline sample's length during the direct martensitic transformation. It is possible that stepwise annealing and subsequent thermal cycling through the martensitic transformation temperature fix residual dislocations, which serve as martensite nuclei. An experiment was prepared involving a single annealing of the sample directly at 800 °C and its effect on thermal expansion in the martensitic transformation region.

The present work was accomplished according to the state assignment of IMSP RAS.

[1] I. I. Musabirov, R. Yu. Gaifullin, K. K. Kirilyuk [et al.], *Chelyabinsk Phys. and Math. Journal*. **10**, 384–394 (2025).

Investigation of the Effect of Aerodynamic Drag on the Damping of Oscillations of an HTS Cryostat on a Magnetic Track

D. E. Kirillov[1, a], M. V. Matyunina[1], V. V. Koledov[1,2], O. O. Pavlukhina[1], M. A. Orshulevich[1], I. V. Maltsev[1], K. A. Kolesov[1,2], D. A. Karpukhin[1,2], D. A. Kuzmin[1]

[1]Chelyabinsk State University, Chelyabinsk, Russia
[2]Kotelnikov Institute of Radioengineering and Electronics of the Russian Academy of Sciences, Moscow, Russia
[a]e-mail: *den4862@yandex.ru*

In recent years, considerable attention has been devoted to the study of magnetic levitation based on high-temperature superconductors (HTS),

driven by the prospects of developing high-speed transportation systems with minimal energy losses [1; 2]. The use of HTS enables the elimination of mechanical friction due to the levitation effect; however, during motion in air, aerodynamic drag becomes significant, leading to oscillation damping and a reduction in velocity.

This work investigates the effect of aerodynamic drag on the dynamics of a cryostat with high-temperature superconductors levitating above a magnetic track consisting of permanent magnets. Experimental studies were carried out using two types of cryostats: titanium and foam-based. To examine the effect of aerodynamic profile on motion damping, plates of various sizes were mounted on the front and rear parts of the cryostat.

A system consisting of two main units was developed to control the cryostat's position above the track and its velocity. The first control unit includes a high-performance 32-bit Russian-made K1921VG015 microcontroller (MCU) based on the RISC–V core, which includes hardware cryptographic modules enabling the implementation of a secure MLT control and monitoring system with an encrypted data exchange protocol. The second unit is a distributed system of laser optoelectronic sensors with a MCU that records the signal reception time. The optoelectronic position and velocity sensors for the control and feedback system were tested, and their metrological characteristics — accuracy, speed, and reliability — were established. Calibration was also performed to ensure the conversion of photodetector signals into precise kinematic parameters of the moving element in real time. Data received from the sensor system allows for the determination and calculation of the cryostat's current velocity and position at any given time. The control program for the second unit is written in C++. The cryostat's equation of motion was derived both without and with aerodynamic drag. The developed model

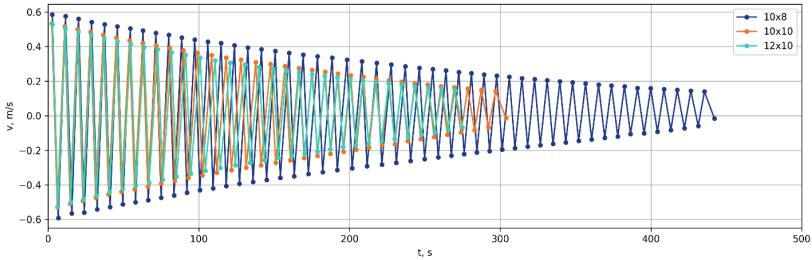


Fig. 1. Experimental velocity-time curves for the titanium cryostat with plates of different sizes

was used to obtain the velocity-time dependence shown in Fig. 1. As can be seen an increase in the characteristic cross-sectional area leads to higher aerodynamic drag and faster decay of velocity.

The obtained results enable a quantitative assessment of the contribution of aerodynamic drag to the dynamics of HTS-based levitating systems and may be useful in the design of magnetic levitation transport systems.

This work was supported by the Russian Science Foundation Project № 25-19-20141 (https://rscf.ru/project/25-19-20141/).

[1] W. Lei, Z. Deng and J. Zheng. *Int. J. Rail Transp*. 12, 1 (2024).

[2] L. Wang, Z. Deng and Y. Li. *Sci. Rep*. 15, 1 (2025).

Ferromagnetic Shape Memory Effect in Heusler Alloys — 30 Years of Discovery

V. V. Koledov[1,a], V. D. Buchelnikov[2], P. S. Smerchansky[1,4], A. P. Kamantsev[1], D. D. Kuznetsov[1], S. D. Suslov[1], E. V. Morozov[1], A. V. Mashirov[1], O. E. Kovalev[3], R. A. Safonov[3], I. F. Gribanov[3], A. V. Golovchan[3], N. Yu. Nyrkov[3], S. V. von Gratowski[1], S. S. Zhdanov[5,1], V. M. Povarnitsyn[5,1]

[1] Kotelnikov Institute of Radioengineering and Electronics of RAS, Moscow, Russia
[2] Chelyabinsk State University, Chelyabinsk, Russia
[3] A.A. Galkin Donetsk Institute for Physics and Engineering, Donetsk, Russia
[4] National Research University Higher School of Economics, Moscow, Russia
[5] Bauman Moscow State Technical University, Moscow, Russia
[a] email: *victor_koledov@mail.ru*

In 1996, a paper [1] was published in which the authors reported large deformations of single crystals of the Ni_2MnGa Heusler alloy under the influence of a magnetic field. The effect was termed magnetic shape memory and attracted considerable attention from researchers, which has not waned to this day. The effect of giant magnetically controlled

deformations can also be observed in polycrystalline alloys; this requires the application of sufficiently strong magnetic fields to induce a reversible thermoelastic magnetostructural transition and the associated shape memory effect (SME) [2]. Modern technologies make it possible to fabricate microscale actuators from composites based on ferromagnetic Heusler alloys with magnetically controlled SME [3]. This paper reviews current global advances in the development and study of new ferromagnetic alloys with thermoelastic martensitic transition and magnetically controlled (SME), applied works on the development of various devices based on magnetically controlled SME, and an analysis of the challenges involved. The paper also presents the authors' latest achievements in this area. The paper reports on the fabrication and experimental study of rapidly quenched $Ni_{37}Co_{13}Mn_{35}Ti_{15}$ Heusler alloy ribbons. The following key results were obtained:

1. A strong, up to 1.6%, reversible SME was detected in rapidly quenched $Ni_{37}Co_{13}Mn_{35}Ti_{15}$ alloy ribbons. A model for its explanation is proposed.

2. Numerical calculations using a thermodynamic model showed that residual tensile stresses induced by the strip during spinning can lead to a decrease in the martensitic transition temperature.

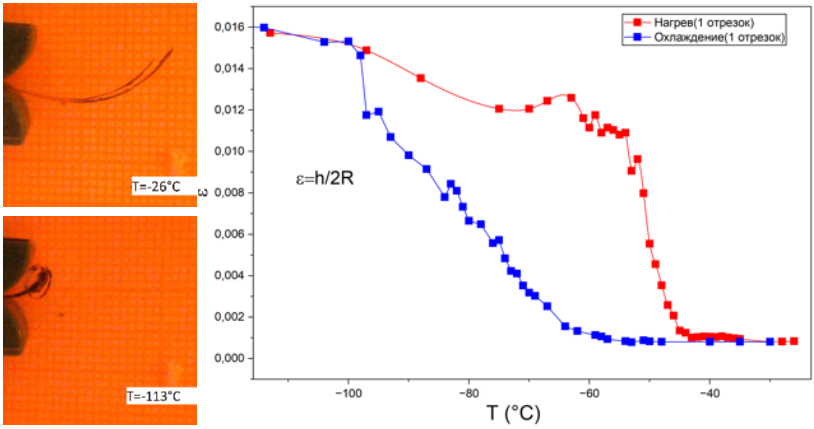


Fig. 1. Reversible shape memory effect in a rapidly quenched ribbon of the ferromagnetic Heusler alloy made of 3D transition elements NiCoMnTi. (a) alloy ribbon sample is in the austenitic high-temperature phase. (b) sample is in the martensitic low-temperature phase. (c) the graph of the dependence of the bending strain of the ribbon sample on temperature

3. The model that takes into account the non-uniformity of the tape thickness explains the appearance of two points of the martensitic phase transition in two layers of the tape and the possibility of two-stage bending/straightening with decreasing temperature.

4. Numerical calculations using the model show that applying a magnetic field causes a decrease in the martensitic transition temperature, regardless of the magnetic field direction. Based on this fact, a protocol for conducting an experiment on magnetically controlling the shape memory effect in a $Ni_{37}Co_{13}Mn_{35}Ti_{15}$ alloy is proposed.

This work was carried out as part of a state task of the Kotelnikov IRE RAS.

[1] Ullakko, K., Huang, J. K., Kantner, C., et al. *Applied Physics Letters*, 1996, 69(13), 1966–1968.

[2] Cherechukin, A. A., Dikshtein, I. E., Ermakov, et al. *Physics Letters A*, 2001, 291(2–3), 175–183.

[3] Kalimullina E., Kamantsev A., Koledov V., et al. *Physica status solidi* (c), 2014, 11 (5–6). *C*. 1023–1025.

Magnetic Levitational Transport Based on High Temperature Superconductors: Modelling of Accelleration and Braking System

V. V. Koledov[1,2, a], M. V. Matyunina[2], S.V. von Gratowski[1], D. A. Suslov[1], I. V. Bychkov[2], O. O. Pavlukhina[2], M. A. Orshulevich[2], I. V. Maltsev[2], A. V. Mashirov[1], D. E. Kirillov[2], R. R. Garipov[2], A. P. Kamantsev[1], K. A. Kolesov[1,2], D. A. Karpukhin[1,2], D. A. Kuzmin[2]

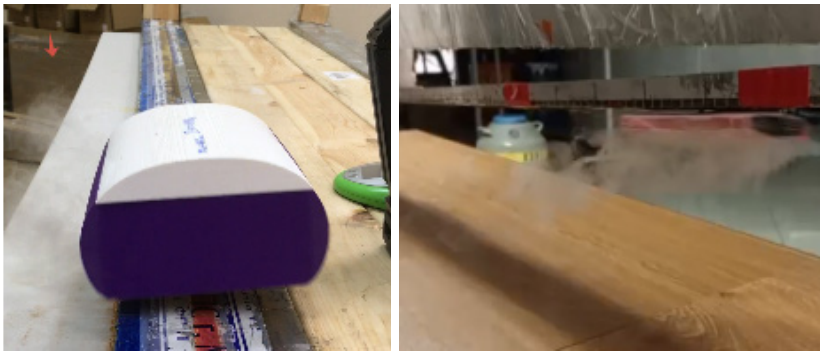
[1]Kotelnikov Institute of Radioengineering and Electronics of RAS, Moscow, Russia

[2] Chelyabinsk State University, Chelyabinsk, Russia

[a]email: *victor_koledov@mail.ru*

The development of high-speed, cost-effective, and environmentally friendly magnetic levitation transport (MLT) in a vacuum tube using

high-temperature superconductors (HTSC) has attracted considerable attention from researchers in our country and abroad [1; 2]. Not only is the absence of friction attractive, but also the stability of HTSC movement along a permanent magnet track, due to the effect of HTSC magnetic flux capture (see Fig. 1).



a *b*

Fig. 1. Stability of magnetic levitation of the MLT model based on high-temperature superconductors: a) suspension of the model above the track; b) suspension of the model below the track

This report describes the results of work on the design and testing of small-scale MLT prototypes made of Y—Ba—Cu—O high-temperature superconducting ceramics cooled with liquid nitrogen. Preliminary data on the derivation of a system of equations for the motion of the MLT prototype along a permanent magnet track, as well as on an experimental study of the prototype's motion along a track with gravitational acceleration and deceleration, are presented (see Fig. 2).

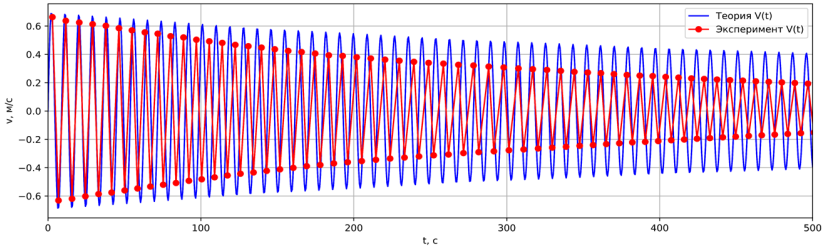


Fig. 2. Experimental and theoretical curves of the dependence of the MLT model speed on time

It has been shown that on short tracks, when a superconductor moves at low speeds, the characteristics of the drag force dependence can be identified by improving the accuracy of measuring the acceleration (damping) of the MLT motion in a vacuum and in air along a gravity path [3]. Motion on paths ranging from 2 to 12 meters in length is being experimentally studied. Accuracy is increased by automating the measurement of the MLT model's velocity along a gravity (curved) path. The effects of not only the cryostat shape and aerodynamic cross-sectional area but also the cryostat material on the model's velocity damping are revealed.

This work was supported by the Russian Science Foundation (RSF) Project No 25-19-20141 (https://rscf.ru/ru/project/25-19-20141/).

[1] Karpukhin D. A., Petrov A. O., Koledov V. V. et al. *Journal of Radioelectronics*.11 (2022).

[2] Deng, Z., Zhang, W., Kou, L., et al. *IEEE Transactions on Applied Superconductivity*, 31(8), 1–5. (2021)

[3] Terentyev Yu.A., Suslov D. A., Koledov V. V., Karpushin D. A., Petrov A. O. Superconducting magnetic levitation transport system. Russian Federation Patent No. 2782548. October 31, 2022.

Trapped Field Profile in Bulk High-temperature Superconductor Solenoid

K. A. Kolesov[1, a], A. V. Mashirov[1], V. V. Koledov[1], A. P. Kamantsev[1]

[1]Kotelnikov Institute of Radioengineering and Electronics of RAS, Moscow, Russia

[a]e-mail: *kolesovkka@mail.ru*

In connection with the growth of development of prototypes and commercial devices of refrigeration machines operating on the principle of magnetic cooling, which are based on the magnetocaloric effect (MCE) [1], the issue of creating a high-intensity magnetic field remains relevant. One application of high-temperature superconductors (HTSC) is the production of tapped field magnets with high magnetic field [2], which

can be used as a source of magnetic field for magnetic cooling devices.

In this study, we conducted a physical experiment to create a solenoid based on HTSC bulk YBCO, trap magnetic flux in it, and study the profile of the trapped magnetic field. For the experiment, three bulk YBCO samples were prepared in the form of cylinders with an outer diameter of 12 mm, an inner diameter of 4 mm, and a thickness of 5 mm. The samples were stacked and placed in a fixed holder. The counter-piece, a rod with a glued-in Hall sensor, moved freely within the inner bore of the samples. The experiment was conducted using a cryostat. Magnetic flux trapping was performed using the FC (field cooling) protocol. This resulted in obtaining the distribution profile of the trapped magnetic flux along the axis of rotation of the samples (Fig. 1). As the experiment showed, a dip in the trapped magnetic flux is observed at the boundary between the lower and middle samples, which is clearly visible as the trapped magnetic flux increases. The maximum trapped magnetic flux occurs at the midpoints of the cross-sections of the upper and lower samples, forming the solenoid. The maximum trapped magnetic field reached about 3 T.

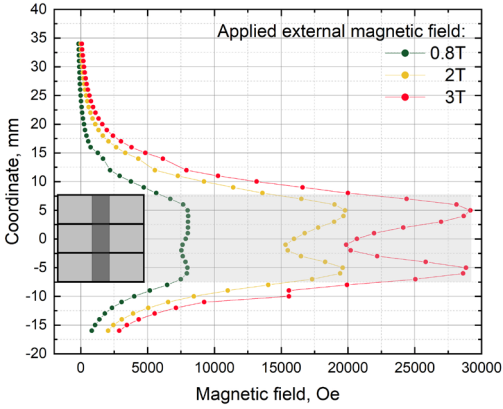


Fig. 1. Trapped field profile

The study was supported by a grant from the Russian Science Foundation № 25-19-00942, https://rscf.ru/project/25-19-00942/

[1] A. M. Tishin, Y. I. Spichkin. *CRC Press*. (2016)

[2] Q. Wang, H. Zhang, L. Hao, T. Coombs. *Superconductor Science and Technology*. 37, 123005 (2024).

Effect of Pressure on the Magnetocaloric Properties of $NiMn_{0.89}Cr_{0.11}Ge$ Alloys with Reduced Curie Temperature and Different Thermal History

I. F. Gribanov[1], R. A. Safonov[1, a], O. E. Kovalev[1], A. V. Golovchan[1], V. V. Burkhovetsky[1], N. Yu. Nyrkov[1]

A. A. Galkin Donetsk Institute for Physics and Engineering, Donetsk, Russia
[a]e-mail: *romansafonov05@mail.ru*

As is well known, in alloys of the $NiMn_{1-x}Cr_xGe$ system with a Cr content of about $x = 0.11$, a giant magnetocaloric effect (MCE) occurs, accompanying a first-order magnetostructural phase transition between the high-temperature paramagnetic phase with a hexagonal Ni_2In-type crystal structure (hex(PM)) and the low-temperature ferromagnetic phase with an orthorhombic TiNiSi-type crystal structure (orth(FM)) [1; 2]. It has been established that the synthesis method commonly used in the literature for such materials, which includes solid-state quenching in water from the homogenization annealing temperature (850 °C), leads to a spread of Curie temperatures in the range $200 < T_C < 280$ K without loss of functional efficiency. In the present work, two samples with reduced T_C were obtained; during quenching, they differed in cooling rate (designated sample 1 and sample 2). This was achieved in the first case by breaking the evacuated quartz ampoule containing the sample when it entered the vessel with water, which ensured direct contact between the sample and the quenching liquid. In the second case, the integrity of the evacuated ampoule containing the sample was preserved during quenching. The paper compares the effect of the cooling factor during quenching in these two cases (frequently encountered in experiments) on the magnetobaric and magnetocaloric properties of the samples. The results are presented below.

As can be seen from Fig. 1, the pressure dependences of the hex(PM)-orth(FM) transition temperatures are nonmonotonic, which contrasts with the previously obtained monotonically decreasing $T_C(P)$ dependences for the case of a higher Curie temperature [1].

A possible interpretation of this behavior, associated with the formation of the crystal structure during quenching, is given in [2] within the framework of the diffuse phase transition model.

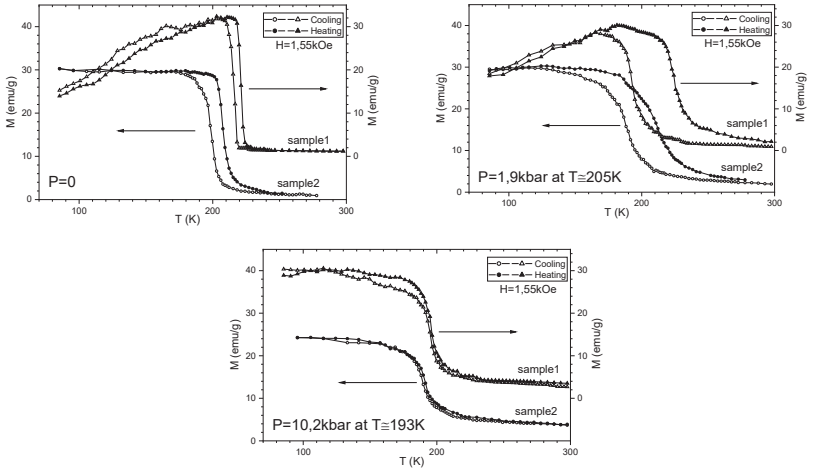


Fig. 1. Temperature dependences of the magnetization of sample 1 and sample 2 at different pressures

The temperature dependence of the entropy change during isothermal magnetization of the studied samples in the vicinity of the hex-(PM)-orth(FM) phase transition was determined in the standard way using the Maxwell relation, while the series of isothermal magnetization

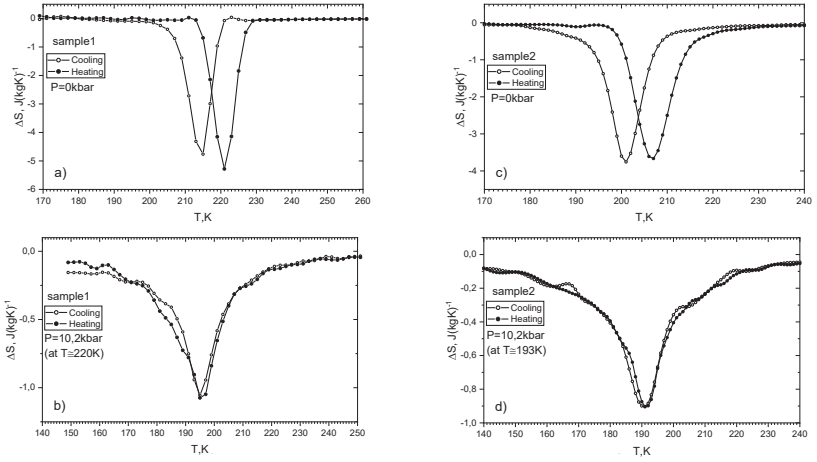


Fig. 2. Temperature dependence of the entropy change during isothermal magnetization of the studied samples 1 (a, b) and 2 (c, d) in a field of ΔH = 0–9.4 kOe at different pressures

curves was obtained by appropriate processing of a series of temperature dependences of magnetization measured in different magnetic fields. The results are shown in Fig. 2, *a–d*.

As can be seen from Figs. 1 and 2, compression of the crystal lattice in both studied samples leads, first, to a nontrivial pressure dependence of the Curie temperature; second, to a decrease in the hysteresis of the hex(PM)-orth(FM) phase transition; and third, to a broadening of this transition, which entails a decrease in the magnitude of the magnetocaloric effect. Variation of the quenching cooling rate of the samples within the range considered here has little effect on their magnetostructural and magnetocaloric properties.

[1] I. F. Gribanov, V. V. Burkhovetsky, V. I. Valkov et al. *Physics and Technology of High Pressures*. 30(1), 83–95 (2020).

[2] V. I. Valkov, A. V. Golovchan, I. F. Gribanov et al. *Physics of the Solid State.* 67(4), 653–667 (2025).

Specific Features of Methods for Preparing the Double-Layered Cobaltite $GdBaCo_2O_{5.5}$

T. N. Tarasenko[1], Ya. Yu. Antonishin [1], O. E. Kovalev[1, a], A. S. Mazur [2]

[1]A.A. Galkin Donetsk Institute for Physics and Engineering, Donetsk
[2]Saint Petersburg State University, Saint Petersburg
[a]email: *oleg_kovalev_2018@mail.ru*

Rare-earth (Ln) cobaltites $LnBaCo_2O_{5.5}$, depending on the synthesis method, the type of Ln ion, and the oxygen content, differ from other layered oxides by a diversity of properties and a rich phase diagram, which, with increasing temperature, includes a whole series of phase transitions associated with various structural, charge, orbital, and spin orderings.

$LnBaCo_2O_{5+\delta}$ compounds have a double perovskite structure. Depending on the oxygen content, cobalt ions may have the valence states Co^{2+}, Co^{3+}, and Co^{4+}. At an oxygen index value of $\delta = 0.5$, all cobalt ions have the same valence, Co^{3+}. In this case, due to the difference in ionic radii between

the larger Ba cation and the smaller Ln cation, a layered perovskite-like orthorhombic (*Pmmm*) crystal structure is formed, with a doubling of the perovskite unit cell along the *b* and *c* axes (Fig. 1) [1].

Polycrystalline samples of $GdBaCo_2O_{5.5}$ were synthesized by two methods: (1) solid-state synthesis and (2) glycine-nitrate combustion.

In the first case, a mixture of powdered oxides Gd_2O_3, Co_3O_4, and barium carbonate $BaCO_3$ (all of high-purity grade), taken in a stoichiometric ratio, was subjected to preliminary calcination at 1000 °C (8 h) and final calcination at 1150°C (30 h), followed by gradual cooling at 100°C/h [2]. X-ray diffraction analysis showed the samples to be single-phase with an orthorhombic (Pmmm) structure (Fig. 2).

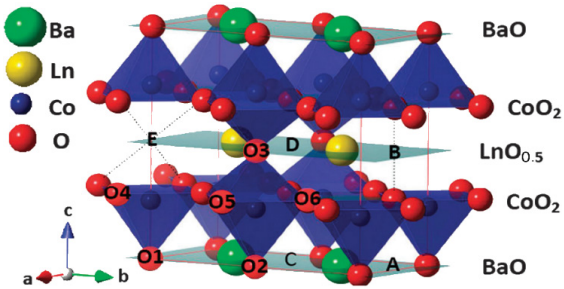


Fig. 1. Crystal structure of $LnBaCo_2O_{5.5}$ (Pmmm)

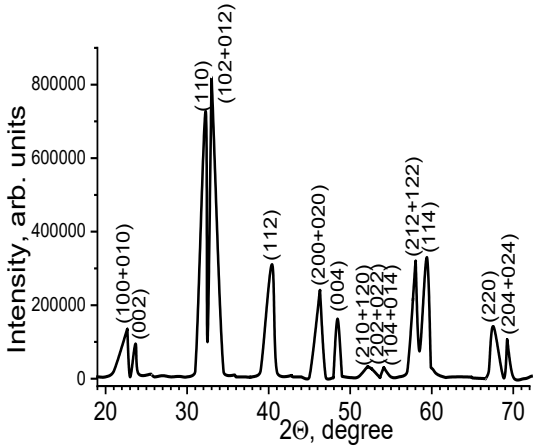


Fig. 2. X-ray diffraction pattern of $GdBaCo_2O_{5.5}$ samples

In the second case, the starting reagents were the metal nitrates $Gd(NO_3)_3 \cdot 6H_2O$, $Ba(NO_3)_2$, and $Co(NO_3)_2 \cdot 6H_2O$, taken in a stoichiometric ratio, and glycine, $C_2H_5NO_2$, the amount of which relative to the metal nitrates was 1.5 [3]. After preliminary dissolution of the nitrates and glycine in distilled water, the mixture was evaporated. The resulting "gel" was heated to the self-ignition temperature of 343 °C. The reaction lasted about 2–3 s. The resulting "ash" was subjected to final annealing at 1100 °C (35 h).

The advantage of the glycine-nitrate combustion method lies in producing a highly dispersed powder of the complex oxide $GdBaCo_2O_5$.

Double layered cobaltites are of great interest for practical applications as cathodes for solid oxide fuel cells (SOFC). In $GdBaCo_2O_{5+\delta}$, with increasing temperature, a sequence of phase transitions is observed: AFM-FM, FM-PM, insulator-metal, as well as a change in the spin state of cobalt ions [2]. Due to the strong coupling "magnetism ↔ crystal structure ↔ oxygen nonstoichiometry ↔ Co spin state" in $GdBaCo_2O_{5+\delta}$, a magnetocaloric effect is possible.

[1] D. Seymour, A. Chroneos, J. A. Kilner, R. W. Grimes, *Phys. Chem. Chem. Phys*., 13, 15305 (2011).

[2] T. N. Tarasenko, T. S. Sivachenko, I. Yu. Reshidova, V. V. Burkhovetskii, A. S. Mazur, *Chemistry and Materials Science*. 11, 5, 247 (2021.).

[3] V. D. Zhuravlev, A. V. Dmitriev, E. V. Vladimirova et al., *Russian Journal of Inorganic Chemistry*. 66, 12, 1770 (2021).

Magnetic Viscosity in Materials with Nonequilibrium Transformations Near Magnetostructural Phase Transitions

A. S. Komlev[1, a], A. R. Vashchenkova[1], S. I. Kostylev[1], V. E. Chernyshev[1], N. S. Perov[1]

[1] Faculty of Physics, M. V. Lomonosov Moscow State University, 119991, Moscow, Russia
[a] e-mail: *komlevas@my.msu.ru*

Magnetic viscosity is a key parameter characterizing the nonequilibrium behavior of magnetic materials. It determines the rate at which a magnetic system responds to time-dependent external stimuli and therefore governs the reproducibility of phase transitions, the shape of hysteresis loops, and the stability of operating regimes in magnetic devices. In modern applications of magnetism — including magnetocaloric systems, spintronics, magnetic recording, and soft magnetic components — the achievable performance is often limited not only by equilibrium properties but by the dynamic conditions of operation, such as field and temperature sweep rates [1].

Experimental studies demonstrate that under non-stationary conditions the "effective" parameters of phase transitions and magnetization processes cease to be intrinsic constants and instead become functions of both the driving rate and the instantaneous state of the system. This work the summary of mechanisms responsible for the emergence of magnetization relaxation under quasi-adiabatic external excitation [2].

For materials exhibiting reversible first-order magnetic phase transitions, such as FeRh and $La(FeSi)_{13}$-based compounds, it is shown that the critical fields of the transition depend nonlinearly on the magnetic field sweep rate [3]. This behavior indicates that conventional approaches based on a constant kinetic coefficient in the Landau—Khalatnikov equation are insufficient. To address this, a modified approach is proposed in which the kinetic coefficient is treated as a magnetization-dependent function. The model provides qualitative agreement with experimental observations and captures the nonlinear evolution of transition parameters with driving rate. Notably, in these systems the crystalline anisotropy

remains essentially unchanged during the phase transition, indicating that the observed relaxation originates primarily from intrinsic phase transformation kinetics rather than structural reconfiguration.

In contrast, studies of amorphous ribbons during crystallization reveal that prolonged magnetization relaxation can arise from the evolution of the internal structure itself. In this case, the relaxation behavior is governed by changes in the type and magnitude of effective magnetic anisotropy during phase formation. The emergence of competing contributions — such as anisotropy energy and internal magnetic (magnetostatic and exchange) fields — leads to a complex, time-dependent energy landscape. As a result, thermally activated reorientation of magnetic moments becomes strongly dependent on temperature and the stage of crystallization, which must be taken into account when optimizing annealing conditions to achieve desired microstructural and magnetic properties [4].

A general conclusion emerging from the analysis of phase transformation kinetics across different systems is that magnetic viscosity should be interpreted as a response to a dynamically evolving energy landscape shaped by both external driving forces and internal interactions/microstructure. Accordingly, adequate theoretical descriptions must allow kinetic parameters to depend on the state variables (H, T, T_{sample}, M, degree of transformation) and explicitly incorporate phase kinetics. From a practical standpoint, this framework enables a transition from the phenomenological description of isolated anomalies (e. g., relaxation time maxima or transition shifts) to the predictive design of processing routes and device operation regimes, where both rate and structure determine the stability of magnetic properties.

This work was supported by the Russian Science Foundation (project № 25-72-00031).

[1] D. Yu. Karpenkov, R. A. Makarin, A. Yu. Karpenkov, A. V. Korotitskiy, A. S. Komlev, M. V. Zhelezniy. *Journal of Alloys and Compounds* 962 171154 (2023).

[2] R. Costa, E. Lovell, R. Almeida, R. Pinto, L. F. Cohen, A. M. Pereira, J. P. Araujo, J. H. Belo. *J. Phys. D: Appl. Phys*. (2023).

[3] A. S. Komlev, R. A. Makarin, T. S. Ilina, D. A. Kiselev, A. M. Chirkova, N. A. Kulesh, A. S. Volegov, V. I. Zverev, N. S. Perov. (2022).

[4] A. Mattoni, L. Colombo. *Phys. Rev.* B 78 075408 (2008).

Polarization Curve and Power Density of Plant Bioelectrochemical System with Different Agricultural Crops

T. E. Kuleshova[1a], O. I. Karmanova [1b], G. G. Panova [1c]

[1] Agrophysical Research Institute, St. Petersburg, Russia
[a] e-mail: *www.piter.ru@bk.ru*
[b] e-mail: *pochtovij_jashik@bk.ru*
[c] e-mail: *gaiane@inbox.ru*

Plant-based bioelectrochemical systems using exoelectrogenic reactions in the plant rhizosphere with the participation of microorganisms to convert the chemical energy of organic compounds into electrical energy are a promising bioenergy technology compatible with the production of plant products [1]. Different plant species and their selection criteria play a decisive role in bioelectric parameters and electricity generation [2].

The aim of this work was to obtain the power and polarization characteristics of bioelectrochemical systems when growing various plant crops of different economic value in them.

The phytotest subjects were the different varieties of lettuce, cucumber, and tomato. The study was conducted under controlled conditions of intensive light culture at the AFI agrobiological testing ground using original bioelectrochemical system designs based on panoponics technology [1]. The results are presented in the figure; the cucumber-based BES exhibited the highest specific power of 8.4 μW/m².

BES appears to be a relevant technology for generating renewable energy, with the correct selection of plant crops being a key factor in its development.

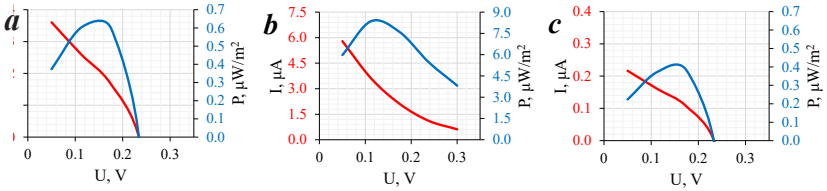


Fig.1. Power density and polarization curves of the BES during cultivation of: a — lettuce, b — cucumber, c — tomato

[1] T. E. Kuleshova, A. S. Galushko, G. G. Panova, E. N. Volkova, W. Apollon, Ch. Shuang, S. Sevda. *Sel'skokhozyaistvennaya Biologiya* (*Agricultural Biology*). 57(3), 425 (2022).

[2] T. Kuleshova, E. Ezerina, V. Vertebny, Yu. Khomyakov. *International Journal of Hydrogen Energy*. 64, 781 (2024).

[3] R. Bhattacharya, V. Parthasarthy, D. Bose, K. Gulia, S. Srivastava, K. R. Roshan and R. Shankar. *Biotechnology and Bioengineering*, 120(6), 1455 (2023).

Temperature Profile of the Plant-environment System Under Natural Conditions and Intensive Light Culture

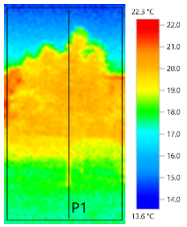
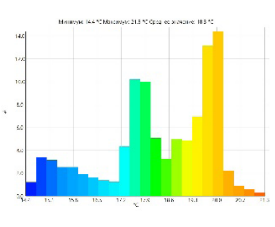
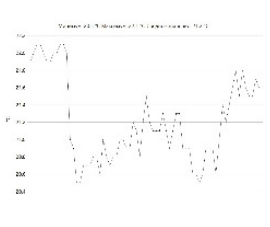
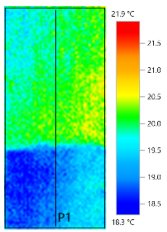
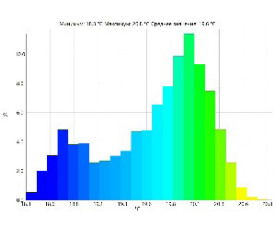
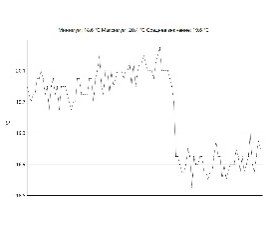
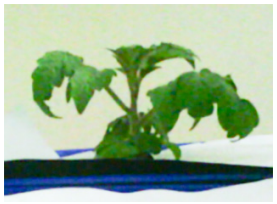
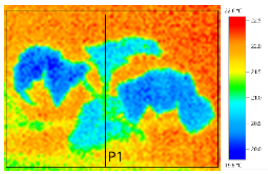
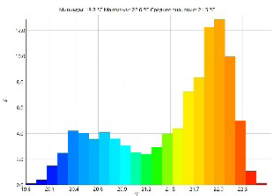
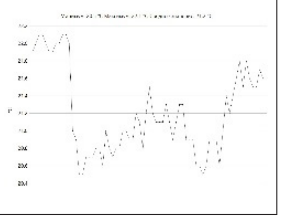
T. E. Kuleshova[1, a], A. V. Dobrokhotov [1, b], V. V. Tarakanov [2, c], V. V. Koledov[3, d], S. V. von Gratowski [3, e]

[1] Agrophysical Research Institute, St. Petersburg, Russia
[2] West Siberian Branch, Sukachev Institute of Forest, Siberian Branch, Russian Academy of Sciences, Novosibirsk, Russia
[3] Kotelnikov Institute of Radio Engineering and Electronics, Russian Academy of Sciences, Moscow, Russia
[a] e-mail: *www.piter.ru@bk.ru*
[b] e-mail: *dobralexey@gmail.com*
[c] e-mail: *tarh012@mail.ru*
[d] e-mail: *svetlana.gratowski@yandex.ru*
[e] e-mail: *victor_koledov@mail.ru*

Plants are poikilothermic organisms, meaning their temperature depends on the ambient temperature but may not be equal to it. Suprathermal plants have a temperature higher than the surrounding air, which is typical for cold climates, while subthermal plants, more common in hot climates, have a temperature lower than the surrounding air [1]. In addition, massive organs with poor heat exchange (leaves and stems of succulents, fleshy fruits of tomatoes, watermelons, tree trunks) can have a temperature 10–20 °C higher than that of the air [1].

Table

Thermal imaging of the plant-environment system

Option	Real image	Thermogram	Histogram	Temperature profile
A tree in a park area within the city limits				
Aboveground part and root system of wheat in a rhizotron				
Tomato in intensive light culture				

Plants are known to be capable of thermogenesis — the production of heat in the process of dissipation of oxidation-reduction energy H^+ and the proton electrochemical gradient (μH^+) during mitochondrial respiration [2]. For example, the kidney-leaf cedar (*Symplocarpus renifolius* Schott ex Tzvelev) is able to maintain an organ temperature of about 20 °C, even if the air temperature drops to –15 °C [3], and the nut-bearing lotus (*Nelumbo nucifera* Gaertn.) — in the range from 30 to 36 °C under ambient temperature fluctuations from 10 to 45 °C [4]. Evergreen conifers can tolerate extremely low temperatures during a long, dark winter and fully restore photosynthesis in the summer. The temperature difference between the trunks of healthy and dying trees during anticyclonic weather reaches 10–14 °C [5].

The aim of this work was to study the temperature gradients of plants and their surrounding air and root environments under various growing conditions with the potential to use the observed caloric effects for phytomonitoring and power generation.

The radiometric temperature profile of the plant-environment system was studied using a testo 868 thermal imager (Testo, Germany) in natural conditions — a park area within the city (coordinates 60.010056, 30.398056) and at the agrobiopolygon of the AFI under conditions of controlled intensive light culture and in a rhizotron.

The measurement results are presented in the table. The temperature difference between the air and the tree under natural conditions during a summer night (measured on August 5, 2025, at 11:40 PM) reached 5.5 °C, between the root system and the above-ground part of the wheat — 1.8 °C, and between the tomato leaf and the air during the dark stage of photosynthesis — 2.5 °C.

Thermal methods for assessing the state of the plant-environment system have the potential to obtain information remotely and are relevant for use in phytomonitoring.

It would be extremely interesting to conduct similar studies on commercially valuable species of woody plants in the boreal forests of Russia.

[1] A. A. Shapovalova. Plant ecology: Textbook. Saratov: Saratov Source Publishing House (2015).

[2] Y. Zhu, J. Lu, J. Wang, F. Chen, F. Leng and H. Li. *Journal of Integrative Plant Biology*. 53(1), 7 (2011).

[3] R. S. Seymour, Y. Ito, Y. Onda and K. Ito. Biology Letters 5, 568 (2009).

[4] J. R. Watling, S. A. Robinson and R. S. Seymour. *Plant Physiology.* 140, 1367 (2006).

[5] V. N. Karasev, M. A. Karaseva, E. M. Romanov and D. I. Mukhortov. *Russian Journal of Ecology*. 48(2), 109 (2017).

Magnetocaloric Effect in Pseudo-binary $Gd_{0.9}Tb_{0.1}NiH_x$ Hydrides with Various Hydrogen Amounts

A. A. Kurganskaya[1,2,a], E. S. Kozlyakova[1], I. S. Tereshina[1], A. N. Vasiliev[1]

[1] Lomonosov Moscow State University, 119991, Leninskie gory 1, Moscow, Russia

[2] Bauman Moscow State Technical University, 105005, Moscow, 2nd Baumanskaya str., 5, Moscow, Russia

[a]e-mail: *kurganskaia.aa17@physics.msu.ru*

The development of high-performance magnetocaloric materials remains a key challenge in materials science, as magnetic refrigeration is widely regarded as a promising alternative to conventional gas-cycle cooling technologies [1]. Among the several classes of magnetocaloric materials that have been identified and extensively investigated to date [2], RNi-type intermetallic compounds are of particular interest since they exhibit a large magnetocaloric effect (MCE) in the temperature range close to the liquefaction point of nitrogen, which makes them promising candidates for low-temperature applications [3; 4]. The properties of these compounds are highly sensitive to external treatments, such as substitutions in both the rare-earth and nickel sublattices. These modifications can significantly influence the saturation magnetization, magnetic anisotropy, and magnetic transition temperature. Previous studies have also demonstrated that the incorporation of hydrogen into the crystal lattice of RNi compounds substantially affects their structural, magnetic, and thermal properties [5–7]. Therefore, this study was aimed at comparing magnetothermal properties of pseudobinary alloy $Gd_{0.9}Tb_{0.1}Ni$ hydrides with different hydrogen contents.

To this purpose, four hydrides were synthesized as follows: $Gd_{0.9}Tb_{0.1}NiH_{0.48}$, $Gd_{0.9}Tb_{0.1}NiH_{0.97}$, $Gd_{0.9}Tb_{0.1}NiH_{1.51}$, and $Gd_{0.9}Tb_{0.1}NiH_{2.72}$. Magnetocaloric properties were studied using two characteristics: the Curie temperature and the magnetocaloric effect. The former was determined by analyzing the temperature derivative of magnetization, the latter by analyzing Maxwell's equations (an indirect method).

$$\Delta S_M(T,H) = \int_0^H \left(\frac{\partial M(T,H)}{\partial T} \right)_H dH. \quad (1)$$

The results of the study are presented in Table 1. New data was compared to that of the $Gd_{0.9}Tb_{0.1}Ni$ alloy and its hydride $Gd_{0.9}Tb_{0.1}NiH_4$ with the maximum amount of hydrogen per f. u. studied previously [8].

Table 1

Magnetothermal properties of $Gd_{0.9}Tb_{0.1}NiH_x$ (x = 0; 0,48; 0,97; 1,51; 2,72; 4,0) compounds

Sample	T_C, K	$-\Delta S_m$, $J \cdot kg^{-1} \cdot K^{-1}$, ($\mu_0 \Delta H = 2$ T)
$Gd_{0.9}Tb_{0.1}Ni$ [8]	65	8,2
$Gd_{0.9}Tb_{0.1}NiH_{0.48}$	66	6,9
$Gd_{0.9}Tb_{0.1}NiH_{0.97}$	66	3,0
$Gd_{0.9}Tb_{0.1}NiH_{1.51}$	66	6,4
$Gd_{0.9}Tb_{0.1}NiH_{2.72}$	66	2,8
$Gd_{0.9}Tb_{0.1}NiH_4$ [8]	15	2,6

Fig. 1 visualizes the dependence of Curie temperature on the amount of interstitial hydrogen atoms in the crystal lattice.

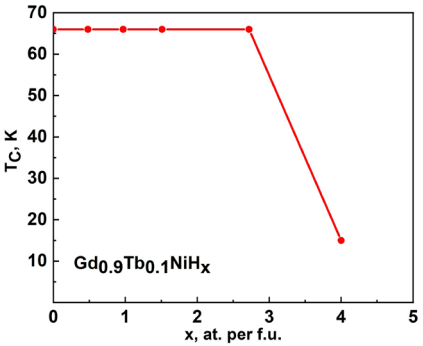


Fig. 1. Curie temperature dependence on the amount of interstitional hydrogen atoms per f. u.

It has been discovered that the radical shift in Curie temperature observed in all previously studied RNi-type hydrides does not occur until the maximum possible amount of hydrogen per formula unit is reached. MCE values seem to be oscillating between that of the initial compound and that of the maximum hydrogen amount hydride. This interesting phenomenon might be explained by supposing that MCE values follow the pattern set by Ruderman — Kittel — Kasuya — Yosida interaction model.

The study was conducted under the state assignment of Lomonosov Moscow State University.

[1] A. M. Tishin, Y. I. Spichckin, Institute of Physics Publishing, Bristol and Philadelphia (2003)

[2] K. A. Gschneidner Jr, V. K. Pecharsky, A. O. Tsokol. *Rep. Prog*. 68(6) 1479 (2005).

[3] I. A. Tanaeva, H. Ikeda, L.J.A. Van Bokhoven, Y. Matsubara, A.T.A.M. De Waele. *Cryogenics*. 43(8) 441 (2003).

[4] P. Kumar, K. G. Suresh, A. K. Nigam, O. Gutfleisch. *Journal of Physics D*. 41(24) 245006 (2008).

[5] A. I. Smarzhevskaya, W. Iwasieczko, V. N. Verbetsky, S. A. Nikitin. *Phys. Status Solidi C*. 11(5–6) 1102 (2014).

[6] S. A. Lushnikov, I. S. Tereshina, V. N. Verbetsky. *Physics of the Solid State*. 61(1) 91 (2019).

[7] W. Iwasieczko, H. Drulis, Y. L. Yaropolov, S. A. Nikitin, V. N. Verbetsky. *J. Alloys Compd*. 509 827 (2011).

[8] I. S. Tereshina, A. Yu. Karpenkov, A. A. Kurganskaya, V. B. Chzhan, S. A. Lushnikov, V. N. Verbetsky, E. S. Kozlyakova, A. N. Vasiliev. *J. Magn. Magn. Mater*. 574 170693 (2023).

Comparative Simulation of Halbach Cylinder with Ring Segments and Rectangular Prisms for Caloric Cooling

D. A. Kuzmin[1,a], I. V. Maltsev[1], D. S. Bataev[1], M. V. Utarbekova[1]

[1]Chelyabinsk State University, Chelyabinsk, Russia
[a]e-mail: *kuzminda@csu.ru*

Magnetic cooling based on the magnetocaloric effect requires compact magnetic field sources with an induction of ~2 T in a working area of ~20 mm diameter. The most promising topology is the Halbach cylinder, which concentrates the field inside the cavity. However, the technological complexity of manufacturing ring segments with radial magnetization stimulates the search for simpler solutions, such as assemblies of rectangular prisms. The aim of this work is a comparative analysis of the magnetic characteristics of the two configurations based on computer simulation.

Calculations were performed using the Magpylib library (Python) by analytical integration. The material used was Nd—Fe—B grade N52 (B_r = 1.45 T, coercivity H_c = 1.15·10⁶ A/m). Geometry: inner cavity radius R_{in} = 15 mm, outer magnet radius R_{out} = 100 mm, height h = 80 mm. Two models were considered: an ideal case of 8 ring segments, each with magnetization varying as $\boldsymbol{M}(\varphi) = M_0(\cos 2\varphi, \sin 2\varphi)$ with φ — a polar angle (see Fig. 1); and more realistic case of 8 rectangular prisms with

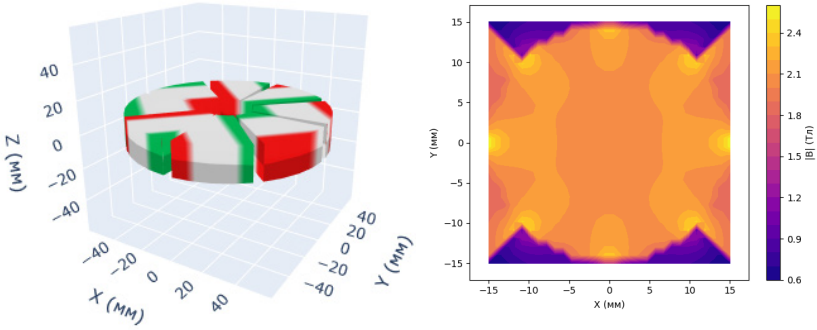


Fig. 1. Scheme and magnetic field distribution in ideal case of 8 ring segments

shape rotation by angle φ_i and local magnetization oriented at angle φ_i (to obtain a field along X) (see Fig. 2). The prism width was chosen without overlap. The central induction, its homogeneity in a region of radius 10 mm, and the field profile along the X-axis were evaluated.

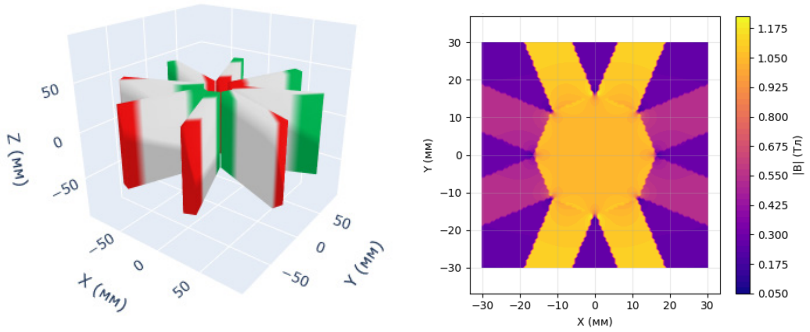


Fig. 2. Scheme and magnetic field distribution in ideal case of 8 rectangular prisms

For the ideal model with ring segments, the central field was 2.089 T with excellent homogeneity: the average field in the 10 mm radius region was 2.097 T, standard deviation 0.007 T (0.3%). The field profile along the X-axis shows a drop to 1.95 T at a distance of 10 mm from the center.

For the assembly of rectangular prisms (width 45.2 mm, depth 85 mm) with the same overall dimensions, the central field was only 1.127 T, and the average field in the working region was 1.09 T with a spread of ±0.15 T (14%). Attempts to increase the prism width to reduce gaps led to overlapping elements, which produced a nonphysical overestimation of the field (up to 2.89 T) and unreliable results. Thus, rectangular prisms without overlap yield a field 46% lower than that of ring segments.

The field reduction in the prism assembly is due to two factors: the rectangular shape does not match the trapezoidal crosssection of a ring sector, resulting in a loss of active magnet volume; and gaps between prisms increase the magnetic reluctance of the external circuit. To achieve 2 T with rectangular prisms, the outer radius would need to be increased to 140–150 mm and the height to 100–120 mm, raising the system mass to 35–40 kg (compared to 18 kg for the ringsegment design).

The developed Halbach cylinder model with Nd—Fe—B ring segments provides an induction of 2.09 T in a 20 mm diameter region with a mass of ~18 kg, fully meeting the requirements for magnetic cooling.

Using rectangular prisms of the same overall size does not reach the target field. It is recommended that a prototype cooling device adopt the ringsegment configuration, despite its higher manufacturing cost.

This work was carried out within the framework of State Assignments (topic FEGG-2025-0012).

Modelling of Force Interaction Between an Hts Ring and a Coil in a Permanent Magnet Levitation System

D. A. Kuzmin[1,a], K. A. Kolesov[2], I. V. Bychkov[1], V. V. Koledov[2], I. V. Maltsev[1], M. V. Matyunina[1]

[1] Chelyabinsk State University, Chelyabinsk, Russia
[2] Kotelnikov Institute of Radioengineering and Electronics of RAS, Moscow, Russia
[a] e-mail: *kuzminda@csu.ru*

High-temperature superconductors (HTS) are promising for magnetic levitation (maglev) transport. A key challenge is the efficient acceleration and braking of vehicles using electromagnetic coils. This work investigates a system comprising an HTS ring, fieldcooled (FC) above a threechain permanent magnet (PM) guideway (NdFeB), and a solenoid coil wound around the track. The aim is to theoretically and experimentally evaluate the forces arising when the coil is energised and to identify the underlying physical mechanism.

A hybrid modelling approach was used, combining analytical estimates, numerical simulations in Magpylib, and an integral Brandt method adapted for a ring geometry. The threechain PM guideway (central chain magnetised upward, side chains downward) was modelled to compute the vertical magnetic field B_z in the region of the HTS ring (outer radius 17.75 mm, inner radius 8 mm, thickness 10 mm, gap from magnet tops 17 mm), see Fig. 1. The average trapping field was ~20 mT, yielding

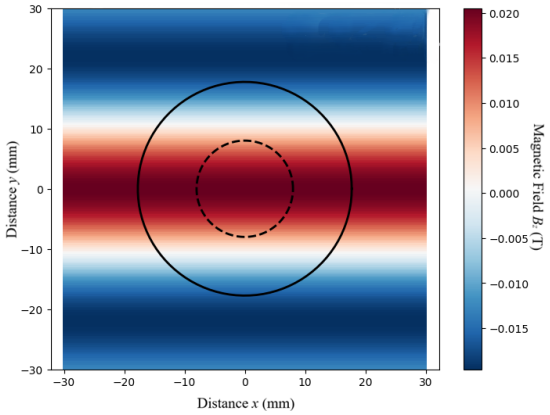


Fig. 1. Non-uniform distribution of threechain PM guideway B_z field

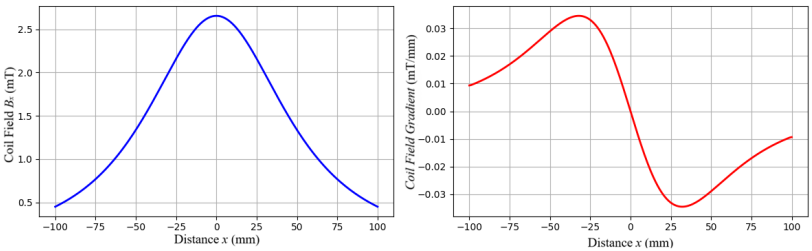


Fig. 2. Longitudinal coil-induced magnetic field and its gradient

a magnetic moment $m_z = \frac{1}{\mu_0}\int B_z\, dV \approx 0.13$ A·m² after FC. The coil (inner radius 57.5 mm, outer radius 77.5 mm, length 28 mm, 700 turns, current 0.4 A) produces an onaxis field $B_x \approx 2.5$ mT and a nonuniform vertical component B_z near the edges, dee Figure 2. The interaction force $F_x = m_z\, \partial B_z / \partial x$ was estimated to be ~2–3 mN. The trapped field distribution was refined using an integral Brandt method accounting for the fielddependent critical current density $J_c(B)$ and the powerlaw $E(J)$ characteristic of HTS.

The classical model of a fixed vertical moment interacting with the coil field would predict a force that reverses sign when the coil current is reversed. However, experiments showed that the HTS ring is always attracted towards the coil centre regardless of the current direction. This observation indicates that the HTS undergoes remagnetisation under the

action of the coil field. Even though the coil's axial field (2.5 mT) is an order of magnitude weaker than the trapping field (20 mT), the component B_x (0.2–0.5 mT) is sufficient to reorient the Abrikosov vortices. In the steady state, the magnetisation becomes aligned with the coil field, leading to an effective susceptibility $\chi \approx +1$ and a force $F_x = \frac{V}{\mu_0} B_x \frac{\partial B_x}{\partial x}$ that is quadratic in the current and always points toward the coil centre.

Alternatively, the HTS ring can be fieldcooled inside the same coil. In that case, the trapped magnetic moment is aligned with the coil axis (horizontal). Upon subsequent energisation of the coil, the interaction between this prealigned moment and the coil's nonuniform field also produces an attractive force toward the coil centre, independent of the current sign. This configuration yields a force formula of the same quadratic form, $F_x = m_x \frac{\partial B_x}{\partial x}$. The trapped moment is $m_x = \left(B_{cooling} / \mu_0 \right) V \approx 0.0157$ A·m² (using the onaxis field 2.5 mT). The gradient of the axial field on the coil edge giving a force $F_x \approx 2.8$ mN.

The calculated force magnitude (2–3 mN) with a moving mass of 85 g gives an acceleration of about 0.03 m/s². Increasing the current to 10 A would raise the force to 0.1–0.2 N, producing accelerations of 1–2 m/s², sufficient for macroscopic motion of a small demonstrator.

A methodology has been developed to quantitatively model forces in an HTSring — PM guideway — coil system, considering remagnetisation even in weak applied fields. It is shown that attraction independent of current polarity arises from the reorientation of trapped vortices. The results provide guidelines for optimising coil parameters (current, geometry) to achieve controlled propulsion in HTSbased levitation systems. Future work will focus on pulsedcurrent operation and the use of ferromagnetic cores to enhance the force.

This work was funded by the Russian Science Foundation grant № 25-19-20141, https://rscf.ru/project/25-19-20141/.

Tailoring Magnetic and Magnetocaloric Properties in Ni—Co—Mn—Ti Melt-spun Ribbons via Annealing

A. S. Kuznetsov[1, a], A. V. Mashirov [1], V. I. Mitsiuk [2, b], A. P. Kamantsev [1], O. E. Kovalev [3, c], N. Yu. Nyrkov [3], R. A. Safonov [3], I. F. Gribanov [3], A. V. Golovchan [3]

[1]Kotelnikov Institute of Radioengineering and Electronics of RAS, Moscow, Russia
[2]Scientific and Practical Center for Materials of NAS, Minsk, Belarus
[3] A. A. Galkin Donetsk Institute for Physics and Engineering, Donetsk, Russia
[a]e-mail: *kuznetsovalserg@gmail.com*
[b]e-mail: *vmitsiuk@gmail.com*
[c]e-mail: *oleg_kovalev_2018@mail.ru*

Heusler alloys based on Ni—Mn are highly promising multicaloric materials due to their pronounced caloric effects during a 1st order magnetostructural phase transition (MSPT) between the low-temperature martensitic (*M*) and high-temperature austenitic (*A*) phases [1]. In recent years, their modifications with cobalt substituted for nickel (Ni_xCo_{50-x}) and titanium substituted for manganese (Mn_yTi_{50-y}), consisting exclusively of *3d*-elements, have gained particular relevance. Alloys of the Ni—Co—Mn—Ti system exhibit easily tunable martensitic transformation temperatures (T_t) and austenite Curie temperatures (T_C), high mechanical stability, and a significant phase transition entropy change ΔS_t, opening up wide possibilities for their application in mechanocaloric and magnetocaloric cooling [2; 3].

In the present work, we report on studies of the magnetic properties of amorphous ribbon samples of the Ni—Co—Mn—Ti system. Ribbon samples of nominal composition $Ni_{37}Co_{13}Mn_{35}Ti_{15}$ were fabricated by the melt-spinning method from a quartz ampoule with a 1 mm orifice, with a nozzletowheel distance of 0.5 mm at a wheel speed of 20 m/s (designated as NCMT20). The as-synthesized samples were divided into two groups: the first group was subjected to heat treatment at 1125 K for 15 minutes followed by quenching in ice water (annealed), while the second group was not heat-treated (as-cast). Studies of the magnetic properties of the NCMT20 melt-spun ribbons in the as-cast and an-

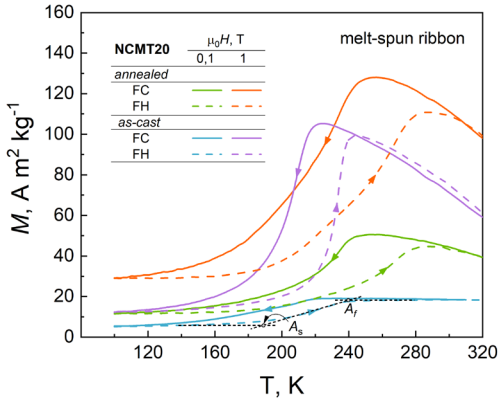


Fig. 1. Temperature dependences of magnetization M(T) for melt-spun ribbons in the as-cast state and after annealing, measured in applied magnetic fields of 0.1 and 1 T

nealed states were carried out using a Cryogenic Ltd. vibrating sample magnetometer by measuring the temperature dependences of magnetization $M(T)$ in the temperature range of the 1st order MSPT from 100 to 320 K under FC and FH protocols in applied magnetic fields of 0.1 and 1 T (see Fig. 1). From the presented FC dependencies, a shift of the first-order MSPT temperature $T_t^{A\rightarrow M}$ of the annealed samples relative to the as-cast ones towards the high-temperature austenitic phase region is observed, along with an increase in the maximum magnetization values across the entire range of applied magnetic fields. The PTs becomes more "broadened" with an increase in the width of the thermal hysteresis ΔT_{hys}. The sensitivity of the 1st MSPT temperature to the applied magnetic field during the martensitic transformation under the FC protocol was determined, yielding values of $dT_t^{A\rightarrow M}/dH = 2$ K T^{-1} for the annealed samples, compared to $dT_t^{A\rightarrow M}/dH = 2.69$ K T^{-1} for the ascast samples. The entropy change ΔS_t during the 1st order MSPT was estimated, with values upon the $A\rightarrow M$ transition in a magnetic field of 1 T amounting to 40.7 J (kg K)$^{-1}$ for the as-cast sample and 43.6 J (kg K)$^{-1}$ for the annealed sample, which is in good agreement with literature data for Ni—Co—Mn—Ti systems [4, 5]. The influence of heat treatment on the magnetic and magnetocaloric properties of the synthesized samples is demonstrated.

The study was supported by a grant from the Russian Science Foundation № 25-19-00942, https://rscf.ru/project/25-19-00942/

[1] Liu, J., Gottschall, T., Skokov, K. et al. Nature Mater 11, 620–626 (2012).

[2] Y. Shen, Z. Wei, W. Sun, Y. Zhang, E. Liu, J. Liu. *Acta Mater*. 188, 677–685 (2020).

[3] A. Aznar, A. Gràcia-Condal, A. Planes et al. *Phys. Rev. Mater*. 3 (4) (2019) 044406.

[4] Beckmann, B., Taubel, A., Gottschall, T. et al. *Acta Mater*. 282, 120460, (2025).

[5] Bez, H. N., Pathak, A. K., Biswas, A. et al. *Acta Mater*. 173, 225–230 (2019).

Effect of Heat Treatment on the Austenite Microstructure and Martensitic Transformation of Rapidly Quenched Ribbons of Heusler Alloy $Ni_{37}Co_{13}Mn_{35}Ti_{15}$

D. D. Kuznetsov[1, a], E. I. Kuznetsova[2, b], A. P. Kamantsev[1], D. V. Danilov[3, c], G. A. Shandryuk[4, d], V. V. Koledov[1]

[1] Kotelnikov Institute of Radioengineering and Electronics of RAS, Moscow, Russia

[2] M. N. Mikheev Institute of Metal Physics of the Ural Branch of the Russian Academy of Sciences, Yekaterinburg, Russia

[3] IRC for Nanotechnology, Research Park, St. Petersburg State University, St. Petersburg, Russia

[4] A. V. Topchiev Institute of Petrochemical Synthesis of Russian Academy of Sciences, Moscow, Russia

[a] e-mail: *kuznetsov.dmitry89@gmail.com*

[b] e-mail: *dk1964@yandex.ru*

[c] e-mail: *d.danilov@spbu.ru*

[d] e-mail: *gosha@ips.ac.ru*

Currently, a significant number of studies have been published on the research and development of functional materials based on all-d-metal Heusler alloys, which exhibit attractive calorimetric properties for energy applications, such as magnetic refrigeration devices with improved cyclic performance [1; 2]. To better tailor the MF to specific

applications, stoichiometry changes or partial atomic substitutions can be used, so attempts have been made to alloy elements to improve the magnetocaloric effect. The $Ni_{2-x}Co_xMn_{1.4}Ti_{0.6}$ system was presented by the authors of [3], who used the strategy of introducing Co atoms into Ni sites in the Ni—Mn—Ti system, which led to the emergence of the first FSMAs among Heusler alloys consisting of only d-metals.

In this study, we conducted an *in situ* transmission electron microscopy and high-resolution transmission electron microscopy study of the A↔M transformation processes in $Ni_{37}Co_{13}Mn_{35}Ti_{15}$ alloys to elucidate the microstructure and its role in phase transformations of metamagnetic shape-memory alloys consisting exclusively of d-metals. The influence of heat treatment conditions on the structural state of the ribbons was examined.

The study was supported by a grant from the Russian Science Foundation. № 25-19-00942, https://rscf.ru/project/25-19-00942/.

[1] H.-L. Yan, L.-D. Wang, H.-X. Liu, X.-M. Huang, N. Jia, Z.-B. Li, B. Yang, Y.-D. Zhang, C.Esling, X.Zhao, L.Zuo. *Materials & Design.* 184, 108180 (2019).

[2] T. Bachagha, J.-J. Suñol. *Metals*. 13, 111 (2023).

[3] Z. Y. Wei, E. K. Liu, J. H. Chen, Y. Li, G. D. Liu, H. Z. Luo, X. K. Xi, H. W. Zhang, W. H. Wang, G. H. Wu. *Appl. Phys. Lett*. 107, 022406 (2015).

Development of Measurement Methods and Study of the Electrodynamic Characteristics of Multiferroics in the Microwave Range Using Inductive-gap Cells

Yu. A. Lupitskaya[1, a], A. A. Fedii [1], I. V. Bychkov [1], D. A. Kalganov [2, b]

[1]Chelyabinsk State University, Chelyabinsk, Russian Federation
[2]ITMO University, Kronverksky Pr. 49, bldg. A, St. Petersburg, Russian Federation
[a]e-mail: *lupitskaya@gmail.com*
[b]e-mail: *kalganov@itmo.ru*

The task of developing new generation devices based on bulk multiferroics and studying their electrodynamic parameters is becoming increasingly relevant and is of scientific and practical interest in the field of modern physical materials science and radio engineering [1].

This paper presents the results of studies of synthesized materials based on various types of multiferroics — lead ferroniobate ceramics and lanthanum manganites. Experimental data on their structure and properties at various stages of synthesis are presented. Electrodynamic characteristics were measured in the 7.5–12 GHz microwave range, including permittivity and magnetic permeability, reflection coefficient, and magnetization over a wide temperature range, including the points of second-order phase transitions. Methods for measuring electric and magnetic permeability were developed and tested using planar inductive slot resonators (Fig. 1), various microwave waveguides, and constant and alternating magnetic fields.

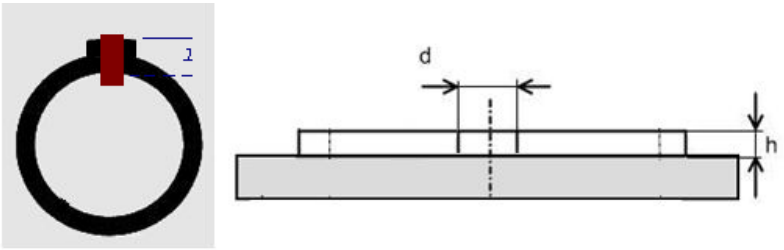


Fig. 1. Schematic diagram of the permittivity measurement in a flat resonator

To account for edge effects and the properties of the substrate (foil-clad fiberglass), measurements were conducted on materials with known permittivity. The studies were performed using specially developed automated hardware and software systems with high accuracy and high-speed processing.

[1] C. W. Nan et al. *J. App. Phys*. 103, 031101 (2008).

Effect of Micro- and Nanosized Refractory Carbide Additives on the Structure and Properties of Deposited Metal

Yu. A. Lupitskaya[1,a], S. I. Saunina[1], A. V. Butakov[1], L.-S. D. Galeeva[1]

[1]Chelyabinsk State University, Chelyabinsk, Russian Federation
[a]e-mail: *lupitskaya@gmail.com*

The formation of a structure with a well-dispersed and separated carbide phase with fine, uniformly sized grains is a prerequisite for producing alloys with high strength properties. According to [1; 2], the introduction of composite microgranules containing nanosized tungsten carbide particles into the ceramic flux contributes to the modification of the structure of the low-carbon weld metal and leads to an increase in its impact toughness by 21–24% at subzero temperatures.

The study demonstrates the effectiveness of using micro- and nanoscale refractory carbide particles in welding flux to modify the weld metal structure. It was also found that all modifiers contribute to improved physical and mechanical properties of the deposited metal compared to an unmodified sample.

The average hardness values of the layers welded last are practically the same when modified with micro- and nano-sized additives, and their increase relative to the unmodified sample of the deposited metal in the case of samples alloyed with particles of refractory carbides was 16% with the addition of titanium carbide particles; 20% with the content of zirconium carbide particles and 40% when using tungsten carbide particles.

The use of nanoscale modifier particles proves to be more cost-effective for serial and mass production. It has been found that the addition of composite granules reduces the grain size of the deposited metal, and its structure becomes more uniform. Preliminary studies of the mechanical properties of deposited metal using fluxes with various modifiers will enable the production of structural materials with increased strength.

[1] À. S. Troshkov, G. N. Sokolov, S. S. Sycheva, V. I. Lysak. *News of Volgograd State Technical University*. 6 (2012) (In Russ.).

[2] N. V. Kobernik, R. S. Mikheev, À. S. Pankratov, À. À. Linnik. *Engineering Bulletin*. 4 (2013) (In Russ.).

Numerical Modelling of a Multi-cascade Magnetocaloric Device Operation

I. V. Maltsev[1, a], I. V. Bychkov[1], M. V. Matyunina[1], V. V. Koledov[1,2]

[1]Chelyabinsk State University, Chelyabinsk, Russia
[2]Kotelnikov Institute of Radioengineering and Electronics of RAS, Moscow, Russia
[a]e-mail: malts_iv@mail.ru

The first prototypes of cooling devices based on materials exhibiting the magnetocaloric effect (MCE) at room temperatures emerged half a century ago [1]. Since then, a large number of experimental devices with various designs based on magnetocaloric materials have been developed [2], the efficiency of which can theoretically reach 30–60% [3]. Moreover, the technology of solid-state cooling devices is more environmentally friendly compared to vapor-compression systems.

In this work, we consider the magnetic cooling cycle of a simple magnetocaloric device (MCD) consisting of several cascades.

The operation scheme of the MCD consists of the following processes:

1. Introducing the working bodies WB_1, …, WB_i (made of magnetocaloric material) into the magnetic field, which results in an increase of their temperature.

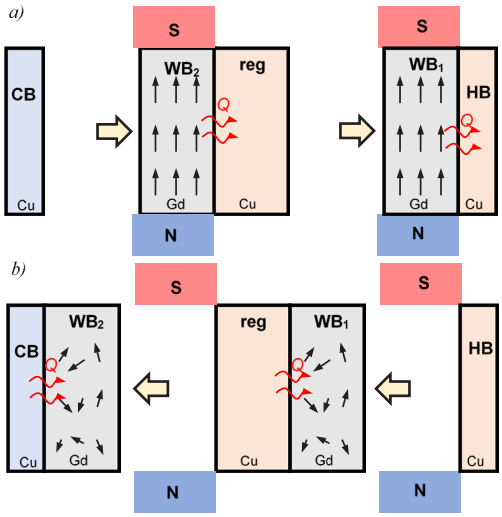


Fig. 1. MCD operation with two cascades: (a) heat removal from WB_1 and WB_2; (b) heat removal from CB and regenerator

2. Contact of WB_1 with the regenerator (reg), …, WB_i with the hot body (HB) for heat removal (Fig. 1a). At this time, temperature distribution relaxation occurs in the cold body (CB).

3. Removing WB_1, …, WB_i from the magnetic field leads to a decrease in their temperature.

4. Contact of WB_1 with the CB, …, WB_i with the regenerator for heat removal from the CB and the regenerator (Fig. 1b). At this time, temperature distribution relaxation occurs in the HB.

During the numerical calculation of the MCD operation, we solved the one-dimensional heat conduction equation at each step via the sweep method with appropriate boundary conditions.

$$\rho c \frac{\partial T}{\partial t} = \lambda \frac{\partial^2 T}{\partial x^2}.$$

Copper was used for CB, HB, and regenerator; gadolinium for WB. For Gd, we accounted for heat capacity's temperature dependence in a 1,5 T field and without it [4]. The temperature dependence of the MCE magnitude $\Delta T_{MCE}(T)$ for Gd was obtained from experimental data [5]. We then calculated the minimum T_{CB} for various values of the initial temperature T_0 and ambient temperature T_{air} in a 5-cascade MCD.

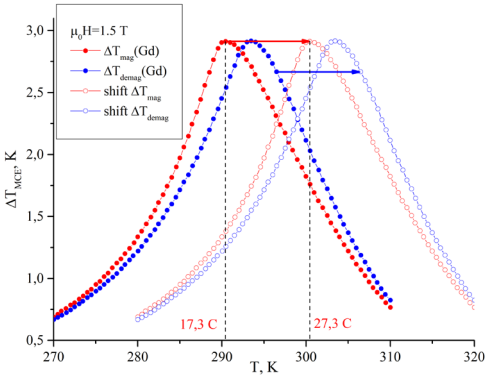


Fig. 2. $\Delta T_{MCE}(T)$ for Gd in a $\mu_0 H$=1.5 T magnetic field (filled circles) [5], and $\Delta T_{MCE}(T)$ obtained by a temperature shift (open circles)

After that, we theoretically determined the optimal $\Delta T_{\text{MCE}}(T)$ for each cascade individually, as shown in Fig. 2. This is equivalent to the case where WB_1, …, WB_5 are made of different materials with the required $\Delta T_{\text{MCE}}(T)$. The results are presented in Table 1.

Table 1

Calculation of the minimum TCB for various initial temperatures T_0

$\Delta T_{\text{MCE}}(T)$ \ T_0, T_{air}		17	19	21	23	25
as Gd for WB_1, …, WB_5	$T_{\text{CB_min}}$	9,75	10,88	12,23	13,67	15,51
	$\Delta T_{\text{CB-HB}}$	7,25	8,12	8,77	9,33	9,49
as Gd for WB_1, while for WB_2 – WB_5 with the temperature shift	$T_{\text{CB_min}}$	5,78	7,37	9,25	11,26	13,32
	$\Delta T_{\text{CB-HB}}$	11,22	11,63	11,75	11,74	11,68

Calculation results indicate that using different materials with optimal $\Delta T_{\text{MCE}}(T)$ for the WB in a multi-cascade MCD allows achieving both a lower T_{CB} and a constant CB-HB temperature difference $\Delta T_{\text{CB-HB}}$ across various T_0 and T_{air}.

This work was funded by the Russian Science Foundation grant № 25-19-20141, https://rscf.ru/project/25-19-20141/.

[1] G. V. Brown. *Int. J. Refrigeration*. 47, 3673–3680 (1976).

[2] B. Yu, M. Liu, P. W. Egolf, A. Kitanovski. *Int. J. Refrigeration*. 33(6), 1029–1060 (2010).

[3] B. F. Yu, Q.Gao, B.Zhang, X. Z. Meng, Z.Chen. *Int. J. Refrig*. 26, 1–15 (2003).

[4] S. Y. Dan'kov, A. M. Tishin, V. K. Pecharsky, K. A. Gschneidner, *Phys. Rev. B.* 57, 3478 (1998).

[5] A. M. Tishin, Y. I. Spichkin, Bristol, Philadelphia, 475 (2003).

Experimental Refrigeration Cycles of a Magnetic Refrigerator Based on $GdNi_2$ Alloy

A. V. Mashirov[1, a], K. A. Kolesov[1], A. S. Kuznetsov[1], I. I. Musabirov[2, b]

[1] Kotelnikov Institute of Radioengineering and Electronics of Russian Academy of Sciences, Moscow, Russia

[2] Institute for Metals Superplasticity Problems of Russian Academy of Sciences, Ufa, Russia

[a]e-mail: *a. v.mashirov@mail.ru*

[b]e-mail: *irekmusabirov@mail.ru*

Recently, intensive research has been conducted into the development of magnetic refrigerators operating at room temperatures [1] and cryogenic magnetic refrigerators [2]. To create the latter, information on heat transfer in a vacuum between periodically contacting surfaces is necessary. The goal of this study is to implement a single-stage cryogenic refrigeration cycle using experimental data to evaluate energy efficiency parameters. To this end, the non-stationary process of heat transfer from a solid working body to a heat sink under high vacuum conditions is considered.

The working body is a magnetocaloric material $GdNi_2$ and the heat sink is a copper disk or cylinder. Heat exchange between the working fbody and heat sink is achieved through contact thermal conductivity. Experimental data on the temperature change of the heat sink and working fluid with the mechanical thermal switch turned on were obtained

through direct measurements. Based on the obtained experimental data, a Brayton refrigeration cycle was partially constructed and the cooling capacity was calculated for various initial temperature differences between the working fluid and heat sink ($\Delta T_{span} \approx 1–3$ K) or when exposed to an external magnetic field of 5 T in the temperature range of 74–78 K.

It was shown that the time to achieve thermal equilibrium for the contact pair of a mechanical thermal switch at an initial heat sink temperature of 75 can range from 12 to 80 seconds, depending on the thermal interface used and the ratio of weight and size parameters. The paper provides a comparison with other studies and similar ones. The magnitude of the magnetocaloric effect for the $GdNi_2$ working fluid in magnetic fields of 3, 5, and 10 T and a temperature range of 48–105 K was experimentally determined. The maximum value of the magnetocaloric effect is 2.87 K at an initial temperature of $T = 75$ K in a magnetic field of 5 T.

The study was supported by a grant from the Russian Science Foundation № 25-19-00942, https://rscf.ru/project/25-19-00942/

[1] Liang J. et al. *Appl. Therm. Eng*. 284, 129144 (2025).

[2] L. Cirillo et al. *Int. J. Refrig*. 179, 184–203 (2025).

Correlation of Lattice Expansion, Phonon Softening, and Superconducting Critical Temperature in Pd_2YSn

M. V. Matyunina[1, a], V. V. Sokolovskiy[1], V. D. Buchelnikov[1]

[1]Chelyabinsk State University, Chelyabinsk, 454001, Russia
[a]e-mail: *matunins.fam@mail.ru*

Based on experimental data on the lattice parameter (a^{exp}) that affects the superconducting transition temperature in the Pd_2YSn alloy [1–3], the phonon dispersion spectra were investigated. Calculations were performed for the $L2_1$ (Fm-3m) crystal lattice within the framework of the density functional theory implemented in the VASP software package [4;

5]. The exchange-correlation interaction was taken into account in the meta-GGA — SCAN approximation [6]. The phonon dispersion relations were obtained from density functional theory simulations using the finite displacement method, as implemented in the Phonopy package [7]. For all alloys, a 32-atom supercell was employed to calculate the second-order interatomic force constants, ensuring accurate results.

Fig. 1 presents the results of phonon spectrum calculations for Pd_2YSn alloy with different lattice constants. The branches do not extend into the negative region along the *y* axis, indicating the dynamic stability of the Pd_2YSn alloy for all three lattice parameters considered. The difference in lattice parameters is less than 0.3%, so the branches visually almost merge. Analysis of the phonon spectrum of the Pd_2YSn alloy reveals several features indicative of enhanced electron-phonon interaction. With increasing lattice parameter, phonon softening (a decrease in mode frequencies) is observed, particularly in the acoustic branches and in the mid-frequency range. Additionally, optical modes dominated by Pd atoms (approx. 1–3 THz) and Sn atoms (3–4 THz) are present. Flat dispersion regions in the W-K and L-U zones are visible, indicating localized vibrations, with the L-U flat bands notably associated with Sn modes. These effects lead to an increased phonon density of states, particularly in the 1–3 THz range, which correlates with the rise in superconducting critical temperature from 3.5 K (at 6.702 Å) [3] to 4.7 K

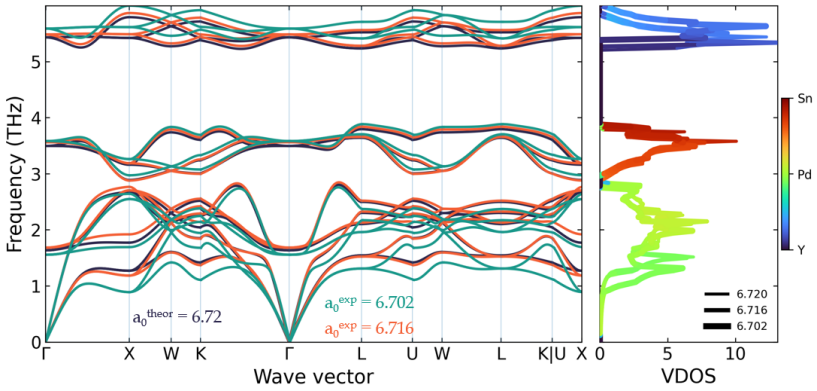


Fig. 1. Phonon dispersion relations for the Pd_2YSn compounds along symmetry lines of the face-centered cubic Brillouin zone with partial and total vibration density of states (VDOS). The aquamarine and orange colors of the branches correspond to two experimental values of lattice constants [1; 3] 6.716 Å and 6.702 Å, respectively. The dark line corresponds to the theoretical value

(at 6.716 Å) [1], confirming the key role of lattice softening in enhancing superconductivity.

This work was supported by the Russian Science Foundation Project № 25-19-20141 (https://rscf.ru/project/25–19–20141/).

[1] T. Klimczuk, C. H. Wang, K. Gofryk, et al. *Phys. Rev. B.* 85 (17), 174505 (2012).

[2] J. H. Wernick, G. W. Hull, T. H. Geballe, et al. *Mater. Lett.* 2 (2), 90–92 (1983).

[3] J. L. Jorda, M. Ishikawa and J. Muller. *J Less-Common Met*. 107, 321–330 (1985).

[4] G. Kresse, J. Furthmüller. *Phys. Rev. B.* 54, 11169 (1996).

[5] G. Kresse, D. Joubert. *Phys Rev B*. 59, 1758–1775 (1999).

[6] J. Sun, A. Ruzsinszky, J. P. Perdew. *Phys. Rev. Lett*. 115, 36402 (2015).

[7] A. Togo. *J. Phys. Soc. Jpn.* 92, 12001 (2023).

Magnetostructural Phase Transitions in Substituted Manganese Arsenide

S. M. Baraishuk[1, a], T. M. Tkachenka[1], A. V. Golovchan[2, b], A. V. Mashirov[3, c], A. V. Gurbanovich[4], A. L. Zhaludkevich [4], V. I. Mitsiuk[4, d]

[1] Belarusian State Agrarian Technical University, Minsk, Belarus
[2] Donetsk Institute for Physics and Engineering named after O. O. Galkin, Donetsk, Russia
[3] Kotelnikov Institute of Radioengineering and Electronics of RAS, Moscow, Russia
[4] SSPA "Scientific-Practical Materials Research Centre of NAS of Belarus", Minsk, Belarus
[a]e-mail: *oldtaty@bsatu.by*
[b]e-mail: *golovchan@donfti.ru*
[c]e-mail: *a. v.mashirov@mail.ru*
de-mail: *mitsiuk@physics.by*

Recently, much attention has been paid to the study of magnetostructural phase transitions, which are accompanied by a change in the elec-

tronic states density near the Fermi surface [1–3]. As the transition progresses, anisotropic deformation of the crystal lattice and heat generation occur. Therefore, to understand the mechanism of such phase transitions it is necessary to study structural and magnetic characteristics of the sample and their dependence on temperature, pressure, alloying, as well as the determination of the magnetostructural phase transition heat.

The useful model objects for this kind of research are manganese arsenide and its alloys since the whole range of magnetostructural first and second kind phase transitions have place in them. Earlier we have studied zinc substituted manganese pnictides [4] due to the possibility of the magnetocaloric effect existence in them.

The purpose of this work is to study the influence of small substitutions in the arsenic sublattice on the magnetostructural phase transitions in MnAs-based alloys. Phosphorus was chosen as substituted element. The outer electron shells of phosphorus and arsenic atoms are similar, therefore, these atoms are well interchangeable which makes it possible to form a single-phase solid solution. At the same time, the size of the divergent phosphorus atom allows to modify the transition. In this work the structural parameters and magnetic properties of $MnAs_{0.93}P_{0.07}$ in strong magnetic fields up to 14 Tesla in the phase transition region are defined.

The work was supported by Grant № T25UZB-053 (Belarusian Republican Foundation for Fundamental Research).

[1] S. Gama, A. Coelho, A. Campos. *Phys. Rev. Lett.* 93, 237202 (2004).

[2] L. Tocado, E. Palacios, R. Burriel. *J.Appl.Phys*. 105, 093918 (2009).

[3] A. Magnus, G. Carvalho, A. A. Coelho [et al.] *Eur. Phys. J. B*. 68, 67 (2009).

[4] V. I. Mitsiuk, A. L. Zhaludkevich, V. I. Val'kov et al. *Phys. Met. Metallogr*. 125, 1832 (2024).

Investigation of Thermoelectric and Magnetostructural Properties of the $Ni_{15}Mn_{13}Sn_4W$ Heusler Alloy

D. M. Moiseev[1,a], V. V. Sokolovskiy[1], V. D. Buchelnikov[1]

[1]Chelyabinsk State University, Chelyabinsk, Russia
[a]e-mail: *danil174821@gmail.com*

Ni—Mn—Sn Heusler alloys are promising materials for spintronics and thermoelectrics due to their flexible electronic structure. One of the key challenges in modern materials science is the creation of efficient thermoelectrics based on the "phonon glass — electron crystal" principle (high conductivity combined with low thermal conductivity).

This work investigates the effect of tungsten (W) doping on the energetic stability, magnetic order, and martensitic transition temperature in Ni-Mn-Sn alloys, which was already considered earlier [1]. The objects of study were Heusler alloys with the compositions $Ni_{15}Mn_{13}Sn_4$ (base) and $Ni_{15}Mn_{13}Sn_4W$ (doped). The investigation of alloy properties was conducted within the framework of Density Functional Theory (DFT) using the VASP software package for geometry optimization and Density of States (DOS) calculations. Modeling was performed on 32-atom supercells under various tetragonal distortions (c/a ranging from 0.8 to 1.5). To evaluate the Seebeck coefficient and electronic thermal conductivity, semi-classical transport theory (BoltzTraP2) was applied. It was confirmed that for both alloys, the most energetically favorable state at $c/a = 1.35$ is the tetragonal martensitic phase with ferrimagnetic ordering (FiM-3).

The substitution of a Ni atom with a 5*d*-element (tungsten) leads to a change in the valence electron concentration and strong hybridization of *d*-orbitals. This "elevates" the energy of the martensitic phase relative to the cubic phase. Calculations showed that tungsten doping reduces the martensitic transition temperature T_M from 348 K to 290 K. The resulting difference ($\Delta T = 58$ K) is in good agreement with available experimental data. It was established that the introduction of W makes the system less sensitive to the type of ferrimagnetic ordering in the tetragonal phase, lowering the energy barrier between the FiM-2 and FiM-3 configurations.

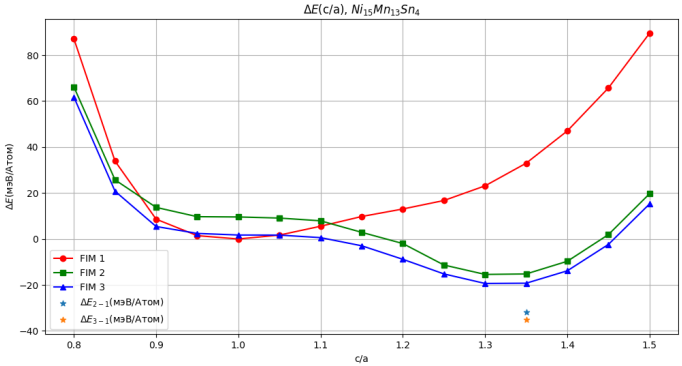


Fig. 1. The dependence of the total energy ΔE of the $Ni_{15}Mn_{13}Sn_4$ alloy unit cell on the magnitude of the tetragonal distortion c/a

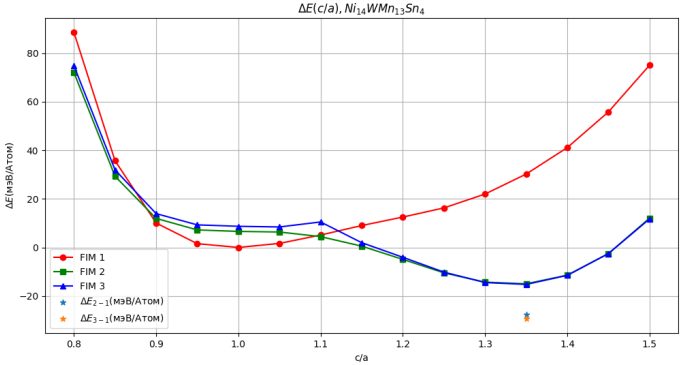


Fig. 2. The dependence of the total energy ΔE of the $Ni_{15}Mn_{13}Sn_4W$ alloy unit cell on the magnitude of the tetragonal distortion c/a

It has been demonstrated that doping with heavy 5*d*-elements (W) allows for effective control of the structural transition temperature in Heusler alloys. This opens up possibilities for tuning materials to specific temperature ranges, which is critical for developing shape-memory devices and magnetocaloric systems operating at room temperature.

This work was supported by the Russian Science Foundation (project No 25-12-20024, https://rscf.ru/en/project/25-12-20024/).

[1] A. G. Gamzatov, A. B. Batdalov, V. V. Sokolovskiy et al. J. Alloy. Compd. 1008 176748 (2024).

The Influence of Temperature Field on the Relaxation Time of Order Parameters During Martensitic Phase Transition in Ni—Mn—In—V and Ni—Co—Mn—Ti Alloys

E. V. Morozov[1, a], V. D. Poimanov[2, b]

[1] Kotelnikov Institute of Radioengineering and Electronics of the Russian Academy of Sciences, Moscow, Russia
[2] Bauman Moscow State Technical University, Moscow, Russia
[a]e-mail: *evgvmorozov@gmail.com*
[b]e-mail: *vladislav-poymanow@yandex.ru*

Development and study of functional materials exhibiting martensitic-type phase transitions are important areas of modern condensed matter physics. This paper describes a theoretical approach to the kinetics of first- and second-order phase transitions using the Landau — Khalatnikov equation.

The studied Ni—Mn—In—V and Ni—Co—Mn—Ti alloys, in addition to phase transitions in the structural subsystem, also undergo transformations in the magnetic subsystem. Therefore, to fully describe these processes, the Landau expansion is used with two order parameters: the structural one (strain ε) and the magnetic one (magnetization M).

The behavior of the order parameter **ε** near the first-order structural phase transition is studied for different temperature fields.

Landau thermodynamic potential:

$$F = a\left(\frac{T}{T_c} - 1\right)\frac{\varepsilon^2}{2} - 2b\frac{\varepsilon^3}{3} + c\frac{\varepsilon^4}{4}\,. \qquad (1)$$

Landau — Khalatnikov equation:

$$\gamma\frac{\partial\varepsilon}{\partial t} = -\frac{\partial F}{\partial\varepsilon}\,. \qquad (2)$$

Relaxation time of the order parameter. Substituting (1) into (2), we obtain: $\tau = \frac{\gamma}{c}$

$$\tau\frac{\partial\varepsilon}{\partial t}=-\varepsilon\left(\varepsilon^2-2\beta\varepsilon+\alpha\left(\frac{T}{T_c}-1\right)\right), \tag{3}$$

where α and β can be recalculated if a, b *and* c.

Temperature regimes

1. The sample is in a homogeneous periodic temperature field with period t_0:

$$T(t)=T_c+\cdot T\sin\left(\frac{2\pi}{t_0}t\right), \tag{4}$$

$\Delta T=20K$. ΔT is the temperature width of the phase transition.

Landau — Khalatnikov equation:

$$\frac{\partial\varepsilon}{\partial t}=-\frac{1}{\tau}\varepsilon\left(\varepsilon^2-2\beta\varepsilon+\alpha\frac{T_1-T_c+\Delta T\sin\left(\frac{2\pi}{t_0}t\right)}{T_c}\right), \tag{5}$$

where T_1 is the temperature at the onset of the phase transition.

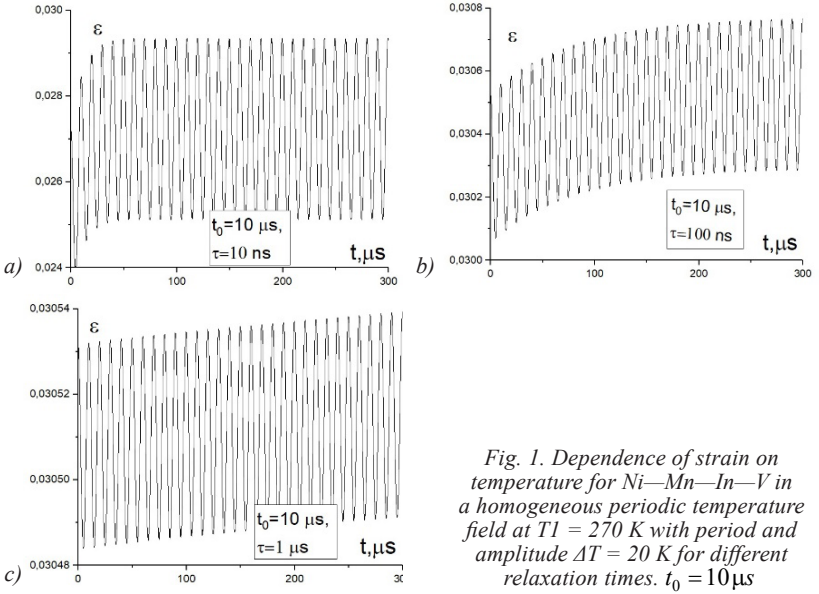


Fig. 1. Dependence of strain on temperature for Ni—Mn—In—V in a homogeneous periodic temperature field at T1 = 270 K with period and amplitude ΔT = 20 K for different relaxation times. $t_0=10\mu s$

Fig. 1 clearly shows the dynamics of the system approaching the equilibrium state.

2. Rectangular temperature pulse: an increase in the interval of 30…60 μs. Initial temperature. $\Delta T = 20 K T_1 = 275$ °C.

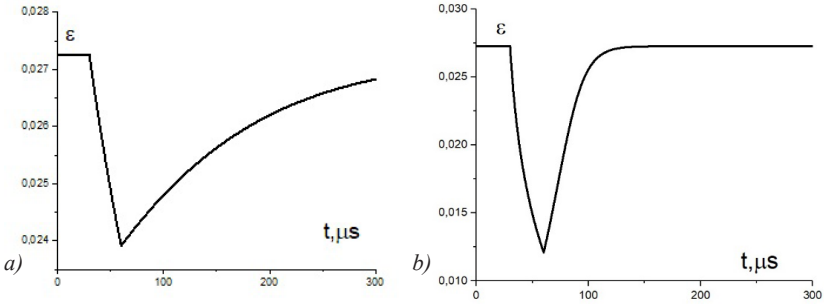


Fig. 2. Dependence of strain on temperature for Ni—Mn—In—V under a single rectangular temperature pulse at T_1 = 275 K with amplitude ΔT = 20 K for different relaxation times

Fig. 2 presents graphs constructed in an analogous way using the method described above.

The study was supported by a grant from the Russian Science Foundation № 25-19-00942, https://rscf.ru/project/25-19-00942/

Magnetomechanical Response of Martensitic Transformation in Ni—Mn—Ga—Si Alloys Across Various Structural States

K. K. Kirilyuk[1], R. Y. Gaifullin[1], V. S. Kalashnikov[2], A. V. Nesolenov[2], Yu. S. Koshkidko[3], E. T. Dilmieva[4], S. V. Taskaev[5], I. I. Musabirov[1, a]

[1]Institute for Metals Superplasticity Problems of RAS, Ufa, Russia
[2]Kotelnikov Institute of Radioengineering and Electronics, RAS, Moscow, Russia
[3]High Field Magnet Laboratory, Nijmegen, Netherlands
[4]Laboratoire National des Champs Magnétiques Intenses, CNRS, Grenoble, France
[5]Chelyabinsk State University, Chelyabinsk 454001, Russia
[a]e-mail: *irekmusabirov@mail.ru*

Heusler alloys exhibit functional properties with potential for practical applications, but their poor mechanical performance and limited thermal stability hinder their widespread use. There are a several methods to increase the thermocycling strength of alloys. The most common method is alloying with elements such as Fe, Cr, Co, and others. Another approach is the formation of a secondary phase, which is most often concentrated along the boundaries of large grains. The authors of the work are developing a method for transforming a as-cast coarse-grained structure into a bimodal "necklace"-type structure by thermomechanical treatment. The treatment may lead to decrease the values of the functional effects due to defects of deformation origins. It is necessary to evaluate the influence the structure type on the thermal characteristics of martensitic transformation.

Thermomechanical treatment by multi-axial isothermal forging significantly improves the mechanical properties of polycrystalline $Ni_{56.2}Mn_{18.8}Ga_{23.2}Si_{1.8}$ alloy. Forging of the equiaxed coarse-grained structure at 973 K with a true strain of $e = 3.19$ results in the formation of a bimodal "necklace"-type microstructure consisting of coarse grains (100–300 μm) surrounded by a dynamically recrystallized fine-grained interlayer. Concurrently, the thermomechanical strength increases from 100 to 300 MPa. Thermal analysis shows that the characteristic temperatures of the martensitic transition decrease by 12–15 K upon forging, while magnetization is reduced by ~7%. The sensitivity of the martensitic

transition temperature to macro-stresses and magnetic field remains comparable for both coarse-grained and bimodal states. The results indicate that the bimodal structure enhances thermocycling strength and stabilizes the functional response, improving the practical applicability of Heusler alloys

The present work was accomplished according to the state assignment of IMSP RAS.

Magnetocaloric Effect in Er and Ho in Cyclic Magnetic Fields

A. A. Mukhuchev[1, a], A. M. Aliev[1]

[1] Institute of Physics named after H. I. Amirkhanov DFRC RAS, Makhachkala, Russia

[a] e-mail: *mukhuch87@mail.ru*

The development of solid-state magnetic coolers based on the magnetocaloric effect (MCE) is a priority area in modern condensed matter physics and cryogenic engineering. In the low-temperature range, rare-earth metals — particularly holmium (Ho) and erbium (Er) — are of particular interest due to their complex magnetic structures, multi magnetic phase transitions, and substantial MCE values. Although the MCE in Ho and Er has been extensively studied under quasi-static conditions and strong magnetic fields (tens of kOe), the practical operating conditions of magnetic refrigerators require materials to withstand cyclic magnetization–demagnetization processes under moderate to weak fields (≤15 kOe). The weak-field regime (≤3 kOe) is particularly important for fundamental studies, as it probes the initial magnetization stage and reveals critical behavior near magnetic phase transitions.

In the 10–30 K temperature range, both materials undergo first-order magnetostructural phase transitions accompanied by significant changes in lattice parameters. Under such conditions, cyclic magnetic field exposure can induce reversible or irreversible degradation of magnetostructu-

ral properties, a key factor in assessing the materials' practical viability. To address this challenge, we developed and implemented a modulation technique for direct measurement of the MCE in the cryogenic temperature range under cyclic magnetic fields with amplitudes up to 3 kOe.

The temperature dependence of the adiabatic temperature change, ΔT_{ad}(T), was obtained for polycrystalline Ho and Er samples. Under a maximum cyclic field amplitude of 3 kOe, the peak adiabatic temperature changes $\Delta T_{ad(max)}$ reached 0.26 K and 0.18 K for Er and Ho respectively. Temporal measurements of ΔT_{ad}(t) at constant temperatures within the magnetostructural transition region demonstrate excellent cyclic stability of the MCE under repeated magnetic field cycling.

The results confirm the high sensitivity of the proposed technique, even in weak magnetic fields, and demonstrate its effectiveness for cryogenic applications. The findings highlight the potential of Ho and Er as active magnetic refrigerants for low-field magnetic cooling systems operating in the 4–30 K range, with applications in infrared detectors, quantum devices, and superconducting magnets. Furthermore, investigating the MCE in weak fields provides new insights into critical phenomena and phase-transition dynamics in rare-earth metals.

The study was supported by the Russian Science Foundation, grant № 24-12-00362, https://rscf.ru/en/project/24-12-00362/

Architecting the Magnetocaloric Future: from Rare-earth and Mn-based Alloys to Flexible Functional Materials for Sustainable Cooling Applications

R. Nagalakshmi[1, a], A. Dzubinska[2], M. Reiffers [2,3]

[1] Intermetallics and NLO Laboratory, Department of Physics, National Institute of Technology Tiruchirappalli, Tamil Nadu, India 625 015
[2] Faculty of Humanities and Natural Sciences, Presov University, 080 01 Presov, Slovakia
[3] Institute of Experimental Physics, Slovak Academy of Science, Kosice, Slovakia
[a] e-mail:*nagaphys@yahoo.com; nagalakshmi@nitt.edu*

The growing environmental concerns associated with conventional vapor-compression refrigeration systems, primarily due to their reliance on high global warming potential refrigerants, necessitate the development of sustainable cooling technologies. Magnetic refrigeration, based on the Magnetocaloric Effect (MCE), offers a promising alternative owing to its zero direct greenhouse gas emissions and high energy efficiency. The MCE is characterized by the isothermal entropy change ($-\Delta S_m$) and relative cooling power (*RCP*), which are critical parameters for evaluating refrigerant performance.

In this lecture, we present the synthesis and investigation of rare-earth and non-rare earth based intermetallic compounds prepared via the Arc Melting technique at our laboratory, NITT, India. Rare-earth compounds based on Gd, Tb, Dy, and Ho have been systematically explored for low-temperature magnetic refrigeration. Multi-phase engineering in Gd- and Dy-based systems enables successive magnetic transitions, resulting in a table-like MCE response and enhanced *RCP*. In contrast, Tb- and Ho-based compounds exhibit large entropy changes; notably, Ho_6FeSb_2 demonstrates $-\Delta S_m$ = 6.37 J/kg·K and *RCP* = 265.6 J/kg under a 2 T magnetic field.

For room-temperature applications, Mn-based materials have been tailored using chemical pressure through elemental substitution. Cu-doped Mn_5Ge_3 exhibits a second-order magnetic transition with negligi-

ble hysteresis ($-\Delta S_m$ = 2.89 J/kg·K, *RCP* = 131.4 J/kg at 2 T), whereas Ag-doped $Ni_{50}Mn_{37}In_{13}$ undergoes a first-order martensitic transition with a significant entropy change ($-\Delta S_m$ = 4.98 J/kg·K), accompanied by markedly reduced thermal and magnetic hysteresis.

Importantly, this study extends beyond bulk materials to emphasize functional material design for practical applications. Melt-spun ribbons derived from Mn-based alloys exhibit refined microstructure and enhanced magnetic response, making them promising candidates for efficient heat exchange in magnetic refrigeration systems. Furthermore, we report on the synthesis of electrospun polymer-based composite fibers incorporating magnetocaloric alloy particles. These flexible and mechanically robust fibrous materials represent a significant step toward scalable device architectures, offering improved surface area, thermal exchange efficiency, and structural adaptability.

Overall, this work provides comprehensive understanding of magnetocaloric materials and their implementation in real-world cooling devices by advancing ribbons and electrospun composites as next-generation functional materials for magnetic refrigeration applications.

[1] T. P. Rashid, K. Arun, I. Curlik, S. Ilkovic, M. Reiffers, A. Dzubinska, and R. Nagalakshmi. *J. Appl. Phys*. 122 093903(2017).

[2] S. R. Athul, K. Arun, S. Swathi, U. D. Remya, M. Reiffers, A. Dzubinska and R. Nagalakshmi. *Physica B.* 673 415471(2024).

[3] S. Swathi, K. Arun, U. D. Remya, M. Reiffers, A. Dzubinska and R. Nagalakshmi. *J. Magn. Magn. Mater*. 586 171224(2023).

[4] S. Swathi, K. Arun, U. D. Remya, M. Reiffers, A. Dzubinska and R. Nagalakshmi. *J. Alloys Compd*. 938 168590(2023).

Torsion Actuator with Shape Memory Effect

A. V. Nezhencev[1,a], V. V. Koledov[1], A. V. Prokunin[1], V. S. Kalashnikiv[1], A.Nesolenov[1], V.Andreev[2]

[1] Kotelnikov Institute of Radioengineering and Electronics of RAS, Moscow, Russia
[2] Institute of Metallurgy of RAS Moscow, Russia
[a] e-mail: *anton.nezhencev@gmail.com*

The development of microactuators utilising the shape memory effect (SME) is a promising area within the field of microelectromechanical systems. A rotary, or torsional, actuator is a key component of microrobotics systems designed, for example, for three-dimensional manipulation of objects. Of particular relevance is the development of miniature torsional actuators used in setups for working with nano-objects inside the vacuum chamber of an electron microscope. However, modern systems have an insufficient controllable angle of rotation and are of considerable size [1–3].

The aim of this work is to develop a prototype actuator based on NiTi wire springs and a screw pair for converting linear motion into rotational motion. A schematic of the 20 mm long torsion actuator is shown in Fig. 1, and the test results for the prototype are presented in Fig. 2.

The conversion of linear motion into rotational motion is achieved by alternately heating two springs connected to a screw pair. The torsional actuator rotates the threaded shaft in the direction determined by the pair of springs to which the discharge current pulse from the capacitor

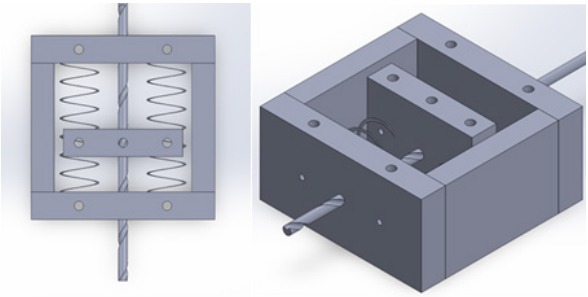


Fig. 1. 3D model of the torsional actuator

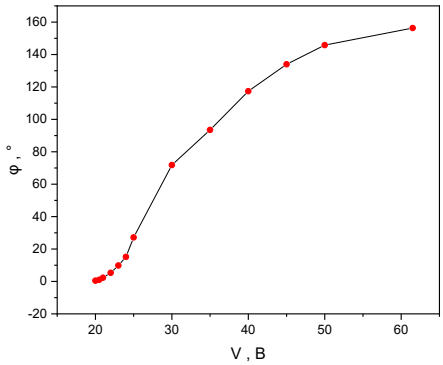


Fig. 2. Plot of rotation angle vs. capacitor charging voltage

is applied. Under the effect of Joule heating, this pair will transition to the austenitic state and contract. Since the austenite-martensite transition temperature is higher than room temperature, upon completion of the control pulse from the capacitor discharge, at room temperature, the actuator shaft will retain its angular position indefinitely, as both springs — whether compressed or extended — will remain in the martensitic state.

The dependence of the rotation angle φ of the axis on the capacitor voltage V is shown in the graph (see Fig. 2). The thickness of the titanium nickelide wire was 0.3 mm. The maximum rotation angle of the axis obtained was 156 degrees.

The report discusses experiments on the use of the proposed actuator during operation in the vacuum chamber of an electron microscope to control the 'bottom-up' nanoassembly of nano-objects using nano-tweezers with an EPF [4].

This work was carried out with the support of a State Assignment from the V. A. Kotelnikov Institute of Radio Engineering, Russian Academy of Sciences.

[1] Jun Sheng and Jaydev P Desai. *Smart Mater. Struct*. 24 105005 (2015)

[2] Barakat, R., Kirsch, S. M., Welsch, F., & Motzki, P. Scientific Reports, 15(1), 9108 (2025).

[3] Lima, F. S., Souto, C. R., Oliveira, A. G., Silvestre, A. D., Alves, R. M., Santos, S. E., … & Lima, A. G. *Sensors*. 24(15), 4973 (2024).

[4] Von Gratowski, S., Koledov, V., Shavrov, V., Petrenko, S., Irzhak, A., Shelyakov, A., & Jede, R. (2017). *Research and Technology: Select Proceedings of FiMPAR T.* 135–154 (2015).

Phase Diagrams of a Four-component Ni—Co—Mn—Ti System

D. V. Novokreshchenov[1, a], V. V. Sokolovskiy[1]

Chelyabinsk State University, Chelyabinsk, Russia
[a]e-mail: *mavarleyne.chelgu@ya.ru*

It is well known that Heusler alloys are capable of significantly altering their properties when their structure is modified or when impurities are added. The promise of researching various multicomponent compositions stems from the wide variety of possible combinations of elements that can make up Heusler alloys, their mechanical properties, and their ability to exhibit the magnetocaloric effect and shape memory effect.

This work is devoted to a systematic study of the system of Heusler alloys based on Ni—Co—Mn—Ti. Calculations were performed using the VASP [1] computational package with an exchange-correlation potential constructed according to the PAW-PBE [2] method within the generalized gradient approximation (GGA). Calculations were performed on 16-atom unit cells for all possible compositions of the form $Ni_xCo_yTi_z$, where the indices *x*, *y*, and *z* took values ranging from 1 to 14 such that the composition contained a total of 16 atoms. For each composition, $L2_1$ and *XA* structures were also generated in the austenitic cubic (225, 216 space group) and martensitic tetragonal (139, 119 space group) phases respectively.

One of the stages of the study was the calculation of the formation energy of the generated compositions and their structural modifications. This parameter allows determining the composition's resistance to decomposition into pure components. The formation energy was calculated as the difference between the ground-state energy of a given composition after relaxation and the sum of the energies of the pure elements:

$$E_{formation} = E_{Ni_xCo_yTi_z} - \left(x \cdot E_{Ni} + y \cdot E_{Co} + z \cdot E_{Ti}\right).$$

Fig. 1 shows ternary diagrams depicting the formation energy of the austenitic (a) and martensitic (b) phases of the Ti—Co—Ni boundary in the overall Ni—Co—Mn—Ti diagram. The number of atoms of the

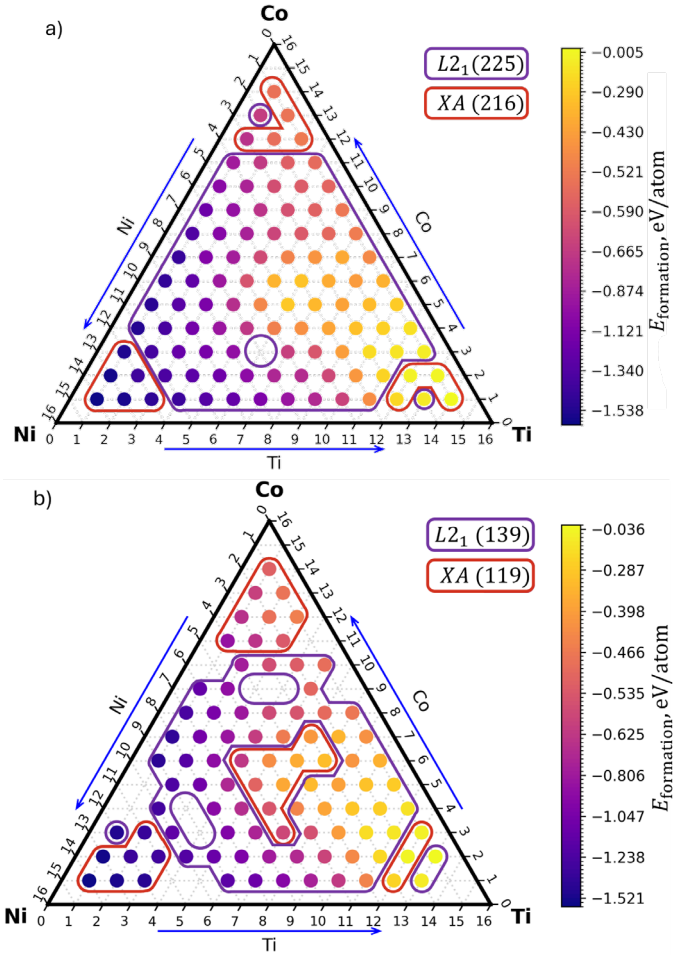


Fig 1. Distribution of the energy of cross-section formation in the Ti—Co—Ni alloy in the austenitic (a) and martensitic (b) phases

corresponding element in the composition is plotted along the axes. The color of the points determines the magnitude of the formation energy according to the color scale. The absence of a composition (corresponding point on the diagram) indicates its positive formation energy; therefore, further consideration of it is not warranted. Colored contours also highlight existence area in which one of the structures ($L2_1$ — 225 and XA — 216) is more favorable based on ground-state energy.

The results demonstrate that compositions with a higher nickel concentration are the most resistant to decomposition into pure elements, while titanium-based compounds possess the highest formation energy, close to zero.

The research was supported by the RSF Russian Science Foundation Project № 25-12-20024, https://rscf.ru/project/25-12-20024/

[1] G. Kresse and J. Furthmüller. *Phys. Rev. B*. 54, 11169 (1996).

[2] J. P. Perdew, K. Burke, and M. Ernzerhof. *Phys. Rev. Lett.* 77, 3865 (1996).

Stretch-hysteresis of Topological Charge in the Model of Elastic Ferromagnetic Monolayer with Strain-Dependent DMI

A. G. Nugumanov[1, a], R. R. Nugumanov[1, b], I. F. Sharafullin[1, c]

[1]Ufa University of Science and Technology, Ufa, Russia
[a]e-mail: *aidar.nugumanov@gmail.com*
[b]e-mail: *nugumanovrb@gmail.com*
[c]e-mail: *sharafullinif@yandex.ru*

Magnetoelasticity in modern solid-state physics is viewed as a full-fledged mechanism influencing effective anisotropy, Dzyaloshinskii-Moriya interaction (DMI), shape and structure of skyrmions and even creating chiral textures in the absence of innate DMI [1–4]. Three main models of magnetoelastic interaction include simple magnetostriction, generalized magnetoelasticity with magnetization gradients and strain-gradient model, which is particularly important for the motion, deformation, and topologically enhanced responses of skyrmions, and more broadly for the relationship between inversion breaking, local chirality, and elastic inhomogeneities [5–8]. We propose and study an alternative model where DMI is directly linked to the strain tensor.

The Hamiltonian of the system is given by:

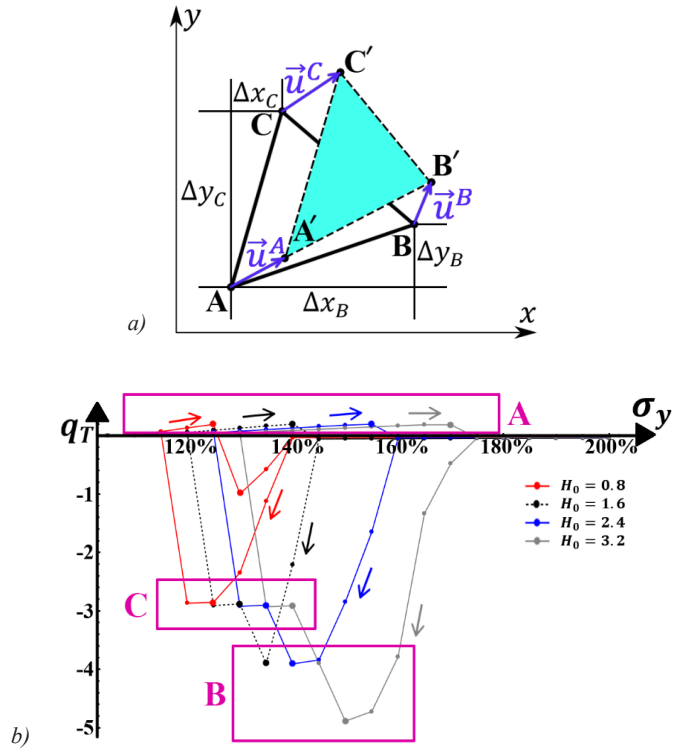


Fig. 1. a) elementary triangle deformation scheme; b) hysteresis of topological charge caused by uniaxial stretch for various values of magnetic field

$$\hat{\mathcal{H}} = \mathcal{H}^{\varepsilon} + \mathcal{H}^{m} + \mathcal{H}^{DM}; \tag{1}$$

$$\mathcal{H}^{\varepsilon} = \frac{\lambda}{2}\left(\varepsilon_{xx} + \varepsilon_{yy}\right)^2 + \mu\left(\varepsilon_{xy}^2 + \varepsilon_{yx}^2\right); \tag{2}$$

$$\mathcal{H}^{m} = -\sum_{i,j} J\left(\vec{r}_i, \vec{r}_j\right)\vec{S}_i\vec{S}_j - \sum_i \vec{H}_0\vec{S}_i; \tag{3}$$

$$\mathcal{H}^{DM} = -\sum_{i,j} \vec{D}_{ij}^{\varepsilon}\left[\vec{S}_i \times \vec{S}_j\right]. \tag{4}$$

In this model exchange parameter J decays exponentially with the increase of the distance between sites, while DMI vector is directed towards nearest neighboring sites and it's magnitude D_{ij}^{ε} linearly depends

on the Euclidian norm of strain tensor $\hat{\varepsilon} = \begin{pmatrix} \varepsilon_{xx} & \varepsilon_{xy} \\ \varepsilon_{yx} & \varepsilon_{yy} \end{pmatrix}$ which is locally calculated from coordinates of deformed film's sites (Fig. 1, *a*):

$$J\left(\vec{r}_i, \vec{r}_j\right) = J_0 \exp\left(1 - \frac{\left|\vec{r}_j - \vec{r}_i\right|}{a_0}\right); \tag{5}$$

$$\vec{D}_{ij}^{\varepsilon} = \frac{1}{2} D_{ij}^{\varepsilon} \frac{\vec{r}_j - \vec{r}_i}{\left|\vec{r}_j - \vec{r}_i\right|}. \tag{6}$$

Fig. 1b shows the hysteresis of topological charge under the continuous stretching (region A) and shrinking (regions B and C).

This research was funded by state assignment, agreement № . 075–03–2024–123/1 dated 02/15/2024.

[1] A. N. Bogdanov, C.Panagopoulos. *Nat. Rev. Phys.* 2, 492 (2020).

[2] T. A. Moore. *Nanotechnology* 36, 072003 (2025).

[3] Y. Ba et al. *Nat. Commun*. 12, 322 (2021).

[4] Y. Hu, X.Wan, B.Wang. *New J. Phys*. 23, 023016 (2021).

[5] J. Sun et al. *Int. J. Mech. Sci*. 285, 109849 (2025).

[6] A. Erickson et al. *Small* 21, e05204 (2025).

[7] L. Liu, W.Chen, Y. Zheng. *Phys. Rev. Lett*. 128, 257201 (2022).

[8] M. Fattouhi, Ph.D. thesis, University of Salamanca (2023).

Laboratory Setup of a Pulsed Magnetometer for Studying Magnetic and Magnetostructural Phase Transitions

N. Yu. Nyrkov[1, a], A. V. Golovchan[1], O. E. Kovalev[1], R. A. Safonov[1], I. F. Gribanov[1], A. V. Shevelev[1], A. P. Kamantsev[1,2], B. M. Todris[1]

[1] A. A. Galkin Donetsk Institute for Physics and Engineering, Donetsk, Russia
[2] Kotelnikov Institute of Radioengineering and Electronics of RAS, Moscow, Russia
[a]e-mail: *nyrkovng@yandex.ru*

One approach to research magnetically induced phase transitions in functional materials is measurement in strong pulsed magnetic fields. Such experiments make it possible to investigate the behavior of a material during an induced phase transition. At the same time, they involve a number of methodological difficulties, since the useful signal from the sample is often comparable in amplitude to the parasitic interference of the measuring system. This imposes stringent requirements on the sensitivity of the measurement chain and the stability of the experimental conditions. In this work, a pulsed magnetometer intended for studying materials with magnetic and magnetostructural transitions is presented.

Measurements in pulsed magnetic fields make it possible, under laboratory conditions, to reach fields sufficient to induce phase transitions in functional magnetic materials and to synchronously record the sample response. In the developed setup, simultaneous in-situ measurements of magnetization and temperature are implemented with a sampling rate of up to 1 MHz. Magnetization is determined by the induction method using a system of oppositely connected measuring and compensation coils, whereas temperature is monitored by a differential microthermocouple attached to the sample.

The magnetic field is generated by discharging a 6.3 mF capacitor bank through a thyristor switch into a solenoid and is monitored from the discharge current using a Rogowski coil followed by signal integration. With an inner solenoid diameter of 9 mm and a sample-channel diameter of 6.5 mm, the setup reaches a field of 14.87 T at a charging voltage of 556 V; the characteristic pulse duration is about 7.5 ms, and the operating

temperature range is 77–375 K. The use of DLP 3D printing in manufacturing the solenoid tooling and elements of the measuring system ensured high precision and reproducibility of the design.

The modular design of the developed pulsed magnetometer (Fig. 1) provides simultaneous recording of $M(H)$ and $T(H)$ during a magnetic-field pulse, and the circuit and structural solutions implemented in the setup make it suitable for studying magnetic and magnetostructural phase transitions in functional materials.

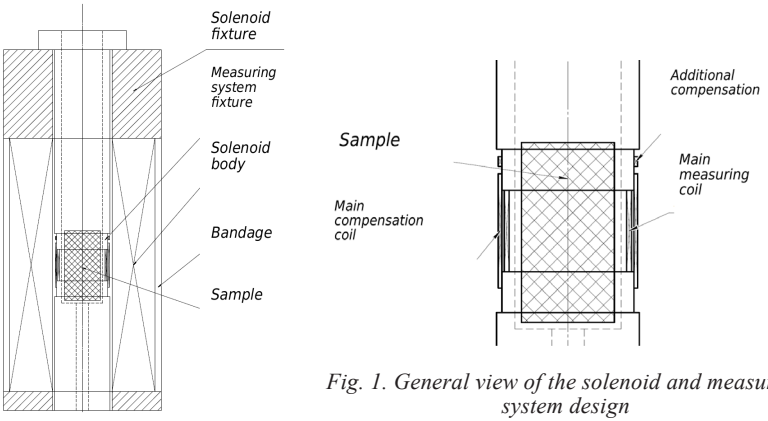


Fig. 1. General view of the solenoid and measuring system design

The study was supported by the Russian Science Foundation, № 25-19-00587, https://rscf.ru/project/25-19-00587/

[1] Kudasov Yu.B., Makarov I. V., Maslov D. A., et al. *Instruments and Experimental Techniques*. 6. 78–85 (2015).

[2] Safonchik M. O., Shakhov M. A. *Instruments and Experimental Techniques*. 4. 74–88 (2025).

[3] Ikeda A., Noda K., Shimbori K. *Journal of Applied Physics*. 136 175902 (2024).

Production, Microstructure and Magnetocaloric Effect of Polycrystalline Ni—Co—Mn—Ti Alloys with Variable Composition

M. A. Orshulevich[1, a], M. V. Utarbekova[1], S. V. Taskaev[1], D. R. Baigutlin[1], Hu Zhang [2], V. D. Buchelnikov[1]

[1] Chelyabinsk State University, Chelyabinsk, Russia
[2] University of Science and Technology Beijing, China
[a] e-mail: *mariya-fks@mail.ru*

In recent years, artificial intelligence (AI) methods have become a powerful tool in materials science, accelerating discovery and optimization of functional materials [1]. Heusler alloys are of particular interest, demonstrating promising caloric and thermoelectric properties, making them attractive for energy and cooling technologies [2; 3]. Traditional methods for discovering such materials require significant time and resources, while machine learning and predictive modeling offer efficient alternatives. Specifically, AI algorithms allow us an analysis of complex relationships between the composition, structure, and functional characteristics of alloys, facilitating a targeted design of new compounds with improved properties. This work reviews modern approaches to applying AI for the search and synthesis of new thermoelectric and caloric materials based on Heusler alloys, as well as their potential applications.

Polycrystalline Ni—Co—Mn—Ti alloys (with varying element contents: $Ni_{34}Co_{16}Mn_{35}Ti_{15}$, $Ni_{34}Co_{16}Mn_{37.5}Ti_{12.5}$, $Ni_{34}Co_{16}Mn_{40}Ti_{10}$, $Ni_{33.8}Co_{14.8}Mn_{36.4}Ti_{15}$, $Ni_{31.6}Co_{16.6}Mn_{39.7}Ti_{12.1}$, $Ni_{37}Co_{13}Mn_{34.4}Ti_{15.5}$, $Ni_{35}Co_{15}Mn_{37}Ti_{13}$) were produced by arc melting in a pure argon atmosphere. The initial metals Ni, Co, and Ti had a purity of over 99.98 wt.%, and Mn — at least 99.5 wt.%. To compensate for manganese losses during melting, additional 1.5 wt.% Mn was introduced. The ingots were remelted and turned over three times to improve homogeneity. Thereafter, the alloy samples were heat-treated in evacuated quartz ampoules and annealed at 1173 K for 96 hours followed by water quenching.

The study of the synthesized samples by scanning electron microscopy with energy-dispersive X-ray spectroscopy (SEM-EDS) confirmed their structural homogeneity. Elemental analysis showed good agree-

ment between the experimentally determined composition and the specified stoichiometric ratios. X-ray structural analysis was performed on a BRUKER D8 ADVANCE diffractometer using Cu Kα radiation. Magnetic properties were studied on a Versa Lab Quantum Design vibrating sample magnetometer in the temperature range of 50–400 K under fields up to 3 T.

The magnetocaloric effect (MCE) was studied in the synthesized alloys. The MCE is a phenomenon resulted in a change in the temperature of magnetic materials under the influence of an external magnetic field.

The isothermal change of magnetic entropy (ΔS_m) was calculated from magnetization data using the Maxwell relation.

The maximum values of ΔS_m are observed near room temperature, that fact making these materials promising for practical application.

In conclusion, the synergy between AI and investigation of the magnetocaloric effect in Heusler alloys opens new ways in materials science. AI's ability to analyze data and predict properties accelerates the development of highly efficient materials, advancing energy-saving technologies.

This work was supported by the Russian Science Foundation (project № 24-12-20016).

[1] Agrawal, A., Choudhary, A. *APL Materials.* 4(5), (2016), 053208.

[2] Liu, J., et al. *Progress in Materials Science.* 112, (2020), 100673.

[3] Carrete, J., et al. *Physical Review X.* 4(1), (2014), 011019.

Insight into Half-metallicity and Structure of $FeRhSb_{1-x}Z_x$ Heusler Alloys

O. O. Pavlukhina[1,a], V. D. Buchelnikov[1], V. V. Sokolovskiy[1]

[1] Chelyabinsk State University, Br. Kashirinykh Str. 129, 454001, Russia
[a] e-mail: *pavluhinaoo@mail.ru*

The Fe—Rh-based alloy have attracted a lot of attention due to the observation of shape memory effect, magnetocaloric effect etc. [1]. It

should be noted that spintronics is one of the most promising applications of Heusler alloys. This is due to the fact that for some alloys, one spin band reveals the semiconductor, while the other exhibits metallic behavior at the Fermi level. The properties of $FeRhSb_{1-x}Z_x$ (x = 0, 0.25, 0.5, 0.75, 1) alloys are investigated. The calculations were performed using density functional theory. The VASP software package was used for the calculations. Half-Heusler alloys have a cubic structure ($C1_b$). Three configurations are possible for these alloys: the α, β, and γ phases. It is shown that the γ-phase is energetically favorable in the case of all the alloys, except for the FeRhSi alloy, for which the β-phase is the equilibrium one. As an example, Figure 1 shows the ground state energies for the α, β and γ phases of the $FeRhSb_{0.75}P_{0.25}$ alloy as a function of the lattice parameter a.

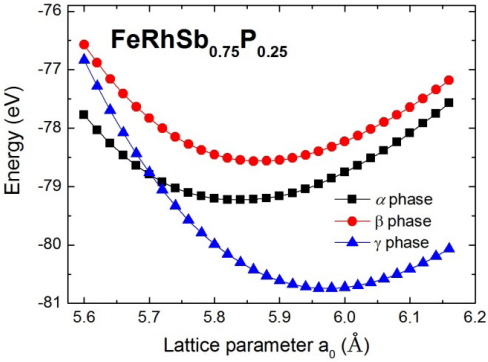


Fig. 1. The total energy difference ΔE of $FeRhSb_{0.75}P_{0.25}$ compounds in the α, β, and γ cubic structures as a function of the lattice parameter

It has been shown that the addition of a fourth element to a three-component alloy leads to a change in the position of the valence band and conduction band with respect to the Fermi level. As an example, for the three-component alloys (FeRhSi and FeRhSb) having a low spin polarization, potentialities have been demonstrated for to provide an increase in spin polarization up to 100% through the addition of a fourth element. Novel half-Heusler alloys having 100% spin polarization are predicted.

This study was supported by the Ministry of Science and Higher Education of the Russian Federation within the framework of the Russian State Assignment under contract № 075-00186-26-00.

[1] J. Winterlik. *Phys Rev. B*. 79, 064508 (2009).

Heating Systems for Actuation of Shape Memory Alloy Nanomechanical Devices

A. V. Prokunin[1, a], V. V. Koledov[1], A. P. Orlov[1], V. A. Luzanov[2], I. I. Musabirov[3]

[1] Kotelnikov IRE RAS, Moscow, Russia
[2] Kotelnikov IRE RAS, Fryazino branch, Fryazino, Russia
[3] Institute of Metal Superplasticity Problems, Ufa, Russia
[a] e-mail: *prokunin.av@phystech.edu*

Direct spatial manipulation of nanoscale objects requires precise positioning, a challenge for thermally actuated shape memory alloy (SMA) nanotweezers. Conventional systems utilize a tungsten needle as a support and a diode heater, but localized heating induces thermal expansion of the needle, causing significant positional drift. This work evaluates three strategies to minimize thermal drift in Ti_2NiCu nanotweezers actuated at 40–65 °C.

Finite element modeling (FEM) simulated thermal expansion of tungsten needles (45 mm length, 0.5 mm shank, ≤1 μm apex). Needles were fabricated via electrochemical etching. Coaxial tips were created using magnetron sputtering of dielectric SiO (1–5 μm) and conductive Cu (0.1–1 μm) layers. Nanotweezer assembly and drift measurements were performed in situ within a SEM/FIB system.

Three heating configurations were investigated:

1) Geometric Optimization of the Tip Profile

A compound tip geometry (truncated cone–cylinder–cone) was modeled. FEM revealed thermal expansion depends predominantly on the cylindrical diameter *d* and negligibly on length *l*. Experimental validation for *d* = 100 μm and 50 μm showed expansion over the 40–65 °C range reduced to 1.2 μm and 0.3 μm, respectively. This confirms that minimizing *d* significantly suppresses drift.

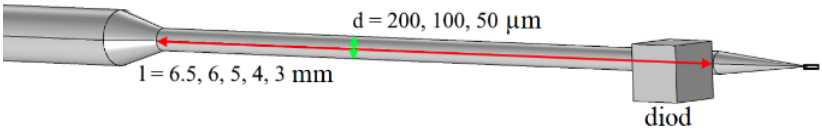


Fig. 1. Model of the needle-diode-nanotweezers system

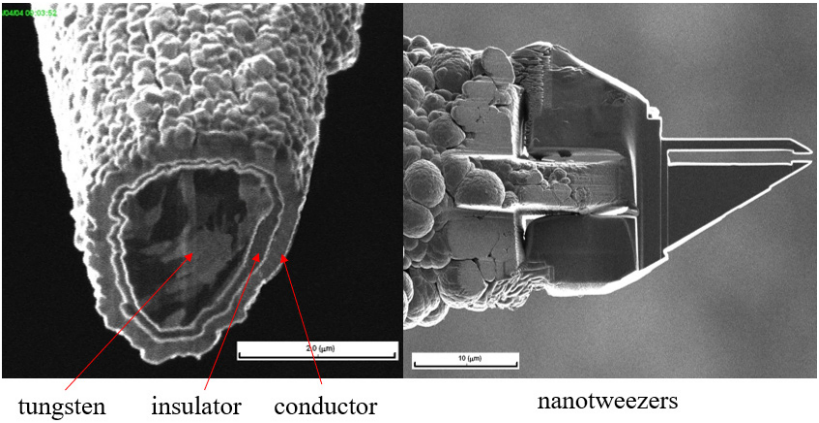


Fig. 2. Coaxial heating system

2) Dual-Needle Ohmic Heating

A prototype with two parallel tungsten needles bridged by the nanotweezer enables localized resistive heating precisely at the contact interface. Modeling predicted drift limited to tens of nanometers. Experiments confirmed sub-100 nm drift; however, the system exhibits mechanical fragility, often failing during transport or installation.

3) Coaxial Needle with Integrated Ohmic Heating

To address the dual-needle system's fragility, a single tungsten needle was coated with SiO and Cu layers. FIB milling exposed a cross-section, and the nanotweezer was attached to bridge the core and outer conductor. Engineered junction resistance (10–100 Ω) ensures localized heating. This prototype demonstrated: Thermal drift <100 nm; Actuation frequencies in the kHz range; High mechanical durability (>10^6 cycles).

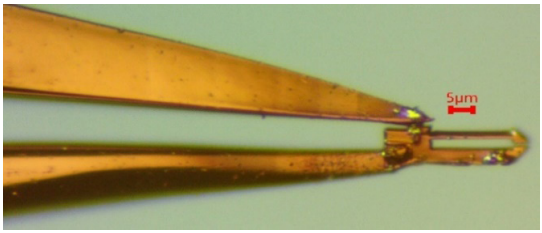


Fig. 3. Dual -needle control system with ohmic heating of nanotweezers

Optimizing tip geometry reduces drift proportional to diameter *d*. The dual-needle ohmic system achieves ultra-low drift but lacks robustness. The coaxial configuration combines sub-100 nm drift with high-speed

actuation and mechanical stability, representing the optimal solution for precise, drift-compensated nanomanipulation and bottom-up nanoassembly.

The work was performed within the framework of the State Assignment of the V. A. Kotelnikov IRE of the Russian Academy of Sciences.

[1] S. Von Gratowski, P. V. Lega, A. V. Prokunin, et al., in Frontiers in Materials Processing, Applications, Research and Technology (Springer, Singapore, 2018), pp. 135–154.

[2] P. V. Lega, A. V. Prokunin, V. V. Koledov, et al. *Mater. Sci. Forum*. 845, 142 (2016).

[3] A. Zhikharev, P. V. Lega, V. V. Koledov, et al. *J. Phys.: Conf. Ser*. 741, 012206 (2016).

[4] P. V. Lega, V. V. Koledov, A. V. Prokunin, et al. *J. Commun. Technol. Electron*. 60, 1124 (2015).

[5] A. Zhikharev, P. V. Lega, V. V. Koledov, et al., in *Proc. 6th IEEE Int. Conf. Manipulation, Manufacturing and Measurement on the Nanoscale (3M-NANO)* (IEEE, 2016), pp. 101–104.

[6] A. V. Prokunin, V. V. Koledov, P. V. Lega, et al., RF Patent No. 2 778 525 (22 August 2022).

[7] A. V. Prokunin, V. V. Koledov, P. V. Lega, et al., RF Patent No. 2 790 934 (28 February 2023).

Effect of Metal Nanoparticles on the Mechanical Properties of Graphene Aerogels

E. A. Rozhnova[1, a], J. A. Baimova[1]

[1]Institute for Metals Superplasticity Problems, Russian Academy of Sciences, Ufa, Russia

[a]e-mail: *rozhnova.elizavetaa@mail.ru*

Graphene aerogels represent carbon materials with high porosity, ultralight weight, and unusual deformation behavior. These properties allow

their application in pollutant adsorption, energy storage, supercapacitors, to name a few. One of the important problems for such materials is the low compression resistance, which leads to an instability of the structure. To improve compressibility resistance, graphene aerogels can be modified by adding other elements into the cells, for example, carbon nanotubes or metal nanoparticles.

This study uses molecular dynamics simulations to examine the mechanical properties of graphene honeycomb aerogels modified with Ni and Al nanoparticles. The behavior of pure graphene aerogels was compared with aerogels containing different distribution and concentration (2.7 and 5.8%) of Ni and Al nanoparticles under compression and tension. The interatomic interactions were described using potentials tested in Ref. [1].

It was found that metal nanoparticles considerably increase the resistance to compression. Stress increase occurred for aerogels with Al nanoparticles at a density of 1.3 g/cm^3, while for aerogels filled with Ni, stress increase occurred at 2.0 g/cm^3. The strengthening mechanism is volume repulsion when Al nanoparticles repel the graphene cell walls, while Ni nanoparticles easily spread along the cell walls and provide less compression resistance, analogous to pure graphene aerogels.

It was established that the tensile properties remained unaffected by the presence of both nanoparticle type, and the same deformation mechanism occurred for all aerogels [2]. The maximum ultimate tensile strength achieved is 160 GPa.

This study demonstrates that embedding weakly interacting metal nanoparticles, such as aluminum, is a highly effective strategy for enhancing the compression resistance of graphene aerogels without compromising their ultra-low weight.

[1] L. R. Safina, E. A. Rozhnova, K. A. Krylova, R. T. Murzaev, J. A. Baimova. *Comput. Phys. Commun*. 301, 109235 (2024).

[2] E. Rozhnova, P. Zakharov, J. Baimova. *Sci*. 7, 176 (2025).

The Influence of Magnetoelectric Interaction on the Spin-wave Spectrum in thin Helimagnetic Films

A. I. Samigullina[1, a], I. F. Sharafullin[1]

[1] Ufa University of Science and Technology, Ufa, Russia
[a] e-mail: *angelasamig2002@gmail.com*

Currently, one of the most dynamically developing areas of quantum electronics is chiral spintronics, which focuses on spin-transport phenomena in materials with chiral symmetry [1]. The presence of a helical magnetization structure, arising from the competition between Heisenberg exchange interactions, Dzyaloshinskii — Moriya interaction, and anisotropy, determines the unique properties of elementary excitations of the magnetic subsystem — spin waves.

Studying the spectrum of elementary excitations in helical magnetic materials is a nontrivial problem, since the periodic spiral structure acts as an effective potential, leading to the formation of the spectrum. Understanding the propagation patterns, spectral characteristics, and excitation mechanisms of spin waves in such materials is an important task for the development of next-generation functional devices, such as nano-oscillators and logic elements based on magnetic helices.

This work studies a model of thin films with Heisenberg spins located at the sites of a body-centered cubic (BCC) lattice, consisting of six magnetic layers and two ferroelectric layers (top and bottom). In this model, the spiral order is formed along the *z*-axis, which is directed perpendicular to the layer surface. The Hamiltonian of the system is as follows:

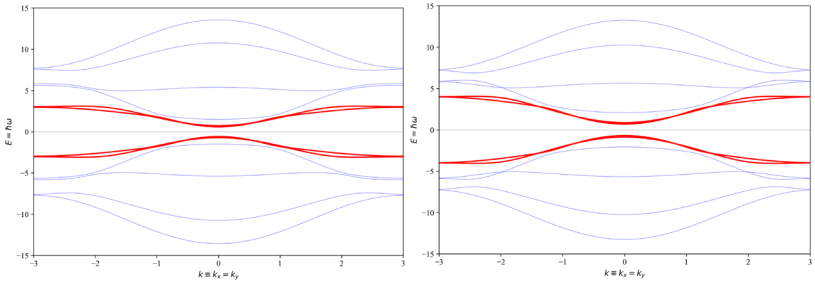
$$H = -J_1 \sum_{i,j} \vec{S}_i \cdot \vec{S}_j - J_2 \sum_{i,i'} \vec{S}_i \cdot \vec{S}_{i'} - \vec{h} \sum_i \vec{S}_i - J_{mf} \sum_{i,j,l} \left[\vec{S}_i \cdot \vec{S}_j \right] \vec{P}_l - J_f \sum_{i,j} \vec{P}_i \vec{P}_j, \quad (1)$$

where the first term in the Hamiltonian describes the ferromagnetic interaction between nearest neighbor (*NN*) spins, the second term describes the antiferromagnetic interaction between next-nearest neighbor (*NNN*) spins along the axis perpendicular to the film plane, the external magnetic field is also directed along the *z*-axis, the fourth term describes the magnetoelectric interaction between the *z*-component of the polarization

vector of the ferroelectric film and the spins of the magnetic film, and the fourth term is the exchange parameter in the ferroelectric layer.

The existence of a helically ordered structure in a BCC lattice is possible only under the condition $|J_2| \geq J_1$. To determine the classical spin configuration of the ground state on the surface, the expression for the spin energy along the *z*-axis was analyzed. The solution to this problem is obtained iteratively. At $J_{mf} = 0.0$ and $J_2 / J_1 = -1.4$, the helix angles within the magnetic layer volume were: $\alpha_1 = \alpha_5 = 17.06°$, $\alpha_2 = \alpha_4 = 39.91°$, $\alpha_3 = 44.12°$. At $J_{mf} = -0.5$ and $J_2 / J_1 = -1.4$: $\alpha_1 = \alpha_5 = 33.36°$, $\alpha_2 = \alpha_4 = 43.70°$, $\alpha_3 = 44.40°$.

Based on the found ground state configuration, the spin-wave spectrum was calculated using the method of two-time temperature Green's functions. The analytical dispersion equation was obtained after diagonalizing the linear transformation, which makes it possible to calculate the frequencies of the spin modes for each pair of wave numbers (Fig. 1).



a) *b)*

Fig. 1. Spin waves with parameter $J_2 / J_1 = -1.4$ at: top — $J_{mf} = 0.0$, bottom — $J_{mf} = -0.5$, where the surface modes of the spin wave are highlighted in red

For a fixed ratio $J_2 / J_1 = -1.4$, a comparison of top ($J_{mf} = 0.0$) and bottom ($J_{mf} = -0.5$) shows a qualitative change in the spin dynamics. An increase in the magnetoelectric interaction $|J_{mf}|$ leads to an increase in the spin deviation angles within the magnetic layer — the noncollinearity becomes more pronounced. At the same time, the dispersion of spin waves intensifies, indicating an increase in spatial inhomogeneity, while the critical temperature decreases.

The work was carried out within the framework of a state assignment, agreement № 075-03-2024-123/1 dated February 15, 2024.

[1] S. El. Hog, I. F. Sharafullin, H. T. Diep et al. *J Magn. Magn. Mater*. 563, 169920 (2022).

Rapidly Quenched Ribbons Produced of Quasi-binary TiNi—TiCu Alloy for the Production of Refrigerators and Heat Pumps Based on the Elastocaloric Effect

N. N. Sitnikov[1, 2, a], R. V. Sundeev[3, 4, b], A. V. Shelyakov[2, c]

[1] State Scientific Center of the Russian Federation "Keldysh Research Center", Moscow, Russia
[2] National Research Nuclear University, National Research Nuclear University MEPhI, Moscow, Russia
[3] I. P. Bardin Science Institute for Ferrous Metallurgy, Moscow, Russia
[4] Institute for Electrophysics and Electric Power of the RAS, Moscow, Russia
[a]e-mail: *sitnikov_nikolay@mail.ru*
[b]e-mail: *sundeev55@yandex.ru*
[c]e-mail: *AVShelyakov@mephi.ru*

Engineers, designers, and materials scientists are currently interested in creating new functional materials for the development of prototype cooling and heating devices that occur during phase transitions in solids. Magnetocaloric and elastocaloric effects (MCE, ECE) hold promise for the creation of alternative solid-state energy systems, such as refrigerators and heat pumps. These effects are associated with changes in the temperature of a material sample under the influence of various external factors, such as magnetic and electric fields, mechanical stress, and others. Most scientific work on this topic is devoted to the study of MCE in magnetic solid-state functional materials and the development of prototype refrigerators and heat pumps based on them. At the same time, ECE are increasingly attracting practical interest as they are less demanding on the design of prototypes.

Promising materials for the production and application ECE of quasi-binary alloys are rapidly quenched alloys based on the quasi-binary TiNi—TiCu system with the addition of Fe, Al, Hf, and other elements. These materials exhibit reversible phase transformations (PT) from the martensitic phase (B19) to the austenitic phase (B2) and back during the heating and cooling cycle. The hysteresis of this transformation ranges from a few degrees to several tens of degrees, depending on the alloying level. The production of quasi-binary TiNi—TiCu alloys by

standard casting methods is problematic, and in some cases impossible, since cooling the melt causes eutectics to precipitate within the formed crystal structure, which embrittles the alloy. These alloys are primarily produced by various sputtering or deposition methods, but their practical use in prototype refrigerators and heat pumps is limited or impossible in this form. A promising method for producing these alloys is melt quenching on a rapidly rotating disk (melt spinning and planar casting methods), which produces thin, elongated ribbons ranging from 20 to 100 μm thick. Such thin ribbons can be used as functional materials for high-speed alternative solid-state energy systems, such as heat pumps and refrigerators.

Depending on the quenching parameters (cooling rate) and the characteristics of the material being quenched, it is possible to obtain ribbons in a completely amorphous or crystalline state, as well as in a mixed amorphous-crystalline state. The study demonstrated that at melt cooling rates of 10^6 ºC/s and above, the entire volume of the TiNi—TiCu alloy ribbon is in an amorphous state, while at melt cooling rates of 10^5 ºC/s and below, the ribbon has a crystalline structure. At intermediate melt cooling rates ($10^5 \div 10^6$ ºC/s), crystallization can occur within the amorphous matrix, ultimately forming an amorphous-crystalline ribbon with a crystalline phase unevenly distributed throughout the volume. However, with uniform heat removal and optimal spinning process parameters, a thin layer of crystalline phase forms on the noncontact surface of the ribbon, resulting in an amorphous-crystalline ribbon with a sharp boundary separating the amorphous and crystalline states into layers. This means the ribbon is a layered structural composite. By varying the melt cooling rate, the ratio of the thicknesses of the amorphous and crystalline layers can be varied. Specifically, reducing the cooling rate from $8{,}9 \cdot 10^5$ to $4{,}2 \cdot 10^5$ ºC/s leads to an increase in the thickness of the crystalline layer from 2 to 12,5 μm.

The amorphous state of the alloy can be converted to a crystalline state through various processes, such as heat treatment, electric pulse heat treatment, and others. Heat treatment of the amorphous state allows for the formation of a crystalline structure with specified characteristics, which in turn determine the PT parameters. Specifically, isothermal treatment at 500 °C for 300 s is used to obtain optimal crystalline characteristics for the TiNi—TiCu alloy from a rapidly quenched amorphous state. The resulting crystalline structure is characterized by

submicron crystals and a PT range of 60–70 °C with pronounced shape memory and ECE effects.

Phase Transitions in $Ni_{2.14}Mn_{0.81}Fe_{0.05}Ga$ Heusler Alloy Under External Magnetic Field and Hydrostatic Pressure

P. S. Smerchanskiy[1,2, a], V. V. Koledov[1, b], A. P. Kamantsev[1], D. D. Kuznetsov[1], O. E. Kovalev[3], R. A. Safonov[3], I. F. Gribanov[3], A. V. Golovchan[3], N. Y. Nyrkov[3], S. S. Zhdanov[4,1], V. M. Povarnitsyn[4,1]

[1] Kotelnikov Institute of Radioengineering and Electronics of Russian Academy of Sciences, 125009, Moscow, Russia

[2] National Research University Higher School of Economics, 109028, Moscow, Russia

[3] A. A. Galkin Donetsk Institute for Physics and Engineering, 283048, Donetsk, Russia

[4] Bauman Moscow State Technical University, 105005, Moscow, Russia

[a] e-mail: *pavelsmerchanskiy@gmail.com*

[b] e-mail: *victor_koledov@mail.ru*

Heusler alloys of Ni_2MnX family, where X = Ga, In, Sn, …, which have been proven to exhibit a giant magnetocaloric effect (MCE) and a magnetically controlled shape memory effect due to a thermoelastic magnetostructural phase transition (MPT), continue to attract attention. Unfortunately, these breakthrough functions are performed in strong magnetic fields at least of several Teslas. Currently, there is an active search for alloys in which these effects could manifest themselves in fields not exceeding those generated by permanent magnets. An accurate measurement and theoretical calculation of the effect of multicomponent alloying on the volumetric magnetostriction constant B could be a guideline for the development of new multifunctional Heusler alloys. Thermodynamic theory shows that B can determine both the sensitivity of the MPT to an external field and the sign of the MCE.

In this paper, the effects of a magnetic field and external hydrostatic pressure on MPT in Heusler alloy $Ni_{2.14}Mn_{0.81}Fe_{0.05}Ga$ with direct MCE are investigated. It is found, that the magnetic field increases the temperature of the MPT, and hydrostatic compression increases the magnetization at the Curie point, slightly affecting its position. The thermodynamical model based on Landau decomposition correctly describes the experimental data taking into account the volumetric magnetostriction constant *B*.

[1] Jiang S., Yang K. *J. Alloys Compd*. 867, 158854 (2022).

[2] Liu J. et al. *Phys. Rev. Mat*. 3, 084409 (2019).

[3] Shavrov V. G. et al. *Phys. Met. Metallogr*. 125 14, 1927–1934. (2024).

[4] Kojima T., Kameoka S., Tsai A. P. *Sci. Technol. Adv. Mater.* 20, 1, 445–455 (2019).

[5] Krenke T. et al. *Phys. Rev. B — Condens. Matter Mater. Phys*. 73, 17, 174413 (2006).

Ab Initio and Monte Carlo Study of Magnetic, Structural, and Magnetocaloric Properties of Ni—Mn—Sn—Cu Heusler Alloy

V. Sokolovskiy[1, a], A. Gamzatov[1,2], A. Kadirbardeev[1,2], V. Buchelnikov[1]

[1] Chelyabinsk State University, Chelyabinsk, Russia
[2] Institute of Physics named after H. I. Amirkhanov DFRC RAS, Makhachkala, Russia
[a] e-mail: *vsokolovsky84@mail.ru*

The Ni—Mn—Sn-based Heusler alloys attract considerable attention due to their multifunctional properties, including magnetic shape memory effect and large magnetocaloric effect (MCE) [1]. The present work reports a comprehensive theoretical investigation of the magnetic and structural properties of the Ni—Mn—Sn—Cu alloy with nominal sample $Ni_{47}Mn_{40}Sn_{12}Cu_1$. The study combines density functional theory (DFT) calculations and Monte Carlo (MC) simulations to determine the

ground state magnetic configuration, lattice parameters, and the stability of austenitic and martensitic phases.

DFT calculations were performed using the projector augmented wave (PAW) method within the generalized gradient approximation (GGA), as implemented in the VASP code [2]. A full geometry optimization of a 2×2×2 supercell (32 atoms) was carried out for the cubic $L2_1$ austenite phase, as well as for the tetragonally distorted $L1_0$ and orthorhombically distorted 4O martensite phases. To determine the ground magnetic state, four magnetic configurations were calculated: ferromagnetic (FM) ordering and three ferrimagnetic (FiM) configurations with antiparallel spin alignment on the Mn_3, Mn_2, or simultaneously on both Mn_2 and Mn_3 sublattices. These three nonequivalent Mn sublattices correspond to regular Mn sites (Mn_1), Sn sites (Mn_2), and Ni sites (Mn_3). The Brillouin zone integration was performed using a 6×6×6 Monkhorst — Pack *k*-point mesh for the cubic austenite structure and a Gamma-centered 6×5×5 *k*-mesh for the tetragonal martensite phase, with a plane-wave energy cutoff of 560 eV. The convergence criterion was set to 10^{-7} eV/atom in total energy, with residual forces below 0.001 eV/Å.

The magnetic exchange coupling constants for the austenitic and martensitic phases of $Ni_{47}Mn_{40}Sn_{12}Cu_1$ were calculated using the spin-polarized relativistic Korringa — Kohn — Rostoker (SPR-KKR) method within the coherent potential approximation (CPA) [3]. The optimized lattice constants obtained from VASP calculations served as input parameters. A 57×57×57 *k*-point mesh (4495 k-points) was employed for Brillouin zone integration, with an energy convergence threshold of 0.01 mRy.

The temperature evolution of the magnetic, structural, and magnetocaloric properties was modeled via the MC method using a Heisenberg–Blume–Emery–Griffiths (BEG) Hamiltonian [4]. The total Hamiltonian includes magnetic, structural, and magnetostructural interaction terms for the austenite and martensite phases. MC simulations were performed on a 9×9×9 supercell (11664 atoms) obtained by multiplying the 16-atom $L2_1$ unit cell. The Mn_2(Cu) and Mn_3 atoms were randomly distributed on the Sn and Ni sites, respectively, to model the $Ni_{47}Mn_{40}Sn_{12}Cu_1$ compound. The MC run included 1×10^5 steps per temperature, with the first 1×10^4 steps discarded for thermal equilibration.

Figure 1(a) presents direct ΔT_{ad} measurements for $Ni_{47}Mn_{40}Sn_{12}Cu_1$ under a 1.8 T field. Cyclic field application (0.2 Hz) gives a direct MCE of $\approx$ 1.1 K near T_C^A and an inverse MCE of $\approx$ –0.15 K near the marten-

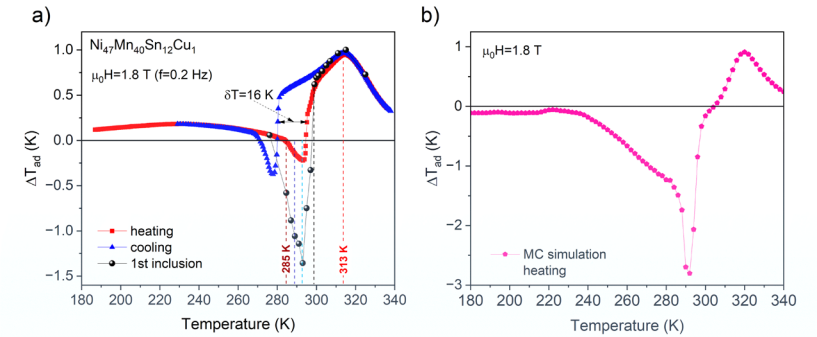


Fig. 1. (a) Temperature dependence of ΔT_{ad} for $Ni_{47}Mn_{40}Sn_{12}Cu_1$ under 1.8 T cyclic field (heating/cooling). Solid circles: single 1.8 T pulse in heating mode. (b) Calculated $\Delta T_{ad}(T)$ at 1.8 T (heating mode)

site–austenite transition. A single field pulse yields a much larger inverse effect of ≈ –1.35 K, attributed to irreversible MSPT kinetics. The theoretical $\Delta T_{ad}(T)$ at 1.8 T is given in Fig. 1(b). In the structural transition region, an inverse MCE of ≈ –2.9 K and a direct MCE of ≈ 1.07 K are observed (ratio ≈ 2.7), consistent with ΔS_m(inv.)/ΔS_m(dir.) ≈ 2.5 at 2 T from [5]. However, the theoretical MCE magnitude is about twice the experimental value, likely because the calculations neglect MSPT kinetics sensitive to the measurement protocol. Optimizing the heating rate and field sweep rate may yield larger experimental MCE values. Nevertheless, the qualitative trend of a reduced direct MCE compared to the inverse MCE under a single field pulse is reproduced experimentally.

This work was supported by the Russian Science Foundation (project No 25-12-20024, https://rscf.ru/en/project/25-12-20024/).

[1] A. G. Gamzatov et al. *J. Mater. Sci*. 58, 8503 (2023).

[2] G. Kresse, J. Furthmüller. *Phys. Rev. B*. 54, 11169 (1996).

[3] H. Ebert et al. *Rep. Prog. Phys*. 74, 096501 (2011).

[4] V. Sokolovskiy et al. *Phys. Metal. Metallogr*. 126, 1424 (2025).

[5] A. Ghotbi Varzaneh et al. *J. Alloys Compd*. 708, 34 (2017).

Mechanical Properties of Stable Austenitic and Martensitic Phases in Ni—Mn—Ga Heusler Alloys: A First-principles Study

Yu. A. Sokolovskaya[1, a], V. Buchelnikov[1]

[1]Chelyabinsk State University, Chelyabinsk, Russia
[a]e-mail: *sya2890@mail.ru*

Ni—Mn—Ga Heusler alloys are renowned for their magnetic shape memory effect, magnetocaloric properties, and magnetostructural coupling. Most research has focused on stoichiometric Ni_2MnGa and nearby compositions, primarily analyzing magnetic and structural phase stability. However, off-stoichiometric compositions remain underexplored, particularly regarding their mechanical behavior [1]. Understanding elastic properties — such as bulk modulus, shear modulus, Young's modulus, Poisson's ratio, and Debye temperature — is essential for practical applications involving actuation, damping, and stress-induced transformations. This work extends previous first-principles studies by systematically computing the mechanical characteristics of compositionally stable austenitic (cubic) and martensitic (tetragonal/orthorhombic) phases across the full ternary Ni—Mn—Ga diagram [2].

We performed density functional theory (DFT) calculations using the projector augmented wave (PAW) method as implemented in VASP [3], with the PBE-GGA exchange-correlation functional. A total of 105 compositions were modeled using 16-atom supercells covering the entire Ni—Mn—Ga ternary diagram. Full structural relaxations (atomic positions and lattice parameters) were conducted for both austenitic and martensitic phases to establish structural and magnetic reference states. The convex hull analysis was applied to determine thermodynamic stability against decomposition into elemental and binary compounds.

From the relaxed structures, we calculated:

- Elastic constants (C_{ij}) for cubic austenite and their equivalents for tetragonal martensite.
- Bulk modulus (B), shear modulus (G), Young's modulus (E), and Poisson's ratio (ν) using Voigt — Reuss — Hill averaging.

- Debye temperature (Θ_D) from average sound velocity.

Only compositions lying on or near the convex hull (stable or metastable) were considered for mechanical analysis.

In the framework of our presentation, all investigated mechanical properties have been systematically represented in the form of ternary composition — structure — property maps. Specifically, for the austenitic phase, ternary contour maps display the distribution of the B and G moduli, which allows for a visual assessment of stiffness and shear resistance as a function of composition. For the martensitic phase, we constructed maps of the Young's modulus anisotropy ratio (E_c/E_a), illustrating the difference in elastic properties along crystallographic directions, as well as maps of the average Debye temperature. Additionally, a separate ternary diagram presents Pugh's criterion (G/B), serving as an indicator of ductility or brittleness. This approach enables rapid identification of composition regions with an optimal combination of stiffness, anisotropy, and ductility, which is particularly important for the targeted search of promising Ni—Mn—Ga compositions suitable for mechanical processing and practical applications as magnetic shape memory alloys.

This work was supported by the Ministry of Science and Higher Education of the Russian Federation within the framework of the Russian State Assignment under contract № 075-00188-26-00.

[1] H.Seiner et al. *Phys. Status Solidi RRL*. 16, 2100632 (2022).

[2] Y. Sokolovskaya et al. *Metals*. 11, 973 (2021).

[3] G. Kresse, J. Furthmüller. *Phys. Rev. B*. 54, 11169 (1996).

Creation of Amorphous-crystalline Composites Using Extreme Impact Methods

R. V. Sundeev[1,2,3,a], A. V. Shalimova[1], S. O. Rogachev[4], V. E. Bazhenov[4]

[1] I. P. Bardin Science Institute for Ferrous Metallurgy, Moscow, Russia
[2] "MIREA — Russian Technological University", Moscow, Russia
[3] Institute for Electrophysics and Electric Power of the RAS, Moscow, Russia
[4] National University of Science and Technology MISIS, Moscow, Russia
[a]e-mail: *sundeev55@yandexl.ru*

It is known that amorphous-nanocrystalline composites can inherit the unique properties of amorphous or nanocrystalline state, e. g., high magnetic softness, extraordinary wear resistance and corrosion resistance, as well as high hardness and strength. On the other hand, the amorphous-nanocrystalline composites are characterized by increased thermal stability and plasticity, which are hardly achieved by amorphous or nanocrystalline alloys separately. One of the directions for preparation of hybrid amorphous-nanocrystalline composites (along with the methods of controlled crystallization of amorphous alloys, mechanical activation, etc.) is the consolidation of freely laying alternating amorphous-crystalline layers by high-pressure torsion (HPT).

Hybrid composites were prepared by stacking samples by the combination of amorphous and crystalline alloys such as two technically pure crystalline copper ribbons and an amorphous $Fe_{75}B_{17}Si_8$ alloy ribbon between them. The consolidation of the constructed composite was carried out by the HPT method at a degree of deformation corresponding to (***n***) 1/4, 1, 5, 10, 20, and 25 revolutions of the movable anvil at a rotation velocity of 1 rpm.

The structure evolution of the layered amorphous-crystalline Cu/FeSiB/Cu composite subjected to HPT at room temperature has been examined by various structural methods. The composite combines a high hardness of the amorphous $Fe_{75}B_{17}Si_8$ phase and the plasticity of the crystalline copper layers. Under the effect of HPT, the copper component of the composite becomes thinner. Simultaneous thinning of the hard amorphous $Fe_{75}B_{17}Si_8$ phase layer is accompanied by the formation of bridges in it. With increasing degree of deformation, the bridges break,

the $Fe_{75}B_{17}Si_8$ amorphous phase is refined, and the hard phase fragments are mixed and distributed along the sample. As a result, the final material consists of a strengthened copper matrix with fragments of the hard amorphous $Fe_{75}B_{17}Si_8$ phase embedded in it. It is assumed that the observed effects are associated with vortex instabilities of deformation in ductile copper layers under the effect of local braking of shear deformation by fragments of the hard amorphous $Fe_{75}B_{17}Si_8$ phase.

The study was supported by the Russian Science Foundation, project № 25-22-00132, https://rscf.ru/en/project/25-22-00132.

Magnetocaloric Effect and Magnetostriction of Medium-entropy Tb—Dy—Ho(Er)—Co Alloys with Laves Phase Structure

I. S. Tereshina[1,2, a], G. A. Politova[3, b], Z. S. Umkhaeva[2, c]

[1]Moscow State University, Moscow, Russia
[2]Kh. Ibragimov Complex Institute RAS, Grozny, Russia
[3]Baikov Institute of Metallurgy and Materials Science RAS, Moscow, Russia
[a]e-mail: *tereshina@physics.msu.ru*
[b]e-mail: *gpolitova@gmail.com*
[c]e-mail: *zargan.umhaeva@yandex.ru*

New multicomponent alloys classified as medium- and high-entropy alloys (MEA and HEA) possess unique properties (demonstrate outstanding mechanical strength under extreme thermal conditions, alongside superior corrosion resistance and ductility). The ability of these alloys to retain the structure of their original compositions while increasing the number of components opens up the possibility of producing new materials for modern technology. MEA and HEA with the general formula RCo_2 (R is a rare earth metal (REM)) possess enormous potential for use as working bodies in magnetic refrigerators or magnetostrictive sensors.

RCo_2 alloys accommodate complex substitutions in both the REM and Co sublattices, as well as combined substitutions in both sublattices

simultaneously. For example, substitution of several rare earth metals (R, R', R'') for one rare earth metal (R) allows for the production of samples with the required set of magnetic properties for practical applications.

Currently, magnetic cooling is a promising and most popular energy technology from both environmental and economic points of view [1]. RCo_2 alloys have enormous potential for use as working bodies in cascade magnetic refrigerators operating in the region of intermediate temperatures (between cryogenic and high) and capable of providing, for example, long-term storage of biomaterials. The purpose of this work was a comparative study of the structural, magnetic, magnetocaloric and magnetostrictive characteristics of medium-entropy Tb—Dy—Ho(Er)—Co alloys consisting of three elements in the rare-earth sublattice, taken in near-equiatomic proportions.

Tb—Dy—Ho(Er)—Co alloys were prepared using arc melting and subsequent homogenizing annealing. Certification of the obtained samples was carried out using X-ray diffraction and thermomagnetic analysis methods. The study of the magnetocaloric effect (MCE) was carried out by direct and indirect methods, while the magnetostrictive properties (including spontaneous magnetostriction) were studied by the tensometric method.

The results of X-ray diffraction analysis for two samples $Tb_{0.3}Dy_{0.35}Ho_{0.35}Co_2$ и $Tb_{0.3}Dy_{0.4}Er_{0.3}Co_2$ are shown in Table 1. It can be seen that the samples with a cubic $MgCu_2$ structure exhibit similar parameters.

Table 1

Structural and magnetic characteristics of medium-entropy alloys Tb—Dy—Ho(Er)—Co

Composition	a, nm	V, nm^3	T_C, K
$Tb_{0.3}Dy_{0.35}Ho_{0.35}Co_2$	0.718(8)	0.370	152
$Tb_{0.3}Dy_{0.4}Er_{0.3}Co_2$	0.717(8)	0.368	145

It has been established that both alloys have close values not only of the crystal lattice parameters, but also of the Curie temperature. However, the transition from a magnetically ordered to a disordered state occurs in different ways: in $Tb_{0.3}Dy_{0.35}Ho_{0.35}Co_2$ it is a first-order transition, and in $Tb_{0.3}Dy_{0.4}Er_{0.3}Co_2$ it is a second-order transition. It is well known that the type of transition has a significant impact on the functional characteristics, namely the magnitude of the magnetothermal and magnetostriction effects. It can be seen (see Fig. 1), for example,

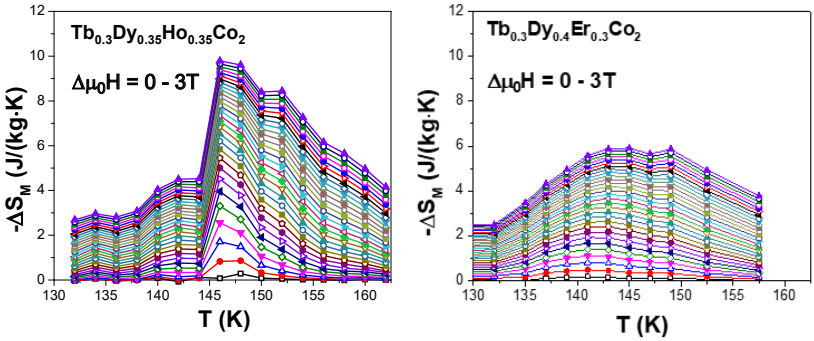


Fig. 1. Temperature dependences of the MCE for the $Tb_{0.3}Dy_{0.35}Ho_{0.35}Co_2$ and $Tb_{0.3}Dy_{0.4}Er_{0.3}Co_2$ alloys obtained by the indirect method

that during a first-order transition the magnitude of the MCE is twice as large. However, it is materials with second-order magnetic phase transitions that, as a rule, are the most promising for use in practice. The operating temperature of the alloys covers the temperature range of 145–152 K, which makes them potential candidates for creating a cooling system for long-term cryopreservation of vaccines and various biological objects.

The work of Politova G. A. was carried out within the framework of a state assignment № 075-00320-26-00.

[1] A. Kitanovski, J. Tušek, U. Tomc, U. Plaznik, M. Ožbolt, and A. Poredoš, *Cham: Springer* (2015).

Interaction of Surface Plasmon-Polaritons with Magnetic Skyrmions in Co/Pt Heterostructures

V. A. Tolkachev[1, a], I. V. Bychkov[1], D. A. Kuzmin[1]

[1] Chelyabinsk State University, Chelyabinsk, Russia
[a] e-mail: *tolkachev.v.a@csu.ru*

Surface plasmon-polaritons (SPPs) are hybrid waves that propagate along a metal–dielectric interface and decay exponentially into both media [1; 2]. They enable the concentration of electromagnetic energy in subwavelength regions, which is important for nanophotonics and sensing. SPPs can also exist at the interface between two metals, such as Co/Pt, opening a pathway toward the integration of plasmonic and magnetic functionalities [3; 4]. Combining Co/Pt with skyrmion excitation allows one to exploit strong spin–orbit coupling in Pt and perpendicular anisotropy in Co to stabilize skyrmions, while SPPs provide optical control [5].

In this work, we investigate the motion of skyrmions at the Co/Pt interface driven by an alternating magnetic field generated by SPPs. The total magnetic energy:

$$F = \int_V \left\{ A\left(\nabla m\right)^2 + D\left[m_z \left(\nabla \mathbf{m}\right) - \left(\mathbf{m}\nabla\right) m_z \right] - \mu_0 \mathbf{MH}_{ext} - \frac{\mu_0}{2} \mathbf{MH}_{demag} \right\} d^3 r,$$

where A is the inhomogeneous exchange constant, D is the constant characterizing the strength of the Dzyaloshinskii — Moriya interaction, which depends on the material properties and the direction of the spin–orbit coupling, $\mathbf{m}$ is the unit vector indicating the direction of the local magnetization, $\mathbf{H}_{demag}$ is the demagnetizing field, and $\mathbf{H}_{ext}$ is the external magnetic field.

The surface electromagnetic wave is described by a solution to Maxwell's equations at the interface between two media. For a TM wave, the magnetic field has the form $H_y\left(x,z,t\right) = H_0 \cdot e^{i\left(k_s x - \omega t\right)} \cdot e^{-\kappa_{1,2}|z|}$, where k_s — is the SPP wave number, $\kappa_{1,2} = \sqrt{k_s^2 - \varepsilon_{1,2}\left(\omega^2 / c^2\right)}$ is the transverse wave number, H_0 — is the magnetic field amplitude at the interface, and

$\varepsilon_{1,2}$ are the permittivities of cobalt and platinum, respectively.

The SPP dispersion relation is

$$k_s = \frac{\omega}{c}\sqrt{\varepsilon_1\varepsilon_2 / (\varepsilon_1 + \varepsilon_2)}\,.$$

Numerical simulations were performed for a Co/Pt structure with parameters typical of skyrmion systems. Fig. 1 shows the dependence of the skyrmion displacement along the y-axis on time for different amplitudes of the alternating magnetic field B_0. It can be seen that as B_0 increases, the amplitude of the periodic motion of the skyrmion increases, indicating a stronger effect of the field. Increasing the field frequency leads to more frequent oscillations of the skyrmion.

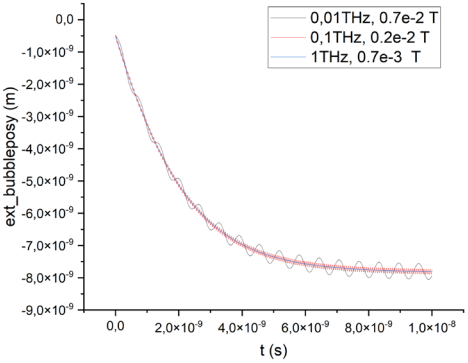


Fig. 1. Dependence of the skyrmion displacement along the y-axis on time

Fig. 2 shows the dependence of the skyrmion oscillation frequency on the frequency of the external electromagnetic wave (SPP). This dependence is found to be non-monotonic, resembling a periodic behavior. Such behavior indicates resonant conditions for the interaction between the surface wave and the intrinsic dynamics of the skyrmion, which can be exploited for frequency selection and motion control.

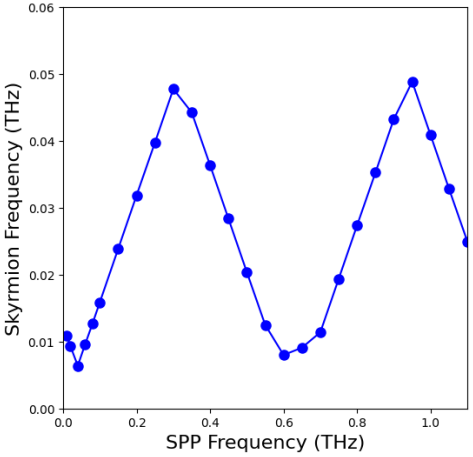


Fig. 2. Dependence of the skyrmion oscillation frequency on the SPP frequency

The obtained results show that the alternating magnetic field generated by

surface plasmon-polaritons allows efficient control of the dynamics of magnetic skyrmions in Co/Pt heterostructures.

The work was carried out within the framework of State Assignments № 075-00188-26-00.

[1] A. Sommerfeld Ann. *Phys. Chem*. 67, 233 (1899).

[2] A. V. Zayats, I. I. Smolyaninov. *J. Opt. A*. 5, S16 (2003).

[3] S. Chung et al. *Phys. Rev. B*. 103, 115430 (2021).

[4] E. Montoya et al. *Adv. Mater*. 32, 2002811 (2020).

[5] X. Chen et al. *Nano Lett*. 22, 512 (2022).

Experimental Study of the Magnetocaloric Effect in Ni—Co—Mn—Ti Heusler Alloys and Prospects for their Application

M. Utarbekova[1, a], M. Orshulevich [1], S. Taskaev [1], Hu Zhang [2], V. Buchelnikov [1]

[1] Chelyabinsk State University, Chelyabinsk, Russia
[2] University of Science and Technology Beijing, China
[a] e-mail: *shchichko.marina.csu@gmail.com*

Magnetocaloric materials (MCMs) are of significant interest for energy-efficient cooling technologies, such as magnetic refrigeration. Among them, Ni—Mn-based Heusler alloys demonstrate a substantial magnetocaloric effect (MCE) due to magnetostructural phase transitions. However, the brittleness of these intermetallics limits their practical application. This work is devoted to investigation new Ni—Co—Mn—Ti alloys, which are composed entirely of transition metals (all-*d* alloys), and which possess improved mechanical properties due to *d*-*d* hybridization [1; 2].

Polycrystalline Ni—Co—Mn—Ti alloys with various compositions (e. g. $Ni_{34}Co_{16}Mn_{35}Ti_{15}$, $Ni_{34}Co_{16}Mn_{40}Ti_{10}$) were synthesized within the study. The alloys were produced by arc melting in a pure argon atmosphere followed by annealing at 1173 K for 96 hours.

Microstructural analysis was performed using Scanning Electron Microscopy (SEM) and Energy Dispersive X-ray Spectroscopy (EDS). Magnetization measurements were carried out using a VersaLab Quantum Design Vibrating Sample Magnetometer (VSM) in fields of up to 3 T and temperatures ranging from 50 to 400 K. X-ray structural studies were conducted on a BRUKER D8 ADVANCE diffractometer (Cu Kα radiation).

The performed X-ray structural analysis confirmed the single-phase state and high crystallinity of all synthesized alloys.

The alloys $Ni_{34}Co_{16}Mn_{40}Ti_{10}$, $Ni_{35}Co_{15}Mn_{37}Ti_{13}$ and $Ni_{37}Co_{13}Mn_{34.5}Ti_{15.5}$ exhibit first-order phase transitions from a weakly magnetic martensite to a ferromagnetic austenite. The critical temperatures (M_s, M_f, A_s, A_f) were determined using the tangent method. For example, for $Ni_{34}Co_{16}Mn_{40}Ti_{10}$: A_f decreases from 427.1 K (1 T) to 418.6 K (3 T), indicating a significant influence of the magnetic field on the phase transition (Fig. 1).

The isothermal change in magnetic entropy (ΔS_m) was calculated from the magnetization data using the Maxwell relation:

$$\Delta S_m\left(T,H\right)=\int_{H_i}^{H_f}\left(\frac{\partial M_{(T,H)}}{\partial T}\right)dH\ . \qquad (1)$$

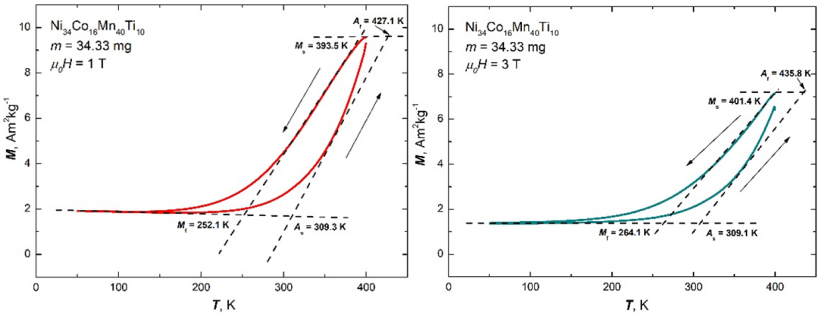


Fig.1. Temperature dependence of magnetization for the $Ni_{34}Co_{16}Mn_{40}Ti_{10}$ alloy in magnetic fields of 1 T and 3 T

The maximum ΔS_m values are observed near room temperature, making these materials promising for practical application.

In summary, the Ni—Co—Mn—Ti system alloys demonstrate a significant magnetocaloric effect (MCE), which is caused by the presence of

magnetostructural transitions. The critical temperatures of these materials exhibit a pronounced dependence on the external magnetic field, creating prerequisites for the targeted control of their functional characteristics. Furthermore, these alloys possess improved mechanical properties compared to traditional Heusler alloys, which broadens the prospects for their application in magnetic cooling devices. Further research in this area should focus on optimizing the chemical composition of the alloys using machine learning methods, as well as on studying multicaloric effects.

This work was supported by the Russian Science Foundation № 24-12-20016.

[1] Z. Guan, J. Bai, Y. Zhang, J. Gu, X. Jiang, X. Liang, R. Huang, Y. Zhang, C. Esling, X. Zhao, L. Zuo. *Rare Met*. 41, 1933–1947, (2022).

[2] Z. Wei, E. Liu, Y. Li, X. Han, Z. Du, H. Luo, G. Liu, X. Xi, H. Zhang, W. Wang, G. Wu. *Appl. Phys. Lett*. 109, 071904 (2016).

Features of Magnetic Inhomogeneities in (111)-oriented Garnet-ferrite Films with Flexomagnetoelectric Effect

R. M. Vakhitov[1, a], A. R. Yumaguzin[1], V. A. Demidova[1]

[1] Ufa University of Science and Technology, Ufa, Russia
[a] e-mail: *vakhitovrm@yahoo.com*

The relevance of studying magnetoelectric materials is determined by the discovery of a number of unique physical properties in them, promising for the development of energy-saving spintronic components. Among such phenomena, which are of fundamental importance for the development of information recording and processing systems, is the flexomagnetoelectric (FME) effect [1]. It consists of the displacement of 180-degree domain walls (180° DW) under the action of an electric field directed along the normal to the film surface. The effect depends significantly on the orientation of the film relative to the crystallographic axes. In particular, it was not detected in the (111)-oriented film. Theoretical

analysis of this situation showed [2] that 180° DW in (111)-type films do indeed respond to an external field, which leads to charge separation in the vicinity of the DW, but their resulting field is practically screened due to the symmetry of the magnetic subsystem. This leads to the fact that the effect seems to be present, but insignificant and difficult to detect.

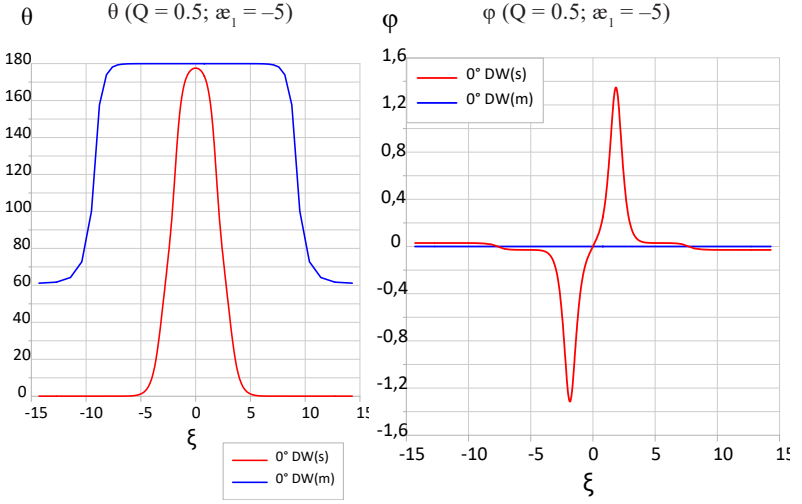


Fig. 1. Structures of 0^0 DW of different topologies, determined through the dependences of the angular variables $\theta(a)$ and $\varphi(b)$ on ξ. Here $æ_1 = K_1 / K_u$, $Q = K_u / 2\pi M_s^2$

In this paper, we investigate the features of the nucleation, structure and properties of 0° DW of different topologies that can exist in a (111)-oriented garnet-ferrite film when an electric field acts on it.

In the energy of magnetic inhomogeneities of the film under consideration, the contribution of the exchange interaction (characterized by the parameter A), uniaxial (K_u) and cubic (K_1) anisotropies, demagnetizing fields in the Winter approximation [3], as well as the contribution of the FME interaction, the energy density of which has the form:

$$w_{int} = \Delta M_s^2 \left[\left(b_1 \cos^2\varphi + b_2 \sin^2\varphi \right) \cos\theta \frac{d\varphi}{dy} + b_2 \sin\theta \sin\varphi \cos\varphi \frac{d\theta}{dy} \right],$$

where θ and φ are the polar and azimuthal angles of the vector $\boldsymbol{M} = M_s \mathbf{m}$, M_s — saturation magnetization, $\boldsymbol{m} = (\sin\theta\cos\varphi, \sin\varphi, \cos\theta\cos\varphi)$ — unit magnetization vector. Here Oz||[111], Oy coincides with the direction

along which the magnet is inhomogeneous, Ɛ — electric field strength (Ɛ||Oz), b1 и b2 — magnetoelectric constants [3].

Numerical solution of the Euler — Lagrange equations for the film under study shows that two types of 0° DW arise in the region $æ_1 < -4.5$. One of them corresponds to the Bloch structure (0° DW(m)) and has, for the values of $(æ_1 = -5, Q = 0.5)$, the limiting values of the angles θ and φ: $\theta = 61$, $\varphi = 0; 2\pi/3; 4\pi/3$ as $y \to \pm\infty$. The other corresponds to the quasi-Bloch structure (0° DW(s)) with the dependence $\varphi = \varphi(y)$, which is an odd function, and has θ, φ: $\theta = 0$, $\varphi = 0$ as $y \to \pm\infty$. In this case, the 0° DW(s) has an energy an order of magnitude lower than that of the 0° DW(m) and, therefore, is an energetically more favorable structure than the 0° DW(m). Calculations show that under the action of a field, charges arise in the vicinity of the wall which, with a further increase in Ɛ, can reach values twice the maximum value of charges induced in the 180° DW in a uniaxial film [3] under the same conditions.

The authors are grateful for the financial support of the State assignment of Russian Federation for the implementation of scientific research by laboratories (№ 075-03-2024-123/1 15.02.2024).

[1] A. S. Logginov, G. A. Meshkov, A. V. Nikolaev, E. P. Nikolaeva, A. P. Pyatakov, A. K. Zvezdin. *Appl. Phys. Lett*. 93, 182510 (2008).

[2] R. M. Vakhitov, A. R. Yumaguzin and G. T. Gridneva. *Phys. Scr.* 98, 125988 (2023).

[3] R. M. Vakhitov, Z. V. Gareeva, R. V. Solonetskiy, F. A. Mazhitova. *Phys. Solid State*. 61, 1043–1051 (2019).

Landau — Khalatnikov Description of Magnetization Relaxation Effects Near First-order Phase Transitions

A. R. Vashchenkova[1, a], A. S. Komlev[1], D. I. Komleva[1]

[1] Faculty of Physics, M. V. Lomonosov Moscow State University, 119991, Moscow, Russia
[a] e-mail: *vashchenkova.ar21@physics.msu.ru*

Magnetic materials undergoing a first-order phase transition are of significant interest to modern science due to their ability to abruptly change their properties in response to relatively weak external fields [1]. This feature makes them promising for use in high-density data storage devices, highly sensitive sensors, and energy-efficient solid-state cooling systems [2; 3]. However, near the first-order phase transition temperature, non-equilibrium processes play a key role: the observed phase transition parameters depend on the rate of change of external conditions, such as the magnetic field and temperature. In these conditions, magnetic viscosity plays an important role. This phenomenon manifests as a change in magnetization over time under fixed external conditions.

Experimental studies of FeRh and $La(Fe, Si)_{13}$ alloys undergoing a first-order phase transition under non-stationary thermal and field excitation have revealed pronounced magnetoviscous effects. It was found that increasing the heating rate leads to a systematic shift of the phase transition temperature toward higher temperatures. When the magnetic field is changed at finite rates, a non-linear shift of the critical transition fields, as well as changes in magnetic susceptibility and coercive force, are observed. These data indicate that the effective transition parameters are not material constants but are determined by the magnetization relaxation dynamics of the material.

To describe the observed dynamics, a theoretical model was used, combining the Landau — Bean — Rodbell thermodynamic potential with the Landau — Khalatnikov relaxation equation:

$$\frac{\partial M}{\partial t} = -G' \frac{\partial F}{\partial M},$$

where G' is the kinetic coefficient that determines the system's response rate. Verification of the model on experimental data for FeRh and $La(Fe, Si)_{13}$ showed that the traditional use of a constant coefficient is fundamentally insufficient [4]. A model with a constant predicts a linear dependence of the critical parameters on the excitation rate, which does not agree with the experimentally observed non-monotonic behavior of the characteristic relaxation time under external excitation.

Qualitative agreement is achieved by introducing the kinetic coefficient as a function of magnetization. The best quantitative agreement with the experiment is provided by a non-monotonic function with a Gaussian-like minimum. This is due to the fact that during the phase transformation, the interaction between magnetic clusters is maximized at intermediate magnetization values, which creates the greatest dynamic obstacle to phase growth and leads to a peak in the relaxation time.

Thus, magnetic viscosity in these materials should be seen as a non-equilibrium response, influenced by the system's state and external factors. The approach developed here will help move from describing dynamic anomalies to modeling specific devices and optimizing how they work in the future. Additionally, the method makes it easier to separate caloric effects from other mechanisms in the relaxation process, which will help improve our understanding of magnetic viscosity in future studies.

This work was supported by the Russian Science Foundation (project № 25-72-00039).

[1] D. Y. Karpenkov et al. *Phys. Rev. Appl*. 13, 034014 (2020).

[2] D. Y. Karpenkov et al. *J. Alloys Compd*. 962, 171154 (2023).

[3] X. Wang et al. *IEEE Trans. Magn*. 49, 686 (2013).

[4] R. M. Costa et al. *J. Phys. D: Appl. Phys*. 56, 155001 (2023).

Quantum Thermal Valve with Magnetocaloric Effect

S. V. von Gratowski[1, a], V. V. Koledov[1]

[1] Kotelnikov Institute of Radioengineering and Electronics of RAS, Moscow, Russia

[a] e-mail: *svetlana.gratowski@yandex.ru*

Modern industry and scientific research require technologies for heat management at cryogenic temperatures (ranging from 0.7 to 120 K), driven by the wide range of applications of such technologies across various industries. These industries include gas liquefaction and transportation, metallurgy, chemicals, energy and hydrogen power, as well as space exploration, medicine and biotechnology, quantum technologies, the food industry, and data centers. Effective management of all these processes requires devices capable of managing heat flows at these temperatures. One such device is a thermal valve. It is also important to note the importance of managing heat flows at low temperatures for many areas of fundamental science.

At low temperatures, many materials and structures, such as superconductors and structures associated with the Josephson effect, exhibit phase coherence. Recently, it was discovered that wave properties of heat, namely, interference of heat flux in a magnetic field, were detected in Josephson structures in a magnetic field [1]. That is, in [1], it was experimentally shown that the heat flux can have coherence. Based on this fundamental work, various devices for quantum superconducting caloritronics have already been created. In [1], a quantum thermal interferometer was proposed, then a thermal diode and a thermoelectric transistor were theoretically proposed and experimentally implemented, T-SQUIPT (thermal transistor/memory), photonic field-effect thermal transistor, heat engines and other devices were experimentally implemented. That is, a whole new scientific field of superconducting coherent spin caloritronics has been created.

Within the physical phenomena and devices of superconducting coherent spin caloritronics, one of the most interesting systems is the superconductor-ferromagnet-superconductor (S/F/S) Josephson junction. A Josephson junction of the SFS type is a complex quantum structure in

which two superconductors are separated by a thin layer of ferromagnetic material. Unlike a classical junction (SIS, where the barrier is a dielectric), in an SFS junction, current is carried by Cooper pairs through a material that inherently destroys superconductivity. This leads to unique effects, the most well-known of which is the formation of a π-junction, among others. SFSs also enable heat flow control via phase and magnetic field. The thermal conductivity of an SFS junction is phase-dependent: it is modulated by the phase difference between the superconducting electrodes. If SIS contacts provide thermal control via the φ phase, then adding a ferromagnetic layer adds a magnetic degree of freedom — the exchange field Hex and the magnetic state M. This changes both the physics and functionality of the device.

Within the physical phenomena and devices of superconducting coherent spin caloritronics, one of the most interesting systems is the superconductor-ferromagnet-superconductor (S/F/S) Josephson junction. A Josephson junction of the SFS type is a complex quantum structure in which two superconductors are separated by a thin layer of ferromagnetic material. Unlike a classical junction (SIS, where the barrier is a dielectric), in an SFS junction, current is carried by Cooper pairs through a material that inherently destroys superconductivity. This leads to unique effects, the most well-known of which is the formation of a π-junction, among others. SFSs also enable heat flow control via phase and magnetic field. The thermal conductivity of an SFS junction is phase-dependent: it is modulated by the phase difference between the superconducting electrodes. If SIS contacts provide thermal control via the φ phase, then adding a ferromagnetic layer adds a magnetic degree of freedom — the exchange field Hex and the magnetic state M. This changes both the physics and functionality of the device.

This paper proposes a phase-transition magnetocaloric quantum thermal valve that controls heat flow through a phase transition between a ferromagnet and a normal metal, or insulator, in an SFS contact. Depending on the configuration of the entire structure, various heat flow control options are possible. Specific materials and device parameters are proposed that make it possible to implement experimentally quantum thermal valve with magnetocaloric effect.

This work was carried out within the framework of a by state assignment of the IRE RAS.

[1] F. Giazotto, M. J. Martínez-Pérez. *Nature.* 492**,** 401–405 (2012).

Partial Phase Transition and Surface Effects in a thin Helimagnet/Ferroelectric Superlattices

A. R. Yuldasheva[1, a], I. F. Sharafullin[1]

[1]Ufa University of Science and Technology, Laboratory of design of new materials, Ufa, Russia
[a]e-mail: *alina.yuldasheva.92@mail.ru*

Helimagnets are a type of magnetic crystal in which spin ordering (ferro-, ferri-, or antiferromagnetic) is accompanied by a rotation by a certain angle at each crystal lattice site along one or more directions over scales much larger than the unit cell dimensions [1]. The reason for such rotation is, for example, the competition between ferromagnetic and antiferromagnetic exchange interactions in the case of a frustrated spin lattice. This provides a promising basis for the creation of spintronic devices in which conducting helimagnets will serve as key functional components [2].

In this work, we consider a model of a magnetoelectric superlattice consisting of a thin helimagnetic film of N_z layers with Heisenberg spins on the sites of a simple cubic lattice and a ferroelectric film with polarization vectors on the sites of a square lattice. The Hamiltonian of the system has the form:

$$H = H_{mag} + H_{fe} + H_{mfe}, \tag{1}$$

$$H_{mag} = -J_1 \sum_{i,j} \vec{S}_i \cdot \vec{S}_j - J_2 \sum_{i,l} S_i \cdot S_l - h \sum_i S_i^z . \tag{2}$$

$\langle i, j \rangle$ — summation over nearest neighbor spins $\vec{S}_i$ and $\vec{S}_j$ interacting ferromagnetically with $J_1 > 0$, $\langle\langle i,l \rangle\rangle$ — summation over spins $\vec{S}_i$ and $\vec{S}_l$ located at next-nearest neighbor sites, interacting antiferromagnetically with $J_2 < 0$. h is the external magnetic field strength applied perpendicular to the film plane.

$$H_{fe} = -J_{fe} \sum_{i,j} \overrightarrow{P_i} \cdot \overrightarrow{P_j} ; \tag{3}$$

$$H_{mfe} = -J_{mfe} \sum_{i,j,k} P_k^z \left(S_i^x S_j^y - S_i^y S_j^x \right). \tag{4}$$

$\langle i,j \rangle$ — summation over nearest neighbor polarization vectors $\vec{P}_i$ and $\vec{P}_j$ with interaction parameter $J_{fe} > 0$. The magnetoelectric interaction between the helimagnetic and ferroelectric films is defined by the Hamiltonian:

$$H_{mfe} = -J_{mfe} \sum_{i,j,k} P_k^z \left(S_i^x S_j^y - S_i^y S_j^x \right), \quad (5)$$

where $J_{mfe} < 0$ is the magnetoelectric interaction parameter. The inclusion of competing interactions J_2 and J_{mfe} leads to the formation of a spiral (helimagnetic) ground state along all three directions.

For the considered model of magnetoelectric coupling between the magnetic film and the ferroelectric film in the superlattice, i. e., between the dipole moment of the ferroelectric film and the in-plane spins of the magnetic film at the interface of the multiferroic superlattice, it is shown that in the ground state, uniform non-collinear spin configurations appear in the magnetic surface layer in the absence of an external magnetic field. When an external magnetic field perpendicular to the film plane is applied, a transition of such configurations into skyrmions occurs. Using Monte-Carlo simulations, a strong deviation in the temperature dependence of the surface magnetization compared to the magnetization of the inner layers was observed. The transition temperature at the surface layer changes with the variation of the surface exchange interaction, i. e., the order on the surface layers is destroyed at lower temperatures than in the in-plane magnetic layers. Such a partial phase transition is not typical for thin films, where disordering of the surface layer rather than the inner layer is more commonly observed. In the case of strong magnetoelectric interaction at the interface, it aligns the spins only in the *xy* plane of the magnetic layer, despite the action of the external magnetic field. Upon increasing the temperature in the superlattice, a first-order transition is observed, since the considered system is frustrated due to the presence of strong competing interactions. Moreover, the phase transition in the magnetic film under strong magnetoelectric interactions occurs only after the phase transition in the ferroelectric film, i. e., upon loss of ferroelectric order at $T \approx 2.3$ (in energy units). Note that at $H = 0$, skyrmions do not form at the interface, and the spin configuration is spiral in the ground state; this configuration also breaks down at $T \approx 2.3$ (transition to the paramagnetic phase) simultaneously with the destruction of the collinear ferroelectric order. At moderate values of the magnetoelectric interaction, second-order phase transitions occur in the system.

This work was carried out within the framework of the state assignment agreement № 075-03-2024-123/1 dated February 15, 2024.

[1] V. A. Chizhikov. *JETP*. 159, 656. (2021).

[2] V. V. Ustinov, I. A. Yasyulevich. *Phys.-Usp.* 195. N. 10. P. 1062–1093. (2025).

Abstract Magnetocaloric Properties of Melt-extracted Gd—Co and Er-doped Gd—Co Crystalline/Crystalline Composite Microwires

Yuhai Qu [1, 2]

[1] School of Physics and Materials Science, Nanchang University, Nanchang, 330031, China

[2] Chongqing Research Institute of Nanchang University, Chongqing, 402660, China

Gadolinium (Gd) is the benchmark magnetocaloric material, yet its performance requires optimization in working temperature range, refrigeration capacity (RC) and heat exchange capacity. Here, we address this by a synergistic strategy combining Co alloying (to form an in-situ dual-phase magnetocaloric system), optional Er alloying (to tune the phase transition temperature) and the melt-extraction technique (to directly shape the alloy into microwires). Using this approach, we fabricated both $Gd_{87.5}Co_{12.5}$ and $Gd_{57.5}Er_{30}Co_{12.5}$ (at.%) crystalline/crystalline composite microwires, allowing a direct comparison between Er-free and Er-doped variants. The resulting microstructure comprises a Gd-rich matrix embedded with magnetocaloric Gd_3Co phase, both of which are crystalline. This dual-phase architecture yields a remarkable magnetic entropy change ($-\Delta S_m$) profile, which delivers an ultra-broad effective temperature span (δT) of above 210 K (defined between the outer half-maximum points of the dual-peak magnetic entropy change vs temperature curve) and a high RC of above 650 J/kg under 5 T. More importantly, it validates a dual-route design paradigm: phase-composition engineering for broadened

δT and RC, coupled with morphology engineering via melt-extraction for enhanced heat exchange. This work establishes a new paradigm for designing next-generation magnetocaloric materials with integrated performance enhancements, particularly for efficient magnetic refrigeration in applications like gas liquefaction.

Method for Measuring Magnetization in Alternating Magnetic Fields

D. M. Yusupov[1,a], A. M. Aliev[1]

[1]Amirkhanov Institute of Physics of Dagestan Federal Research Center, Russian Academy of Sciences, Makhachkala, Russia
[a]e-mail: *dibir.usupov@mail.ru*

Magnetocaloric materials continue to be in the focus of attention as working materials for promising magnetic cooling technology. Dozens of different materials with giant values of the magnetocaloric effect (MCE) are currently known. Recent studies in cyclic magnetic fields show that not all of them are promising in terms of the stability of magnetocaloric properties, as well as the dependence of these properties on the frequency of the magnetic field. Most of the materials studied in cyclic magnetic fields show a strong dependence on the frequency of the magnetic field, but it is difficult to establish the nature of this phenomenon only using the data on the adiabatic temperature change. Therefore, an important task is to study the parameters associated with the MCE, such as magnetization and magnetostriction (the latter in the case of the first-order phase transitions) in cyclic magnetic fields.

In this paper, a method for studying magnetization in alternating (AC) magnetic fields is proposed. The method is based on the law of electromagnetic induction, which states that for any closed circuit, the electromotive force (EMF) generated in it by a magnetic field is equal to the rate of change of the magnetic flux through this circuit, taken with a minus sign. As such a circuit, we used two oppositely wound coils. This is done

in order to minimize the EMF induced in the coil without a sample. But due to the non-ideality of the coil geometry and its placement in an alternating magnetic field, some value of an EMF will be induced in the AC field. The difference in EMF in the coil in an AC magnetic field with and without a sample will be proportional to the magnetization of the sample.

The reference magnetocaloric material gadolinium Gd was selected for testing and calibration the technique. Magnetization in alternating magnetic fields was also studied for other rare earth elements terbium Tb and dysprosium Dy. The studies were carried out both in a constant magnetic field using the vibration technique and in AC magnetic fields with a frequency of 0.3 Hz and a field change amplitude of up to 3 kOe. The measurements of the temperature dependences of magnetization for Gd, Tb and Dy at a low frequency of the field are in agreement with the results obtained by the vibration magnetometry method.

The work was supported by the Russian Science Foundation, grant № 24-12-00362.

Ground State of Mn_3Al Heusler Compound: Insights From *ab initio*

I. V. Artamonov[1,a], M. A. Zagrebin[1,b]

[1]Chelyabinsk State University, Chelyabinsk, Russia
[a]e-mail: *artamonovvv97@mail.ru*
[b]e-mail: *miczag@mail.ru*

Despite advancements in applied physics, the production of alloys with a specific configuration and rigorously defined properties often leads to the formation of secondary and/or competing phases. Specifically, for the Mn_3Al Heusler alloy, the β-Mn phase acts as a «competitor». The Mn-Al-based alloys themselves are of significant interest to modern spintronics as a potential compensated ferrimagnet. However, their synthesis in the target cubic Heusler structure ($L2_1$ or $D0_3$ type) is challenging due to the high stability of the competing β-Mn phase ($P4_132$ и $P4_332$) [1; 2].

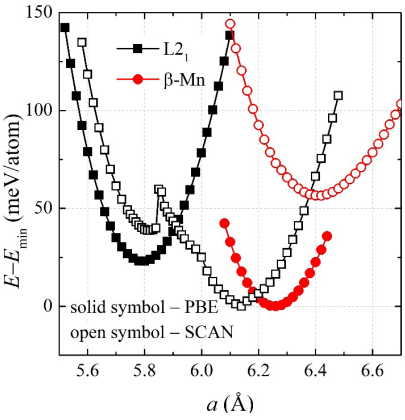


Fig. 1. Relative energies referenced to the global minimum per atom

In this work, a comparative analysis of the energetic stability of various magnetic states of the Mn_3Al alloy with the β-Mn (space group $P4_132$) and $L2_1$ (space group Fm-$3m$) structures is performed as a function of atomic ordering. Calculations were carried out within the density functional theory framework as implemented in the Vienna Ab-initio Simulation Package (VASP) [3; 4]. We employed both the generalized gradient approximation with the Perdew — Burke — Ernzerhof (GGA-PBE) [5] and the meta-generalized gradient approximation using the Strongly Constrained and Appropriately Normed (Meta-GGA SCAN) [6] functionals. As for magnetic structure of the phases considered in the calculations, ferrimagnetic and antiferromagnetic configurations for $L2_1$ and β-Mn were used, respectively. The obtained dependencies of the total energy on the lattice parameter $E(a)$ reveal a competing relationship between magnetic order and crystal symmetry (Fig. 1).Several β-Mn configurations are established to be energetically more favorable compared to the ordered $L2_1$ phase, which is due to the specific occupancy of the inequivalent 8c and 12d positions. It is shown that the minimization of energy in these states is achieved through the formation of a complex antiferromagnetic (possibly non-collinear) order, which effectively relieves magnetic frustration in the triangular sublattices of manganese.

The presence of intersection points of the energy curves and the small difference in energy minima (≈30 and ≈50 meV) indicate a critical sensitivity of phase stability to changes in interatomic distances. Such a high degree of thermodynamic competition explains the possibility of phase coexistence and points to the potential for controlling the phase composition of the alloy through external pressure or thermal treatment.

The study was financially supported by the Ministry of Science and Higher Education of the Russian Federation as part of the state assignment № 075-00188-26-00.

[1] M. Vasundhara, V. V. Marchenkov, V. G. Pushin, N. I. Kourov, V. Y. Irkhin, E. B. Marchenkova. *J. Magn. Magn. Mater*. 513, 167093 (2020).

[2] V. V. Marchenkov, V. Yu. Irkhin, E. B. Marchenkova, A. A. Semiannikova, P. S. Korenistov. *Phys. Lett. A*. 471, 128803 (2023).

[3] G. Kresse, J. Furthmüller. *Phys. Rev. B*. 54, 11169 (1996).

[4] G. Kresse, D. Joubert. *Phys. Rev.* B. 59, 1758 (1999).

[5] J. P. Perdew, K. Burke, M. Ernzerhof. *Phys. Rev. Lett*. 77, 3865 (1996).

[6] J. Sun, A. Ruzsinszky, J. P. Perdew. *Phys. Rev. Lett*. 115, 036402 (2015).

Influence of Impurity Phases in Chromium (IV) Oxide on Magnetic and Magnetocaloric Properties

Z. Zhao [1], C. Liu [1], I. E. Graboy [1], A. G. Gamzatov [2], K. Qiao [3], H. Zhang [3]

[1]Lomonosov Moscow State University, Faculty of Materials Science, Moscow, Russia
[2]Amirkhanov Institute of Physics, DFRC, RAS, 367003, Makhachkala, Russia
[3]University of Science and Technology Beijing, Beijing, China
e-mail: *2283266092@qq.com*

Materials exhibiting the magnetocaloric effect (MCE) are of great interest for the development of magnetic refrigerators and devices for achieving ultra-low temperatures (~0.001 K). Magnetic domain structure, which depends on the microstructure and interphase boundaries of the material, plays a key role in the dynamics of the phase transition. This work is devoted to the role of impurity phases in the frequency stability of the MCE in the ferromagnet CrO_2 (T_C ~ 391 K).

Two methods were used to synthesize CrO_2 with impurity phases. The first was thermal decomposition of CrO_3 in the temperature range 380–500 °C under high oxygen pressure (~150 atm). It was found that the composition of the obtained powders depends on the temperature and duration of annealing. At low temperatures, Cr_2O_5 was observed as an impurity phase. Increasing the temperature led to the formation of Cr_2O_3 as an impurity. The main drawback of this method is the poorly controllable amount of impurities and their high concentration (> 10 mol.%).

To obtain samples with a lower content of impurity phases, pure CrO_2 was impregnated with a solution of $Cr(NO_3)_3$of known concentration, followed by decomposition in oxygen at 300 °C. In this case, Cr_2O_3 was the only second phase.

Magnetic susceptibility measurements showed that an increase in the CrO_2 fraction leads to an increase in the specific magnetization. At the same time, the type of impurity plays a decisive role in the value of saturation magnetization (M_s), especially for samples with a high (> 10 mol.%) content of impurity phase. For example, samples with the same amount of Cr_2O_3 and Cr_2O_5 differed by a factor of two in M_s. When Cr_2O_5 and Cr_2O_3 were present simultaneously, an increase in the proportion of Cr_2O_3 in the mixture led to an increase in M_s. We believe that this effect is related not only to the diamagnetism of Cr_2O_5 and the antiferromagnetism of Cr_2O_3, but also to the ability of Cr_2O_3 to form coherent boundaries with CrO_2, which minimizes the destruction of the ferromagnetic order.

This work also presents the results of magnetization measurements M(T) in heating and cooling modes in a magnetic field of 100 Oe (see Fig. 1(a)) and direct measurements of the adiabatic temperature change ΔT_{ad} in magnetic fields of 1.8 and 8 T (Fig. 1(b)). Direct measurements of the adiabatic temperature change in a magnetic field of 1.8 T showed that the maximum $\Delta T_{ad} \approx 0.66$ K is observed for the sample with 3% Cr_2O_3, whereas at 1.5%, 5%, and 7% it was about 0.45 K. Since the saturation magnetization hardly changes over the entire range of 1.5–7% Cr_2O_3, the observed maximum ΔT_{ad} at 3% is associated with an optimal balance

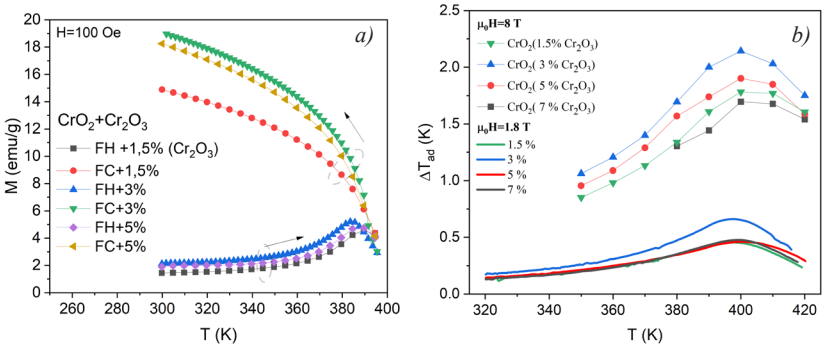


Fig. 1. a) Dependence M(T) for three concentrations of Cr_2O_3 measured in FH and FC modes. b) Dependence of ΔT_{ad} on temperature in magnetic fields of 1.8 and 8 T

between pinning and magnetic dilution, rather than with a change in the magnetic moment. To confirm this mechanism, additional measurements were performed in a high magnetic field of 8 T. They showed that the optimal concentration of 3% Cr_2O_3 is maintained: the maximum ΔT_{ad}. For samples with Cr_2O_3 contents of 1.5 %, 5%, and 7%, the ΔT_{ad} values in an 8 T Kadfield were 1.78 K, 1.9 K, and 1.69 K, respectively, confirming the nonmonotonic dependence of the MCE on the concentration of the secondary phase. Thus, the measurements in high fields fully support the model of competition between pinning and magnetic dilution. All studied samples, including the optimal composition with 3% Cr_2O_3, demonstrated high stability of the MCE under cyclic magnetization. No degradation of the effect or hysteresis was observed, which confirms the suitability of the material for real magnetic cooling devices.

The conducted studies allow us to conclude that the MCE in CrO_2 is not only determined by the mole fraction of the secondary phase Cr_2O_3, reaching a maximum at its value of ~3 % due to optimal pinning, but is also characterized by high stability under cyclic magnetization. This confirms the practical potential of CrO_2 as a working body in magnetic cooling systems.

The work was supported by a grant from the Russian Science Foundation, project № 24-12-00156, https://rscf.ru/project/24-43-00156/.

A phenomenological Model for Multi-stimulus Magnetic Refrigeration: T_{ad} for Second-order Phase Transitions

M. V. Zheleznyi[1,2]

[1]National University of Science and Technology MISIS, Moscow, Russia
[2]Lomonosov Moscow State University, Moscow, Russia
e-mail: *markiron@mail.ru*

In this work, a phenomenological model of the behavior of the working body of a magnetic refrigerator operating on a multistage cooling cycle

has been developed. In particular, analytical expressions were obtained for calculating the contributions of lattice and magnetic entropies to the total entropy change under a phase transition. Based on the developed model, an analytical dependence of the adiabatic temperature changes and specific heat of a magnetocaloric material undergoing a second-order phase transition has been obtained. This dependence can be implemented in models of a magnetocaloric refrigerator being developed using the finite element method, to simulate the temperature change and specific heat variation of the refrigerant during its magnetization and demagnetization.

In this work, using the formalism of the quantum-statistical operator (density matrix), expressions are obtained for the contributions of thermal vibrations and quasi-elastic energy to the Gibbs thermodynamic potential, taking into account inharmonic effects. Then, an expression for the magnetic contribution to the Gibbs potential is obtained in the simplest mean-field (molecular effective field) approximation for a model system of localized magnetic moments. After appropriate transformations, an expression for the total Gibbs potential as a function of temperature, external magnetic field, and magnetization is obtained in the form of a power series in the dimensionless magnetization $\mathfrak{m}(t;h)$ of the system.

Furthermore, using the total Gibbs potential, a third-degree equation of magnetic state (thermodynamic equilibrium) is derived, which is justified in the case of a second-order magnetic phase transition. This equation allows us to explicitly obtain expressions describing the temperature and field dependences of magnetization in both the ferromagnetic and paramagnetic states. Below are these explicit dimensionless dependences of the magnetization $\mathfrak{m}(t;h)$.

$$\begin{cases} m(t;h) = th\left[2\cdot\sqrt{\dfrac{1-t}{t}}\cdot cos\left[\dfrac{\pi}{6}-\dfrac{1}{3}\cdot arcsin\left[\dfrac{3\cdot h\cdot\sqrt{t}}{2\cdot(1-t)^{\frac{3}{2}}}\right]\right]\right], if\ t<1\left(ferromagnetic\ state\right); \\ m(t;h) = th\left[2\cdot\sqrt{\dfrac{t-1}{t}}\cdot sh\left[\dfrac{1}{3}\cdot arsh\left[\dfrac{3\cdot h\cdot\sqrt{t}}{2\cdot(t-1)^{\frac{3}{2}}}\right]\right]\right], if\ t>1\left(paramagnetic\ state\right). \end{cases} \tag{1}$$

If we use the formulas of system (1) to find the indicated first-order partial derivatives of the magnetization function $\mathfrak{m}(t;h)$ for both the

"ferromagnetic" solution (for $t<1$) and the "paramagnetic" solution (for $t>1$), we can similarly obtain the explicit form of the two-branch system Δt as a function of the arguments t and h.

$$\ddot{A}t(t;h) \cong -\frac{h \cdot t \cdot \left(\frac{\partial m(t;h)}{\partial t}\right)_h}{\left[C_{p,lat}\left(\frac{\theta_D}{t}\right) + t \cdot \frac{\left\{\left(\frac{\partial m(t;h)}{\partial t}\right)_h\right\}^2}{\left(\frac{\partial m(t;h)}{\partial h}\right)_t}\right]}. \quad (2)$$

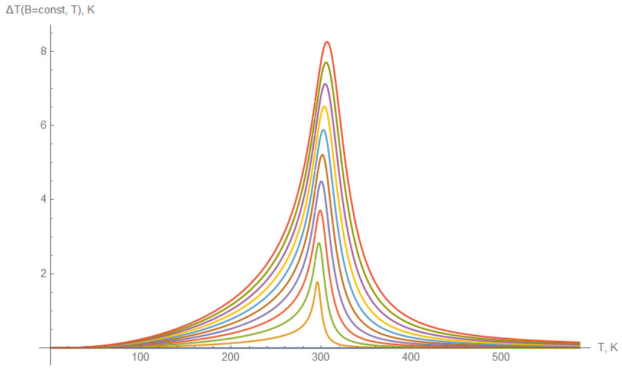


Fig. 1. Dependence of the equilibrium ΔT-effect on the temperature T for different values of the external magnetic induction B

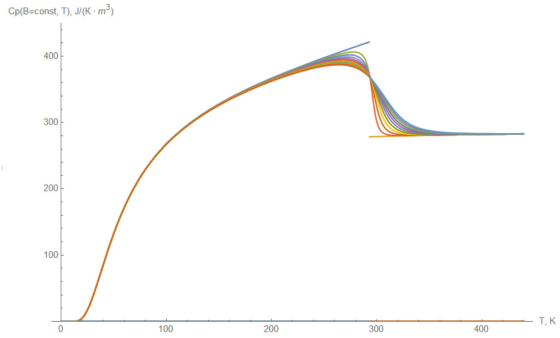


Fig. 2. Dependence of the equilibrium specific heat Cp on temperature T for different values of the external magnetic induction B

In this manner, the total heat capacity of the system under consideration can be computed as the sum of the "lattice" contribution and the "magnetic" contribution.

Figures 1 and 2 show the temperature dependences of the $\Delta T_{ad}(T; B)$ effect and the total heat capacity $C_p(T; B)$, plotted over a range of the external magnetic induction B from 0 to 5 T in steps of 0.5 T for $\Delta T_{ad}(T; B)$ and from 0 to 10 T in steps of 1 T, respectively.

This work was carried out within the framework of a state assignment and partially supported by the RSF, project № 25-22-00371.

Scaling Analysis of the Adiabatic Temperature Change in Alternating Magnetic Fields

A. M. Aliev[1, a], N. Z. Abdulkadirova[1], Z. Z. Alisultanov[1,2]

[1]Amirkhanov Institute of Physics DFRC RAS, Makhachkala, Russia
[1,2]Abrikosov Center for Theoretical Physics, MIPT, Dolgoprudnyi, Russia
[a] e-mail: *lowtemp@mail.ru*

Magnetic phase transitions and the associated critical phenomena are of considerable interest from both fundamental and applied perspectives. One of the key methods for investigating such transitions is scaling analysis, which enables the identification of universal behavior in thermodynamic quantities near the phase transition point. Of particular interest is the application of the scaling approach to the study of the magnetocaloric effect (MCE).

In this work, we perform a scaling analysis of the adiabatic temperature change in a gadolinium single crystal subjected to alternating magnetic fields. We demonstrate that, in the high-field regime ($H > 2$ T), the data obey nearly ideal scaling of the form:

$$\frac{\Delta T}{H^n} = F\left(\frac{t}{H^{1/\beta}}\right), \tag{1}$$

with the exponent $n = 2/3$, corresponding to the mean-field approximation, where $F(x)$ is a universal scaling function. This result is in excellent

agreement with theoretical predictions, as strong magnetic fields suppress critical fluctuations, thereby validating the mean-field theory, which neglects fluctuation effects.

In the low-field regime ($H < 0.3$ T), however, scaling breaks down: no value of the exponent n in Eq. (1) can collapse all experimental $\Delta T_{ad}(T)$ curves obtained at different fields onto a single universal dependence. This indicates that the scaling hypothesis ceases to hold in weak fields. We show that accounting for the field dependence of the heat capacity cannot explain the observed scaling violation in this regime.

Based on these findings, we conclude that the deviation from scaling behavior in weak fields is associated with magnetization mechanisms not captured by the standard scaling theory of critical phenomena. The most probable candidates are processes related to the magnetic domain structure of the material — specifically, domain growth and domain-wall motion, which become the dominant magnetization mechanisms precisely in the low-field limit.

We further demonstrate that, in the weak-field regime, the field dependence of the MCE follows $\Delta T_{ad} \propto H^{\lambda+}$. Whereas scaling theory predicts $\Delta T_{ad} \propto H^{2/3}$ in strong fields, we obtain $\Delta T_{ad} \propto H^2$ for $\lambda = 1$ in weak fields. This fundamentally distinct behavior explains why no single scaling exponent *n* can ensure data collapse across the entire field range.

This work was supported by the Russian Science Foundation, Project No. 24-12-00362.

Magnetocaloric effect of sublimated dysprosium in high steady and pulsed magnetic fields

Yu. S. Koshkid'ko [1], J. Ćwik[1], C. Salazar Mejia[2], N. A. Dormidontov [3], P. A. Prokofev[3], A. S. Bakulina[3], A. A. Nikitin[4], A. A. Khomich[4], R. R. Gimaev[5], A. S. Andreenko[5], Zh. P. Burmii [6], A. A. Telitsa[5], V. I. Zverev [5], N. B. Kolchugina[3]

[1] Institute of Low Temperature and Structure Research, Polish Academy of Sciences, Wrocław, 50-950 Poland
e-mail: *y.koshkidko@intibs.pl*
[2] Hochfeld-Magnetlabor Dresden (HLD-EMFL), Helmholtz-Zentrum Dresden-Rossendorf, 01328 Dresden, Germany
[3] Baikov Institute of Metallurgy and Materials Sciences, Russian Academy of Sciences, Leninskii pr. 49, Moscow, 119334 Russia
[4] National Research Center Kurchatov Institute, pl. Akademika Kurchatova 1, Moscow, 123182 Russia
[5] Moscow State University, Faculty of Physics, Leninskie Gory 1, Moscow, Russia
[6]Institute of Microelectronics Technology and High-Purity Materials, Russian Academy of Sciences, Chernogolovka, Russia

As is known, rare-earth metals (REMs) are promising magnetocaloric materials. The magnitude of the magnetocaloric effect (MCE) of REMs significantly depends on their purity. This paper presents results of studies of the magnetic and magnetocaloric properties of sublimed dysprosium, prepared in the course of the present study, with an emphasis on its impurity and structure perfection. The comprehensive analysis of the chemical composition of sublimed dysprosium, which was performed for the first time by atom probe tomography, showed that the metal corresponds to high-purity rare-earth metals (3N+). The study of the MCE of polycrystalline sublimed dysprosium by direct method in magnetic fields up to 50 T showed high adiabatic temperature change, which is comparable with those observed for single crystals. The vacuum sublimation, which is more economical and technologically advanced in contrast to single crystal growing, can be used to create magnetocaloric REM-based materials with high MCE values.

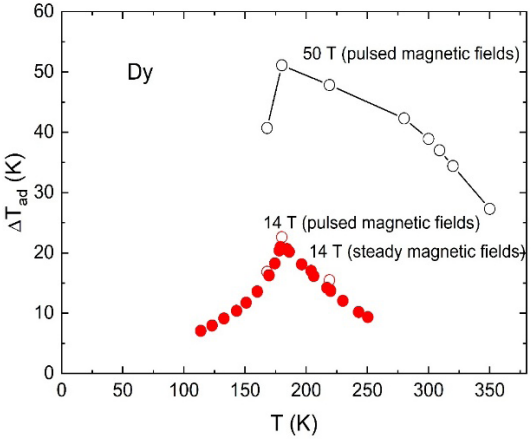


Fig. 1. Temperature dependences of MCE (ΔTad) for sublimed Dy measured in steady fields of to 14 T and pulsed magnetic fields of 14 and 50 T (open symbols)

The authors acknowledge support from Hochfeld-Magnetlabor Dresden (HLD), Helmholtz-Zentrum Dresden–Rossendorf (HZDR), member of the European Magnetic Field Laboratory (EMFL).

Contents

Abdrakhmanov D. I., Sharafullin I. F.
Localized Phase of Skyrmions in a Ferromagnetic Film with a Defect 3

Abdulkadirova N. Z., Gamzatov A. G., Aliev A. M., Jing Wang, Fengxia Hu
Direct Measurements of Adiabatic Temperature Change in $DyCo_2$ Alloy in Ultra-low Magnetic Fields. 5

Alieva M. D., Abdulkadirova N. Z., Gamzatov A. G., Aliev A. M.
Magnetocaloric Effect of the $Tb_{0.25}Dy_{0.25}Ho_{0.25}Er_{0.25}Co_2$ Alloy in Weak Magnetic Fields 6

Anikeev S. G., Artyukhova N. V., Pakholkina S. A., Bolshevich E. A.
Application of Reactive Additive and Electron Beam Processing to Create Porous-Monolithic Material Based on TiNi. 7

Artyukhova N. V., Anikeev S. G., Pakholkina S. A., Bolshevich E. A., Loban' V. V.
The Influence of Chromium Alloying on the Structural Features and Phase Composition of a Monolithic Material Based on Ti_2Ni 9

Batdalov A. B., Mukhuchev A. A., Khovailo A. V.
Effect of Alloying on the Thermoelectric Properties of the Half-Heusler FeVSb Alloy at Low Temperatures 12

Belova O. V., Morkovin S. S., Kolesov K. A., Mashirov A. V.
Temperature Relaxation Time of the Elements of the Gas Thermal Switch of a Cryogenic Magnetic Refrigerator 14

Buchelnikov V. D., Sokolovskiy V. V., Taskaev S. V.
Thermoelectric Properties of Selected Double Half-Heusler Alloys 16

Bybik M. S., Kamantsev A. P., Kalenov D. S., Orlov A. P., Lopukhin K. V., Koledov V. V., Amirov A. A., Shandryuk G. A., Kuzmin D. A., Bychkov I. V.
Electrocaloric Effect During Ferroelectric Phase Transition in Ceramic Samples $BaTiO_3$ 17

Kuzmin D. A., Ekomasov E. G., Bychkov I. V.
Spin Wave Emission Upon the Decay of a Discrete Breather in a Chain of Magnetic Nanoparticles 19

Dilmieva E. T.
Hysteresis and Kinetics of 1st Order Phase Transitions in Heusler Alloys Under High Magnetic Fields 21

Ekomasov E. G., Faskhutdinov R. A., Kabanov D. K., Kudashev V. S.
Dynamics and Structural Changes of Magnetic Vortices of Different Polarity in Spin-transfer Nanooscillators 23

Erager K. R., Sokolovskiy V. V., Buchelnikov V. D.
Phase Stability and Martensitic Transformations in Ni—Co—Ti Heusler Alloys 24

Filippov M. A., Vakhitov R. M., Khakimullina A. A., Akhmetova A. A.
Stability of Magnetic Skyrmions in Nanomodified Films to the Influence of External Magnetic Fields 25

Gaifullin R. Yu., Nagimov M. I., Mitsiuk V. I., Aliev A. M., Mukhuchev A. A., Kadyrbardiev A. T., Musabirov I. I.
Influence of Thermo-mechanical Treatment on the Microstructure, Magnetic and Magnetocaloric Properties of $Ni_{50}Mn_{18.5}Ga_{25}Cu_{6.5}$ Alloy 27

Gamzatov A. G., Abdulkadirova N. Z., Aliev A. M., Jing Wang, Fengxia Hu
Dynamics of the Magnetocaloric Effect in $DyCo_2$ and $Dy_{0.25}Tb_{0.25}Ho_{0.25}Er_{0.25}Co_2$ Alloys: Frequency and Cyclic Stability. 29

Garipov R. R., Sokolovskiy V. V., Matunina M. V.
The Effect of Hydrostatic Pressure on the Magnetic and Structural Properties of the $Ni_{1.5}Co_{0.5}Mn_{1.375}Ti_{0.625}$ Alloy 30

Kutynia K., Przybył A., Gębara P.
The Effect of Substitution of Mn by Pd on the Structure and Thermomagnetic Properties of the $Mn_{1-x}Pd_xCoGe$ Alloys (where x = 0.03, 0.05, 0.07 and 0.1) 32

Golovchan A. V.
Symmetry of Phase Transitions in Ni_2MnIn 33

Igoshev P. A., Vedernikova A. G., Gamzatov A. G.
The Modeling of a Dynamic Magnetocaloric Effect in $(LaFe_{11.6}Si_{1.4})_{100-x}Cu_x$ (x = 0, 5, 10, 15) Alloy Doped by Cu 35

Igoshev P. A., Boyko A. N.
The Study of Ferrimagnetic Ordering and Magnetocaloric Effect in the Hubbard Model for a Simple Cubic and a Base-centered Cubic Lattices 37

Vakhitov R. M., Ilyasova G. F., Filippov M. A., Solonetsky R. V.
Transformation of kπ-skyrmions on Columnar Defects of the "Potential Well" Type 40

J. Wang, P. Zhang, Y. Zhang, Y. Fang, O. Ivasenko
Confined Crystallization of Patterned $MAPbBr_{3-x}Cl_x$ Microcrystals 42

Gratowski S. V., Izmaïlov G. N., Koledov V. V.
To Possibility of Magnetic Field Quanta Using for Coherent Caloritronics . . 44

Kabanov D. K., Ekomasov E. G., Sharafullin I. F.
Oscillations of Magnetic Solitons in Multilayer Structures as a Basis for Creating a Spin-wave Generator 46

Kadirbardeev A. T., Gamzatov A. G., Aliev A. M., K. Qiao, H. Zhang
Reversibility of the Inverse Magnetocaloric Effect During Forward and Reverse Martensitic Transitions in Heusler Alloy $Ni_{36.5}Co_{13.5}Mn_{35}Ti_{15}$ . . 47

Gamzatov Adler, Igoshev Petr, Abdulkadirova Nurizhat, Kadirbardeev Anvar
Relation Between Magnetic and Magnetocaloric Properties Near the Phase Transition Point in the La—Fe(Mn, Co—Si) Alloy 49

Kamantsev A. P., Karpukhin D. A., Morozov E. V., Butvina L. N.
Elastocaloric Effect in 3d-metals Ribbons Measured by Thermal Imager and Ultrafast Fiber-optical Temperature Sensor 50

Urzhumtsev O. I., Kanurin D. A., Amirov A. A.
Machine Learning and Neural Networks Methods for Magnetocaloric Materials 52

Karpenkov D. Yu., Makarin R. A., Karpenkov A. Yu., Zheleznyi M. V.
Multistimulus Magnetic Refrigeration: from Materials to Cooling Cycles . . 53

Karpukhin D. A., Koledov V. V., Musabirov I. I., Aliev A. M., Gamzatov A. G., Abdulkadirova N. Z., Taskaev S. V.
Experimental Technique for Studying the Kinetics of the Heusler Alloy $Ni_{50.5}Mn_{33.4}In_{15.6}V_{0.5}$ During the Phase Transition Near the Curie point 56

Kazakov D. Y., Bychkov I. V., Kuzmin D. A., Fazlitdinova A. G.
Microwave Response of VO_2 and $V_{0.98}W_{0.02}O_2$ Powder Materials in the 8–12 GHz Microwave Range in the Phase Transition Region 58

Khakimullina A. A., Vakhitov R. M., Filippov M. A.
The Influence of Defects in Nanomodified Films on the Properties of Magnetic Skyrmions 60

Khanov L. N., Aliev A. M.
Magnetocaloric Effect and Magnetostriction in Cyclic Magnetic Fields 62

D-H. Kim
Magnetization Dynamics in Various Magnetic Films 65

Kirilyuk K. K., Musabirov I. I.
Thermal Expansion and Microstructural Evolution of a Ni—Mn—Ga—Si Alloy Following Stepwise Annealing of the Deformed State 66

Kirillov D. E., Matyunina M. V., Koledov V. V., Pavlukhina O. O., Orshulevich M. A., Maltsev I. V., Kolesov K. A., Karpukhin D. A., Kuzmin D. A.
Investigation of the Effect of Aerodynamic Drag on the Damping of Oscillations of an HTS Cryostat on a Magnetic Track 67

Koledov V. V. , Buchelnikov V. D., Smerchansky P. S., Kamantsev A. P., Kuznetsov D. D., Suslov S. D., Morozov E. V., Mashirov A. V., Kovalev O. E., Safonov R. A., Gribanov I. F., Golovchan A. V., Nyrkov N. Yu., von Gratowski S. V., Zhdanov S. S., Povarnitsyn V. M.
Ferromagnetic Shape Memory Effect in Heusler Alloys — 30 Years of Discovery 69

Koledov V. V., Matyunina M. V., von Gratowski S.V., Suslov D. A., Bychkov I. V., Pavlukhina O. O., Orshulevich M. A., Maltsev I. V., Mashirov A. V., Kirillov D. E., Garipov R. R., Kamantsev A. P., Kolesov K. A., Karpukhin D. A., Kuzmin D. A.
Magnetic Levitational Transport Based on High Temperature Superconductors: Modelling of Accelleration and Braking System 71

Kolesov K. A., Mashirov A. V., Koledov V. V., Kamantsev A. P.
Trapped Field Profile in Bulk High-temperature Superconductor Solenoid . . 73

Gribanov I. F., Safonov R. A., Kovalev O. E., Golovchan A. V., Burkhovetsky V. V., Nyrkov N. Yu.
Effect of Pressure on the Magnetocaloric Properties of $NiMn_{0.89}Cr_{0.11}Ge$ Alloys with Reduced Curie Temperature and Different Thermal History . . . 75

Tarasenko T. N., Antonishin Ya. Yu., Kovalev O. E., Mazur A. S.
Specific Features of Methods for Preparing the Double-Layered Cobaltite $GdBaCo_2O_{5.5}$ 77

Komlev A. S., Vashchenkova A. R., Kostylev S. I., Chernyshev V. E., Perov N. S.
Magnetic Viscosity in Materials with Nonequilibrium Transformations Near Magnetostructural Phase Transitions 80

Kuleshova T. E., Karmanova O. I., Panova G. G.
Polarization Curve and Power Density of Plant Bioelectrochemical System with Different Agricultural Crops 82

Kuleshova T. E., Dobrokhotov A. V., Tarakanov V. V., Koledov V. V., von Gratowski S. V.
Temperature Profile of the Plant-environment System Under Natural Conditions and Intensive Light Culture 83

Kurganskaya A. A., Kozlyakova E. S., Tereshina I. S., Vasiliev A. N.
Magnetocaloric Effect in Pseudo-binary $Gd_{0.9}Tb_{0.1}NiH_x$ Hydrides with Various Hydrogen Amounts 86

Kuzmin D. A., Maltsev I. V., Bataev D. S., Utarbekova M. V.
Comparative Simulation of Halbach Cylinder with Ring Segments and Rectangular Prisms for Caloric Cooling 89

Kuzmin D. A., Kolesov K. A., Bychkov I. V., Koledov V. V., Maltsev I. V., Matyunina M. V.
Modelling of Force Interaction Between an Hts Ring and a Coil in a Permanent Magnet Levitation System 91

Kuznetsov A. S., Mashirov A. V., Mitsiuk V. I., Kamantsev A. P., Kovalev O. E., Nyrkov N. Yu., Safonov R. A., Gribanov I. F., Golovchan A. V.
Tailoring Magnetic and Magnetocaloric Properties in Ni—Co—Mn—Ti Melt-spun Ribbons via Annealing 94

Kuznetsov D. D., Kuznetsova E. I., Kamantsev A. P., Danilov D. V., Shandryuk G. A., Koledov V. V.
Effect of Heat Treatment on the Austenite Microstructure and Martensitic Transformation of Rapidly Quenched Ribbons of Heusler Alloy $Ni_{37}Co_{13}Mn_{35}Ti_{15}$ 96

Lupitskaya Yu. A., Fedii A. A., Bychkov I. V., Kalganov D. A.
Development of Measurement Methods and Study of the Electrodynamic Characteristics of Multiferroics in the Microwave Range Using Inductive-gap Cells 98

Lupitskaya Yu. A., Saunina S. I., Butakov A. V., Galeeva L.-S. D.
Effect of Micro- and Nanosized Refractory Carbide Additives on the Structure and Properties of Deposited Metal 99

Maltsev I. V., Bychkov I. V., Matyunina M. V., Koledov V. V.
Numerical Modelling of a Multi-cascade Magnetocaloric Device Operation 100

Mashirov A. V., Kolesov K. A., Kuznetsov A. S., Musabirov I. I.
Experimental Refrigeration Cycles of a Magnetic Refrigerator Based on $GdNi_2$ Alloy 103

Matyunina M. V., Sokolovskiy V. V., Buchelnikov V. D.
Correlation of Lattice Expansion, Phonon Softening, and Superconducting Critical Temperature in Pd_2YSn 104

Baraishuk S. M., Tkachenka T. M., Golovchan A. V., Mashirov A. V., Gurbanovich A. V., Zhaludkevich A. L., Mitsiuk V. I.
Magnetostructural Phase Transitions in Substituted Manganese Arsenide . . 106

Moiseev D. M., Sokolovskiy V. V., Buchelnikov V. D.
Investigation of Thermoelectric and Magnetostructural Properties of the $Ni_{15}Mn_{13}Sn_4W$ Heusler Alloy. 108

Morozov E. V., Poimanov V. D.
The Influence of Temperature Field on the Relaxation Time of Order Parameters During Martensitic Phase Transition in Ni—Mn—In—V and Ni—Co—Mn—Ti Alloys 110

Kirilyuk K. K., Gaifullin R. Y., Kalashnikov V. S., Nesolenov A. V., Koshkidko Yu. S., Dilmieva E. T., Taskaev S. V., Musabirov I. I.
Magnetomechanical Response of Martensitic Transformation in Ni—Mn—Ga—Si Alloys Across Various Structural States. 113

Mukhuchev A. A., Aliev A. M.
Magnetocaloric Effect in Er and Ho in Cyclic Magnetic Fields 114

Nagalakshmi R., Dzubinska A., Reiffers M.
Architecting the Magnetocaloric Future: from Rare-earth and Mn-based Alloys to Flexible Functional Materials for Sustainable Cooling Applications. 116

Nezhencev A. V., Koledov V. V., Prokunin A. V., Kalashnikiv V. S., Nesolenov A., Andreev V.
Torsion Actuator with Shape Memory Effect 118

Novokreshchenov D. V., Sokolovskiy V. V.
Phase Diagrams of a Four-component Ni—Co—Mn—Ti System 120

Nugumanov A. G., Nugumanov R. R., Sharafullin I. F.
Stretch-hysteresis of Topological Charge in the Model of Elastic Ferromagnetic Monolayer with Strain-Dependent DMI 122

Nyrkov N. Yu., Golovchan A. V., Kovalev O. E., Safonov R. A., Gribanov I. F., Shevelev A. V., Kamantsev A. P., Todris B. M.
Laboratory Setup of a Pulsed Magnetometer for Studying Magnetic and Magnetostructural Phase Transitions 125

Orshulevich M. A., Utarbekova M. V., Taskaev S. V., Baigutlin D. R., Hu Zhang, Buchelnikov V. D.
Production, Microstructure and Magnetocaloric Effect of Polycrystalline Ni—Co—Mn—Ti Alloys with Variable Composition. 127

Pavlukhina O. O., Buchelnikov V. D., Sokolovskiy V. V.
Insight into Half-metallicity and Structure of $FeRhSb_{1-x}Z_x$ Heusler Alloys . . 128

Prokunin A. V., Koledov V. V., Orlov A. P., Luzanov V. A., Musabirov I. I.
Heating Systems for Actuation of Shape Memory Alloy Nanomechanical Devices 130

Rozhnova E. A., Baimova J. A.
Effect of Metal Nanoparticles on the Mechanical Properties of Graphene Aerogels 132

Samigullina A. I., Sharafullin I. F.
The Influence of Magnetoelectric Interaction on the Spin-wave Spectrum in thin Helimagnetic Films 134

Sitnikov N. N., Sundeev R. V., Shelyakov A. V.
Rapidly Quenched Ribbons Produced of Quasi-binary TiNi—TiCu Alloy for the Production of Refrigerators and Heat Pumps Based on the Elastocaloric Effect. 136

Smerchanskiy P. S., Koledov V. V., Kamantsev A. P., Kuznetsov D. D., Kovalev O. E., Safonov R. A., Gribanov I. F., Golovchan A. V., Nyrkov N. Y., Zhdanov S. S., Povarnitsyn V. M.
Phase Transitions in $Ni_{2,14}Mn_{0,81}Fe_{0.05}Ga$ Heusler Alloy Under External Magnetic Field and Hydrostatic Pressure 138

Sokolovskiy V., Gamzatov A., Kadirbardeev A., Buchelnikov V.
Ab Initio and Monte Carlo Study of Magnetic, Structural, and Magnetocaloric Properties of Ni—Mn—Sn—Cu Heusler Alloy 139

Sokolovskaya Yu. A., Buchelnikov V.
Mechanical Properties of Stable Austenitic and Martensitic Phases in Ni—Mn—Ga Heusler Alloys: A First-principles Study. 142

Sundeev R. V., Shalimova A. V., Rogachev S. O., Bazhenov V. E.
Creation of Amorphous-crystalline Composites Using Extreme Impact Methods. 144

Tereshina I. S., Politova G. A., Umkhaeva Z. S.
Magnetocaloric Effect and Magnetostriction of Medium-entropy Tb—Dy—Ho(Er)—Co Alloys with Laves Phase Structure. 145

Tolkachev V. A., Bychkov I. V., Kuzmin D. A.
Interaction of Surface Plasmon-Polaritons with Magnetic Skyrmions in Co/Pt Heterostructures 148

Utarbekova M., Orshulevich M., Taskaev S., Hu Zhang, Buchelnikov V.
Experimental Study of the Magnetocaloric Effect in Ni—Co—Mn—Ti Heusler Alloys and Prospects for their Application . . 150

Vakhitov R. M., Yumaguzin A. R., Demidova V. A.
Features of Magnetic Inhomogeneities in (111)-oriented Garnet-ferrite Films with Flexomagnetoelectric Effect 152

Vashchenkova A. R., Komlev A. S., Komleva D. I.
Landau — Khalatnikov Description of Magnetization Relaxation Effects Near First-order Phase Transitions 155

von Gratowski S. V., Koledov V. V.
Quantum Thermal Valve with Magnetocaloric Effect 157

Yuldasheva A. R., Sharafullin I. F.
Partial Phase Transition and Surface Effects in a thin Helimagnet/
Ferroelectric Superlattices 159

Yuhai Qu
Abstract Magnetocaloric Properties of Melt-extracted Gd—Co
and Er-doped Gd—Co Crystalline/Crystalline Composite Microwires 161

Yusupov D. M., Aliev A. M.
Method for Measuring Magnetization in Alternating Magnetic Fields 162

Artamonov I. V., Zagrebin M. A.
Ground State of Mn_3Al Heusler Compound: Insights From *ab initio* 163

Z. Zhao, C. Liu, Graboy I. E., Gamzatov A. G., K. Qiao, H. Zhang
Influence of Impurity Phases in Chromium (IV) Oxide on Magnetic
and Magnetocaloric Properties 165

Zheleznyi M. V.
A phenomenological Model for Multi-stimulus Magnetic Refrigeration:
T_{ad} for Second-order Phase Transitions 167

Aliev A. M., Abdulkadirova N. Z., Alisultanov Z.Z.
Scaling Analysis of the Adiabatic Temperature Change in Alternating
Magnetic Fields 170

Koshkid'ko Yu. S., Ćwik J., Salazar Mejia C., Dormidontov N. A., Prokofev P. A., Bakulina A. S., Nikitin A. A., Khomich A. A., Gimaev R. R., Andreenko A. S., Burmii Zh. P., Telitsa A. A., Zverev V. I., Kolchugina N. B.
Magnetocaloric effect of sublimated dysprosium
in high steady and pulsed magnetic fields 172

Scientific edition

DAGESTAN CALORIC DAYS
Functional Materials and Their Applications
Book of Abstracts

May 27-31, 2026, Manas, Dagestan, Russia

Layout by *M. V. Trifonova.* Cover design by *S. S. Feldman*

Signed for printing on 20.05.26. Format: 60×84 $^1/_{16}$.
Conventional printed sheets: 10,5. Educational and publishing sheets: 10,0.
Print run: 500 copies. Order No. 185

Chelyabinsk State University.
129 Bratyev Kashirinykh St., Chelyabinsk, 454001, Russia

Printed by the Publishing House of Chelyabinsk State University
57b Molodogvardeytsev St., Chelyabinsk, 454021, Russia